AN ABSTRACT OF THE THESIS OF

Alan Edward Peterson for the degree Master of Science

in The Department of Physical Sciences presented on November 10, 2016

Title: NEW GEOSPATIAL TECHNIQUES AND METHODS APPLIED TO STRUCTURAL GEOLOGY IN EAST-CENTRAL KANSAS

Thesis Chair: Dr. James Sandusky Aber

Abstract approved:

The wealth of previous geological work done in central and eastern Kansas is of immense help in interpreting newly available data such as high-resolution imagery and LiDAR. The surficial geology (easily defined marker beds of white limestone), land cover (grasses), typical land use (mostly untilled), and difficulty in gaining physical access in the Flint Hills of Kansas make this region particularly well suited to investigation through remote means.

The study area overlies a complex collection of basement faults. These basement faults have been activated and reactivated in the past due to a variety of tectonic events. The Nemaha Fault Zone is thought to be the result of spreading at the Midcontinent Rift farther to the west. This collection of rhombic basement blocks was reactivated later as terranes collided with the now eastern and southeastern margin of the craton. Forces transmitted across the North American craton by these and other collisions exploited preexisting basement faults. Some of these are extensions of transverse fracture zones extending all the way to the Atlantic Mid-Ocean Ridge. These structures are inferred to

account for the Fall River, Chesapeake, Bolivar-Mansfield, and Central Missouri Tectonic Zones among others.

The structural anomaly that is Elmdale Dome and its adjacent structures were recognized early in the 20th century. It has been the focus of further study in the time since then. The application of new technology and data to the study of this region in this research has uncovered additional information concerning the bedrock structure of the region.

The dipping strata and associated landforms overlying the Humboldt Fault may be easily traced from north-central Oklahoma to the glaciated region of northeastern Kansas. Moderately dipping strata associated with the eastern boundary of the Nemaha Fault, found when mapping strike and dip, or analyzing hillshaded LiDAR, generally match previously mapped subsurface faults. Areas with localized anomalous dips generally overlie recognized structural features. Newly mapped fault trends and lineaments sometimes match recognized basement faults and structures, while some do not. These likely overlie unrecognized basement structures. Oblique movement is recorded in various Riedel trends and associated dipping strata in Chase and surrounding counties. Other fault trends found near basement fault zones appear to be normal in nature. Linear fault zones west of the Humboldt front parallel the orientation of the Humboldt Fault (south-southwest to north-northeast). These are possibly the result of adjustments along backthrusts or reverse faults created by the main thrust of the Nemaha Fault Zone during the active period of the Midcontinent Rift ending ~1.1 Ga. These and other structures were reactivated later during Paleozoic and more recent Laurentian orogenies. It is also likely that displacement along transverse faults associated with seafloor spreading in the

Atlantic was transmitted into the cratonic interior during the Mesozoic and Cenozoic. Adjustments along basement structures were broadcast upwards through the sedimentary column.

New technology allows for new methods of data collection and visualization in this realm. This trend of improving geospatial data and the accompanying improved possibility for analysis is likely to continue to advance our knowledge of past tectonic events and resulting geologic structures.

Approved by the department Chair

Committee Member

Committee Member

Committee Member

Dean of the Graduate School and Distance Education

NEW GEOSPATIAL TECHNIQUES AND METHODS APPLIED TO STRUCTURAL GEOLOGY IN EAST-CENTRAL KANSAS

A Thesis

Presented to

The Department of Physical Sciences

EMPORIA STATE UNIVERSITY

In Partial Fulfillment

of the Requirements for the Degree

Master of Science

by

Alan Edward Peterson

2016

ACKNOWLEDGEMENTS

I would like to thank my thesis chair, Dr. James S. Aber for the speedy correspondence required to complete this thesis and for teaching in a manner that invited further exploration of the subject matter outside of classwork. I would like to thank Dr. Richard O. Sleezer for giving me a deep understanding of Geographic Information Systems software and for his continuous input in different pursuits in this field including this work. I would also like to thank Dr. Alivia J. Allison for introducing me to the finer aspects required in understanding faulting in a real world context and for input on various facets of this thesis.

As a child, family vacations consisted largely of geological field trips. I would like to thank my parents in this respect for introducing an understanding of geological and natural processes and for supporting me through the course of my academic career.

Table of Contents

Figures

Formulas

Chapter 1. Introduction

The structural geology of the Flint Hills appears to consist of relatively simple layer cake strata (e.g. horizontal or gently dipping sedimentary rock sequences), but appearances are sometimes deceiving. Although the gross geology may be nearly horizontal to gently dipping sedimentary rocks, locally more complex yet subtle geologic structures (e.g. folds, faults, and joints) have strongly influenced the development of topography in different ways throughout the region. One difficulty with studying these features is that most of the land is privately owned. Gaining access to intensively study subtle geologic structures is time consuming, and a method of accurately detecting and quantitatively studying structures remotely could facilitate new insight concerning the structural and geomorphic history of the Flint Hills. Geographic information systems (GIS) technology facilitates the use of modern GIS datasets (high-resolution imagery, LiDAR, etc.) coupled with historical geologic/structural analyses and field research to gain greater insight into the influences of structure on topography in the Flint Hills.

The focus of this research effort is on using modern GIS technology and datasets to intensively study that part of the Flint Hills that the author is quite familiar with (Figure 1). I grew up on the periphery of the Flint Hills, and some of my early memories are of his father working to complete his master's research in Earth Science at Emporia State University. His study area was in the Flint Hills of Chase and Morris County. It was my father who pointed out a strange geomorphic feature on Elmdale Hill in Chase County, which is one of my intensive study areas for this thesis research. His observation, coupled with the strangely linear drainage patterns in the area and the prevailing stream position within each waterways' respective alluvial valley in this part

of Kansas, made me curious about structural influences on geomorphic processes in this area.

As a teenager I roamed the headwaters of the North Fork of the Verdigris River. I completed my undergraduate field geology mapping project in this area and the cumulative effect of these experiences has been to make me curious about a variety of geologic, geomorphic, and structural observations I have made over the past 15 years. During my undergraduate career, I developed an interest in modern computer mapping technology (GIS and remote sensing), which has made me aware of the potential for such analyses to enhance our understanding of geomorphic processes and how they are related to underlying geology and geologic structures. My intent with this thesis research is to combine my intimate knowledge of Flint Hills' geology, with my curiosity about the relationships between structures and topography, and my capabilities to perform GIS analyses to gain new perspectives on how the current Flint Hills landscapes formed.

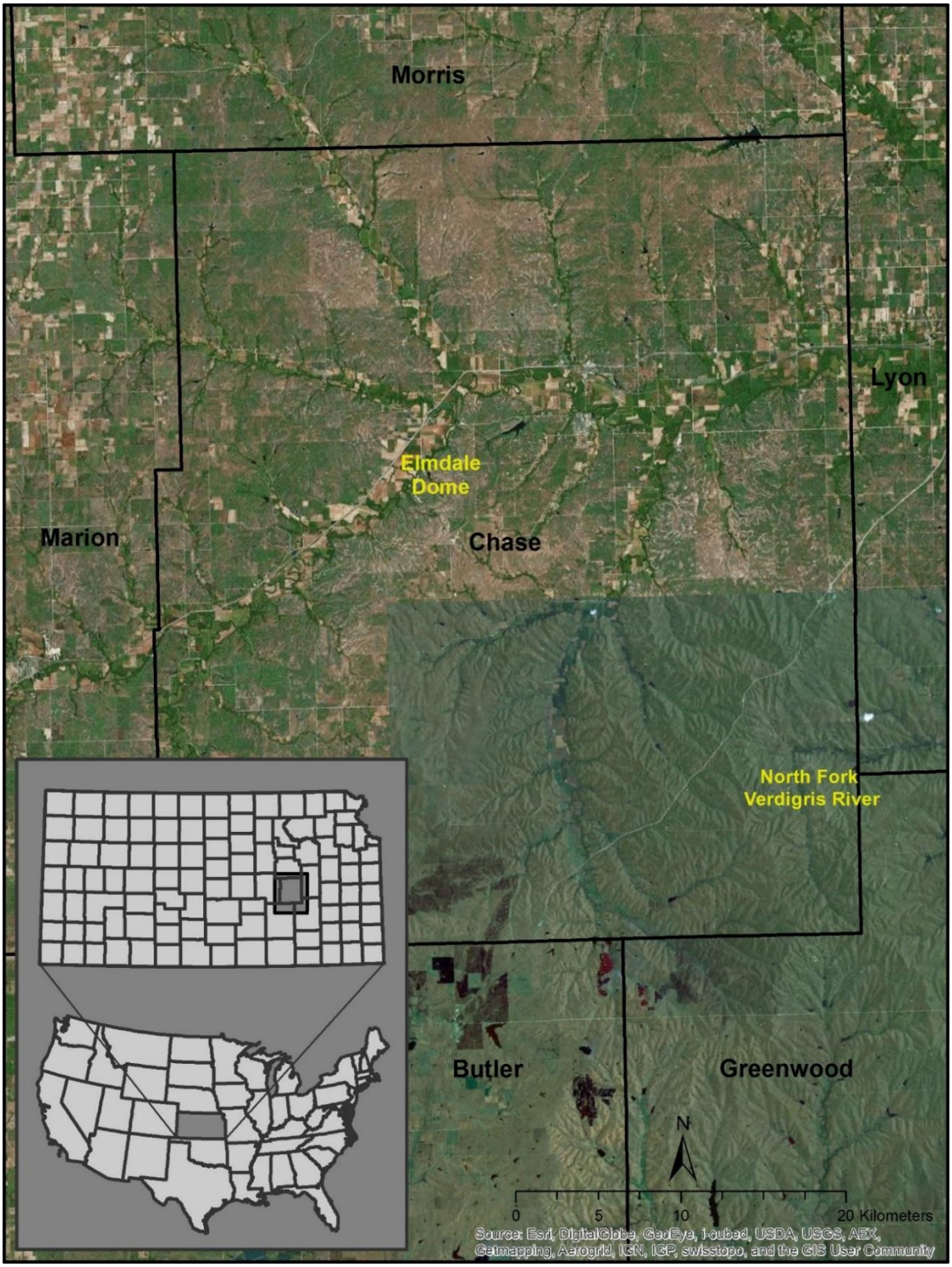

Figure 1. The study area.

My interest in the area, and my penchant for all things GIS related, pressed me to investigate. The recent release of high-resolution imagery acquired during a regional drought when vegetative cover was minimal, and the recent acquisition of LiDAR high-resolution elevation data, combined with the highly visible 'stone lines' associated with the characteristic regional geology and minimal tree cover, make it possible to interpret structural geology within the study area in a new way. The intent was to investigate the structural and geomorphic history of the study region utilizing as many tools as are available for use in pursuit of a greater knowledge of the factors affecting processes that have created Flint Hills' topography. Some methods worked far better than expected, others did not. The more effective methods for interpreting geologic features are examined further in this work. Previous research, which is quite extensive in the area, provided a framework for understanding the conclusions of my research.

Tectonic Context

The strata that make up Elmdale Hill overlie an old geologic basement structure referred to as the Humboldt Fault system. This is the eastern edge of the Nemaha Fault Zone. Other names for the Nemaha Fault Zone used in previous literature include Nemaha Fault (McBee, 2003), Nemaha Ridge (Merriam, 2010), Nemaha Anticline (Merriam, 2010), Nemaha Uplift, and Nemaha Tectonic Zone. The eastern front of the Nemaha is often referred to as the Humboldt Fault Zone (Berendsen and Blair, 1986). The Humboldt Fault system extends from central Oklahoma northward to east-central Nebraska (Figure 2).

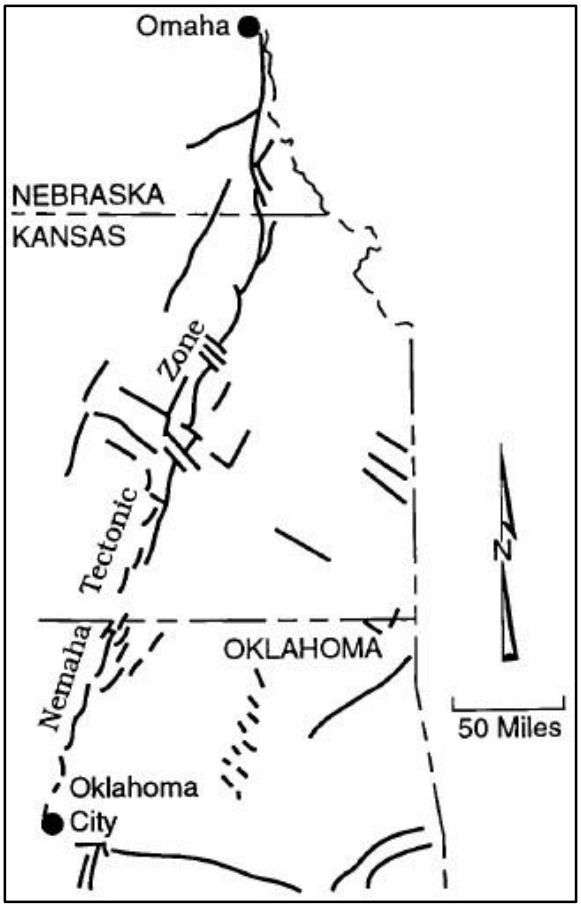

Figure 2. Generalized trend of the Nemaha tectonic zone in Nebraska, Kansas, and Oklahoma. From Structural Development of the Nemaha Tectonic Zone in Kansas (Berendsen and Blair, 1995).

The Nemaha Fault complex is a collection of discrete rhombic fault blocks in a 'zipper' structure that parallels the Mid-Continent Rift to the west. Its proximity and orientation relative to the Mid-Continent Rift system (MCR) have led to the consensus of some that the Humboldt Fault system is the result of reactivation of structural weaknesses parallel to the MCR when the MCR was an active rift feature ending ~1.1 Ga (Berendsen, 1986; Hauser, 1996; Keller, 1983). Other tectonic zones with a similar structural style

are found further to the north parallel to the MCR (Sims, 1990). Other authors refute this connection citing earlier dextral compressional or transpressional structural influences from the OlympicParadox-Wichita fault zone 1.7-1.6 Ga. (Baars, 1995). The MCR extends from south-central Kansas into the Great Lakes Region. It is buried under thick sedimentary strata in Kansas, but there is some information about its depth available from well logs and published analyses. For example, it was pierced by the Texaco Poersch #1 deep well in Washington County, Kansas which was drilled to a depth of 3444 meters in 1984 (Berendsen et al., 1988).

Following the active rifting period, the resulting basin was filled by sediments eroded from the flanks of the ancient rift. This infilling of sediment is clearly visible in the northern United States where the rift is exposed at the surface. The Texaco Poersch #1 well shows repeated basaltic flows separated by sedimentary sequences. In the well, the basalt flows lie atop the primary sedimentary sequence understood to be the erosional infilling of the basin. This sedimentary sequence has been interpreted as being the result of high angle reverse faulting as a result of the episodic Appalachian mountain building era (Berendsen et al., 1988). The expected erosional unconformities associated with compression at the Nemaha Ridge coincide temporally with all three major orogenies associated with the construction of the Appalachian Mountains. The direction of compression relative to the area of interest, thus, changed progressively as first the Taconic Orogeny pushed against the cratonic margin from the east, the Acadian from the east-southeast, and the Alleghenian-Ouachita Orogeny from the southeast and south (Berendsen and Blair, 1986; Gay, 2003). In the Great Lakes Region flood basalts are

exposed at the surface, and the overlying sedimentary infill sequence is visible (Somanas et al., 1989).

Repeated transverse faults perpendicular to the MCR along the length of the failed rift such as the Fall River Tectonic Zone (FRTZ), and the Bolivar-Mansfield Tectonic Zone (BMTZ), have been interpreted as being the extensions of transverse faults proliferating from minor accommodation structures along the MCR (Horral et al., 1982). These transverse faults were likely reactivated during Appalachian mountain building. The visible topographic feature at Elmdale Hill is the surface expression of the easternmost margin of the Nemaha Fault (Berendsen and Blair, 1986). The eastern margin of the Nemaha is referred to as the Humboldt Fault in the remainder of the text. In a cross section in northern Chase County, there is interpreted to be approximately 460 meters of offset between the hanging wall to the west and the foot wall to the east (Figure 3; Jewett et al., 1951). The scarp of the Humboldt Fault is buried under Permian and older strata. The sedimentary fill has muted the expression of the basement fault at the surface despite periodic uplift during Appalachian mountain building.

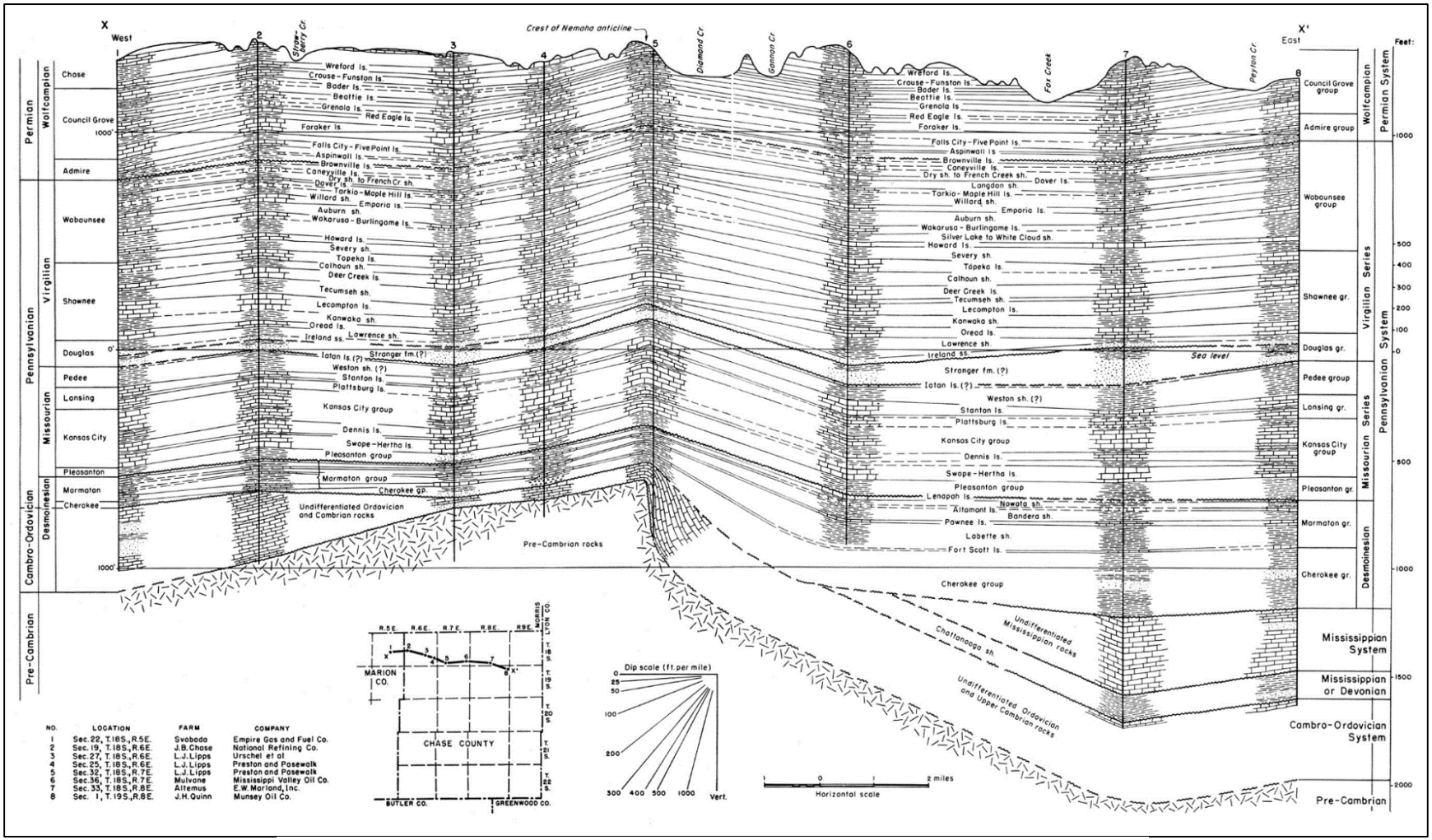

Figure 3. A cross-section through northern Chase County (Jewett et al., 1951).

The feature that caps Elmdale Hill is the node from which the focus of my study radiated. The prominent ridge extending from the top of Elmdale Hill south is the result of relatively, for Kansas, steeply dipping strata dipping to the east. This steeply dipping strata was recognized early, and it was first described by Prosser and Beede (1904) in the USGS Cottonwood Falls Folio. An early well drilled in the area designated "Elmdale Well no. 1" was drilled in 1914 one mile south of Elmdale in the river valley. The surface elevation is 361 meters above mean sea level. The well struck what was termed as 'granite' at about 550 meters below the surface. An excerpt from the Kansas Geological Survey Bulletin number 2, 1915, pages 27-29, "The Crystalline Rocks of Kansas" illustrates the surprise of the on-site driller, one Mr. A. L. Derby.

"Dear Sir

Enclosed you will find record of the well which I am drilling on the Chase County poor farm. We have this well down to a depth of 1980 feet, and from 1700 feet we have had what we consider granite, practically all the way, or nearly 300 feet of this same formation.

According to our contract, we will have to drill this well to a depth to a depth of 2500 feet, unless Mississippian limestone is found at a less depth. As this formation in which we are drilling is very hard and very treacherous to drill, we can not keep the hole going straight. I am enclosing you samples of this formation, under separate cover, and I wish you would examine these samples and the record closely and give me an opinion as soon as possible as to what this formation is, and about how much more of it we should encounter and about we should find the Mississippian limestone. This formation looks a great deal more like granite to me than it does like Mississippian limestone.

As our contract would end when we reach the Mississippian limestone, I wish you would also give me an opinion on that as to whether or not you would consider our contract completed with this formation. An early reply would be very much appreciated.

Very truly, A. L. Derby."

As reported in the Well Report, *"The well was abandoned in granite at a depth of 2500'* (Kansas, 2016)*."*

While much is known of geologic structures and tectonic history of Flint Hills region of Kansas (Berendsen and Blair, 1986), surface expressions of structural features are subtle, and no truly comprehensive field study of faults, fractures and folds has been conducted. There is no incentive for the Kansas Geological Survey or private companies to perform such an investigation unless there are significant economic interests, natural hazards, or environmental concerns. This lack of a sufficient motivation leaves the pursuit of detailed structural knowledge to the purely academic.

Carrying out a detailed, survey of surface-exposed geologic structures in east-central Kansas would be problematic for at least three reasons:

1. The remote nature of the study area. It is not near major population centers and most of the land is used for grazing cattle. Road access is limited to section roads (where they exist) and some of them are limited maintenance.
2. The difficulty of gaining access to large areas of land to perform on-site structural studies in an area predominantly owned by either private land owners or ranching corporations operated by out of state committees is

difficult. Access to an individual pasture may be relatively easy but unfettered access to a hundred sections of land is a logistic nightmare.

3. The time and money required to conduct a detailed surficial geology survey over a large area is prohibitive.

New data and technology have become available in the past decade that may facilitate the remote identification and measurement of structural feature characteristics at an unprecedented precision and scale. These new datasets include LiDAR and high resolution aerial photography (NG911, DASC, 2014; ESRI basemaps, ArcGIS®, 2016, etc.). LiDAR provides higher spatial resolution and more precise elevation data than has ever been available with older elevation datasets. Multiple high resolution aerial photography datasets can be used in conjunction with LiDAR to identify unusual topographic features and rock outcroppings across a variety of spatial scales. In addition, the three-dimensional modeling capabilities of GIS software (e.g. hill shading, etc.) coupled with the capability to convert old, analog paper maps into useful GIS datasets, and the availability of the new datasets mentioned above provide opportunities for spatial analysis that were simply not possible even ten years ago.

Research Questions

The purpose of this study is to examine the feasibility of using modern GIS techniques and datasets (imagery and LiDAR) coupled with georectified historical published map data and well log data to gain new perspectives on the geomorphic history of Chase County and surrounding areas in the context of the influence of the underlying geologic structures on the geomorphic processes that have formed the Flint Hills.

Specifically, the focus is on investigating how the movement of basement structures over time contributed to the linear and angular patterns of stream valleys and the development of landforms characteristic of dipping strata observed in the region. A secondary research question is related to determining the feasibility of acquiring accurate measurements of strike-and-dip remotely using high-resolution imagery and LiDAR elevation data. If strike-and-dip measurements may be accurately determined remotely it obviates the need to obtain permission from land owners and it may facilitate rapid investigation of tilted strata without excessive field work.

Chapter 2. Methods

Georectification

Maps developed in the past are often times sources of important information even though they are based on old analyses and are not available as GIS datasets (e.g. Berendsen and Blair, 1986, Figure 4). It is possible to convert paper maps into useful GIS datasets if they are digitized and accurately overlain on existing GIS datasets. The process to convert historical maps into GIS datasets involves several steps. First the maps must be scanned to create an appropriate digital image. Next the image must be geo-rectified using GIS software to assign known coordinate values to pixels and warping the image so that it is an accurate overlay on other GIS datasets. Finally the data on the now rectified map may be digitized to create GIS dataset that may be used for additional analysis. This process allows information contained in analog sources to be converted to digital GIS dataset. For example, the original paper maps from Subsurface structural maps over the Central North American rift system (CNARS) (Berendsen and Blair, 1986), central Kansas were scanned into .pdf format, converted to .tiff format, and then georectified using control points from every township corner using ArcGIS 10.x software. The georectification tool was used to input the control points manually. The user must place a point on the scanned image and a second point on a matching location in an existing GIS dataset with a known coordinate system based on a known map projection. This process assigns geographic coordinates to the digital version of the paper map (Figure 5). The more control points that are used, the more precise the georectification generally is.

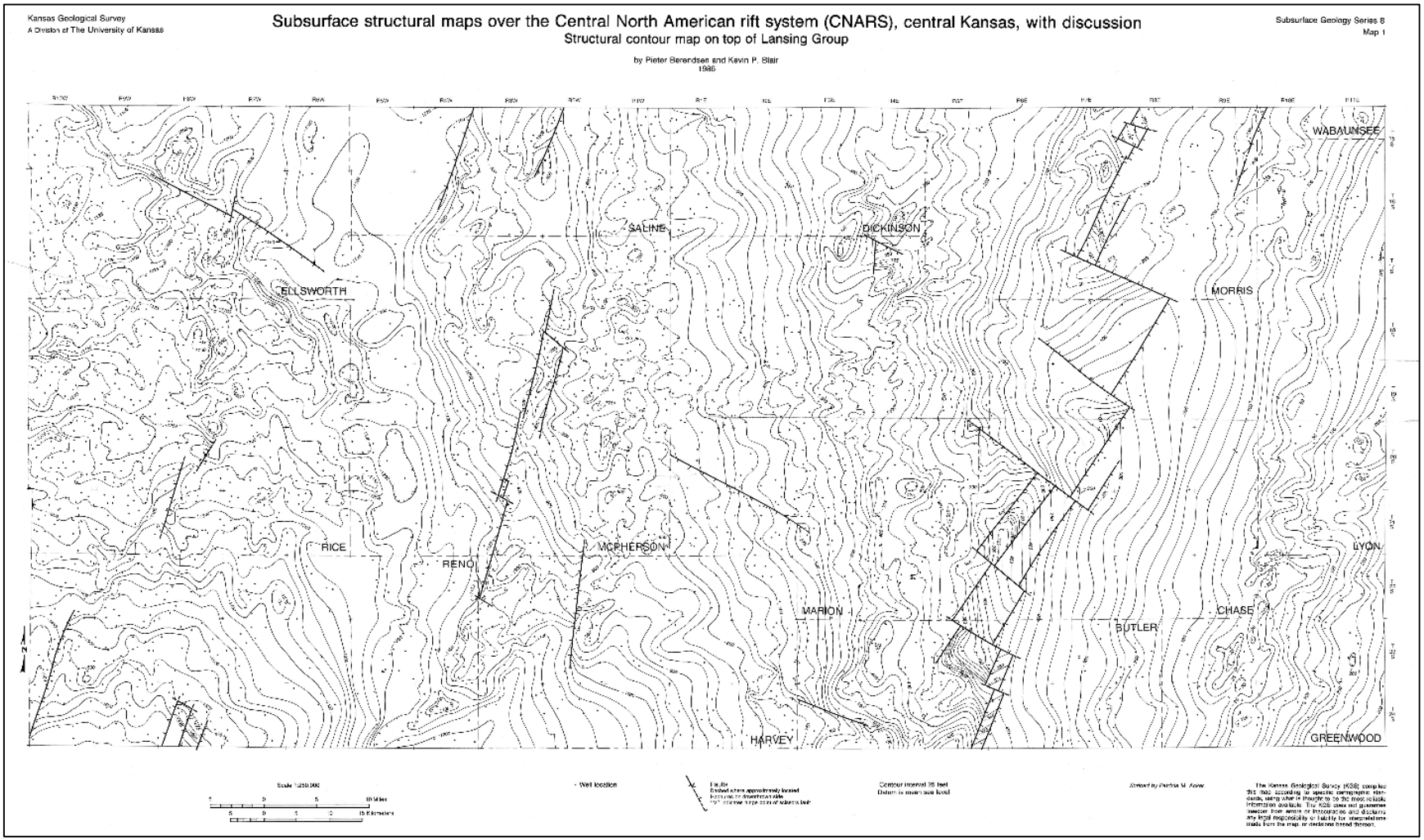

Figure 4. The original paper map (Berendsen and Blair, 1986).

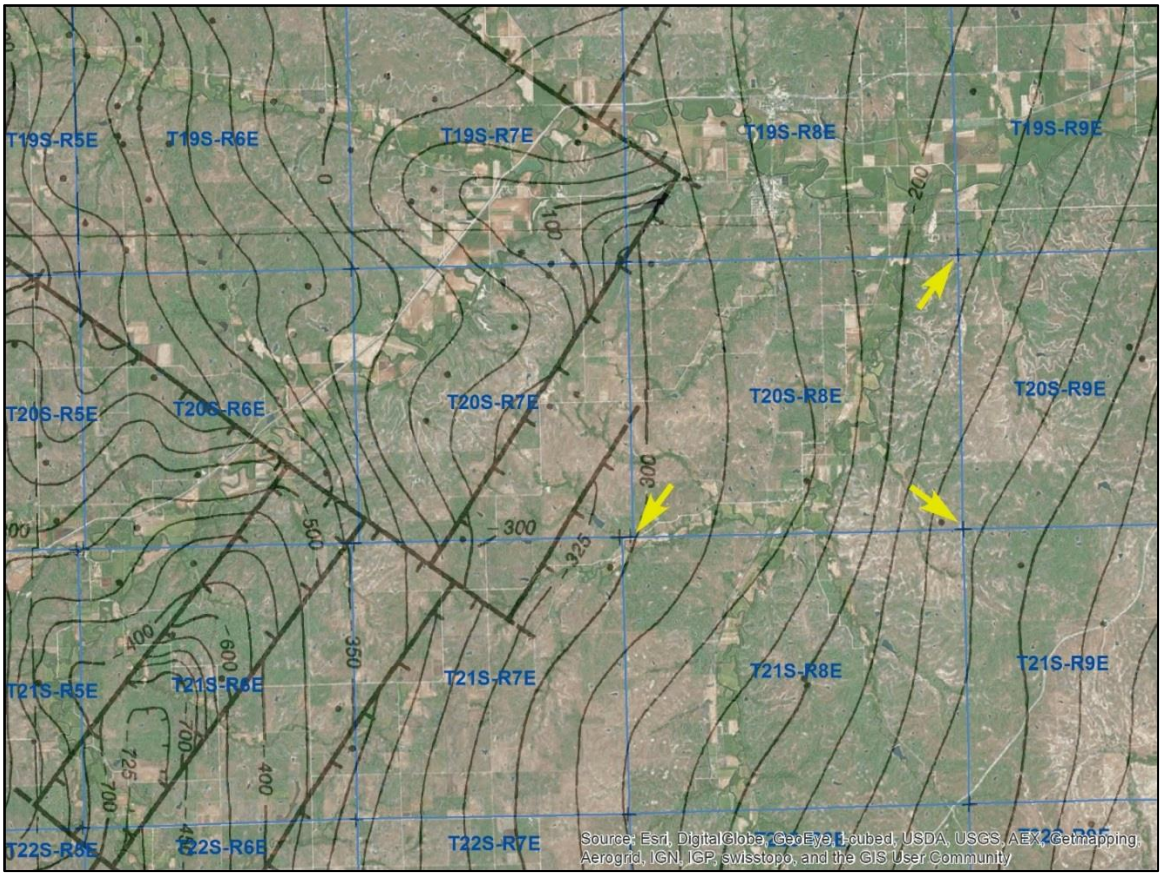

Figure 5. Showing the alignment of township corners on the scanned paper map with GCP at township corners. The original paper map has been made semi-transparent so that it is possible to see that the township corners are aligned with those of a GIS dataset in geographic space. Black dots are well tops used as control points in the map's creation (Berendsen and Blair, 1986).

Once rectified, it is possible to convert the information to a more useful digital format. The example used in describing this process is a structural contour map from Berendsen and Blair (1986). The contour lines in the map were subsequently digitized to create a polyline shapefile that is in turn attributed with elevation data. By digitizing the

polyline traced on top of a contour line and attributing it with the value of the original contour on the paper map (Figure 6), the data contained in the map may be converted to a digital GIS format that may be used to create three-dimensional views of bedrock topography by interpolating a continuous grid of elevation values that is essentially a subsurface bedrock digital elevation model. The GIS datasets (contours, elevation grid, and three-dimensional view) were then used in a series of overlay analyses to determine relationships between landforms observed at the surface and subsurface bedrock topography and structures. For example, data in a digital format might be simultaneously displayed along with other data in the same area. A map of surface faults was displayed as an overlay on subsurface structure and surface topography datasets to investigate spatial relationships among the location of surface faults, surface topography, and subsurface structures.

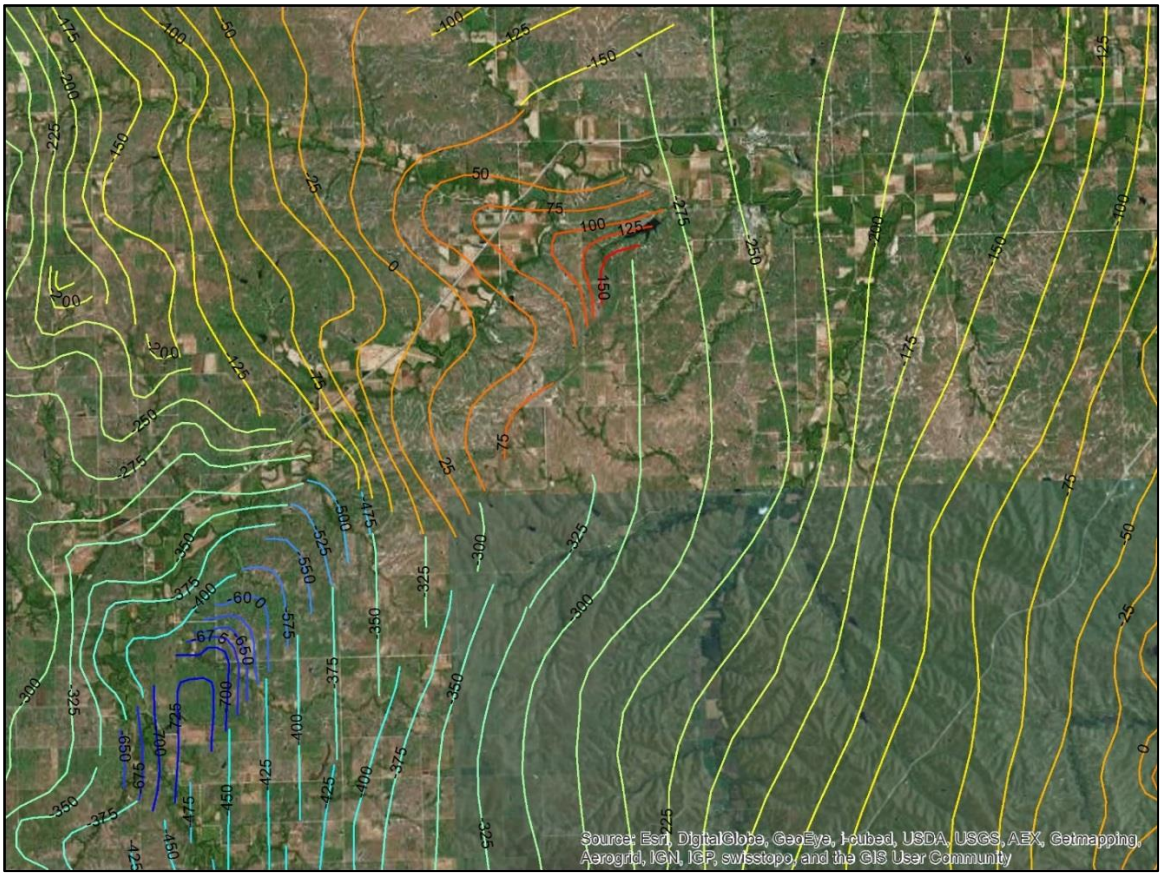

Figure 6. Structural contours on top of the Lansing Formation traced from the paper map.

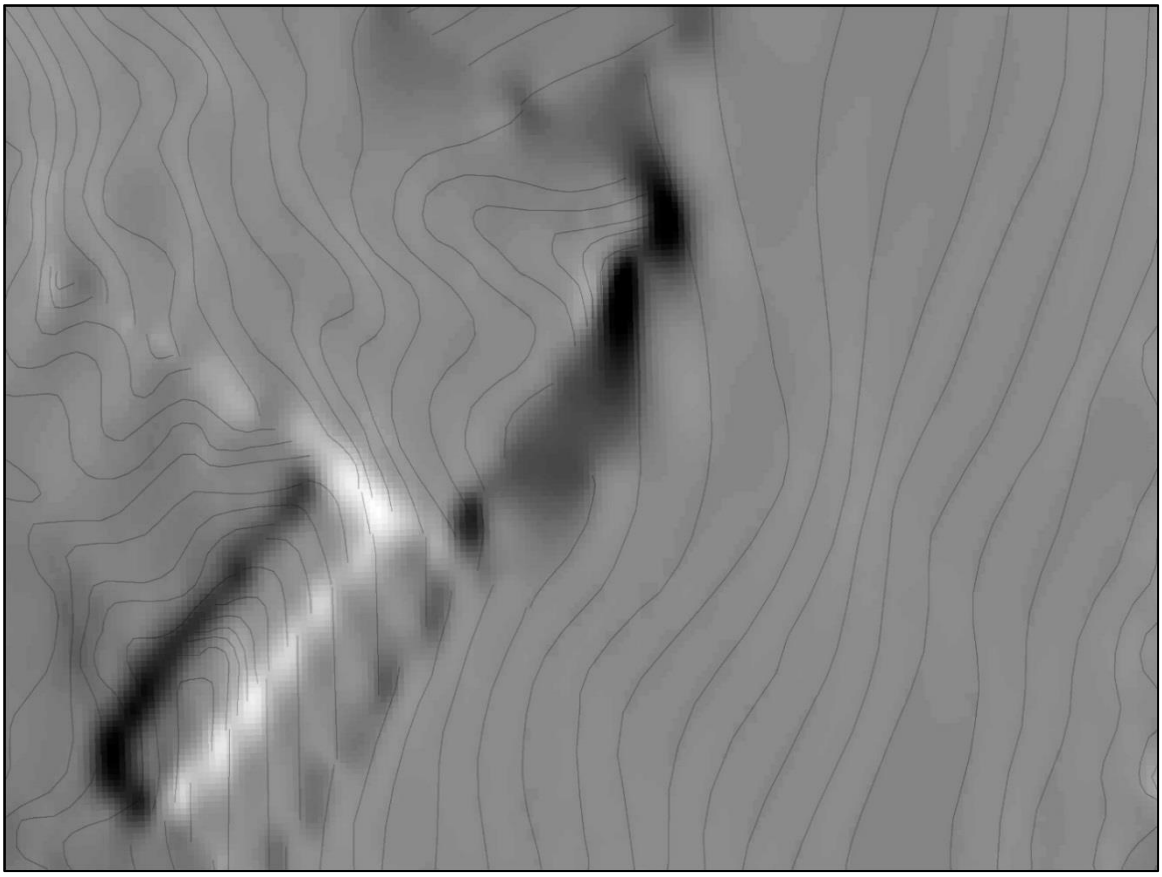

Figure 7. A hillshade of the surface derived from the digitized contours. The contours are left in place (gray lines) for reference.

Well Logs Analyses

The well tops shapefile from the Kansas Geological Survey lacked many of the points that I was able to acquire by manually sorting through a multitude of boxes filled with scout cards found at Emporia State University. The information contained in a scout card may be given spatial coordinates in a GIS dataset by converting the U.S. Public Land Survey description (Township, Range, Section, and part of section) into a set of geographic point coordinates. The method used in this example consisted of manually

placing a point in a shapefile where the card specified that the well had been drilled within the township, range and section specified. When the location for the well had been established, the data on the card could be manually entered into the data table associated with that point. Well tops were particularly important. When many points are displayed simultaneously with the datum depth to the same formation, structural features become apparent. The structural contour maps from Berendsen and Blair (1986) were derived from similar well log data. The added points from the ESU collection of scout cards provided extra detail in some areas and served as a check on the accuracy of the data from Berendsen and Blair (1986). The well log points were also overlain on depictions of surface topography e.g. shaded relief maps, (Figure 9) to investigate relationships between subsurface and surface features.

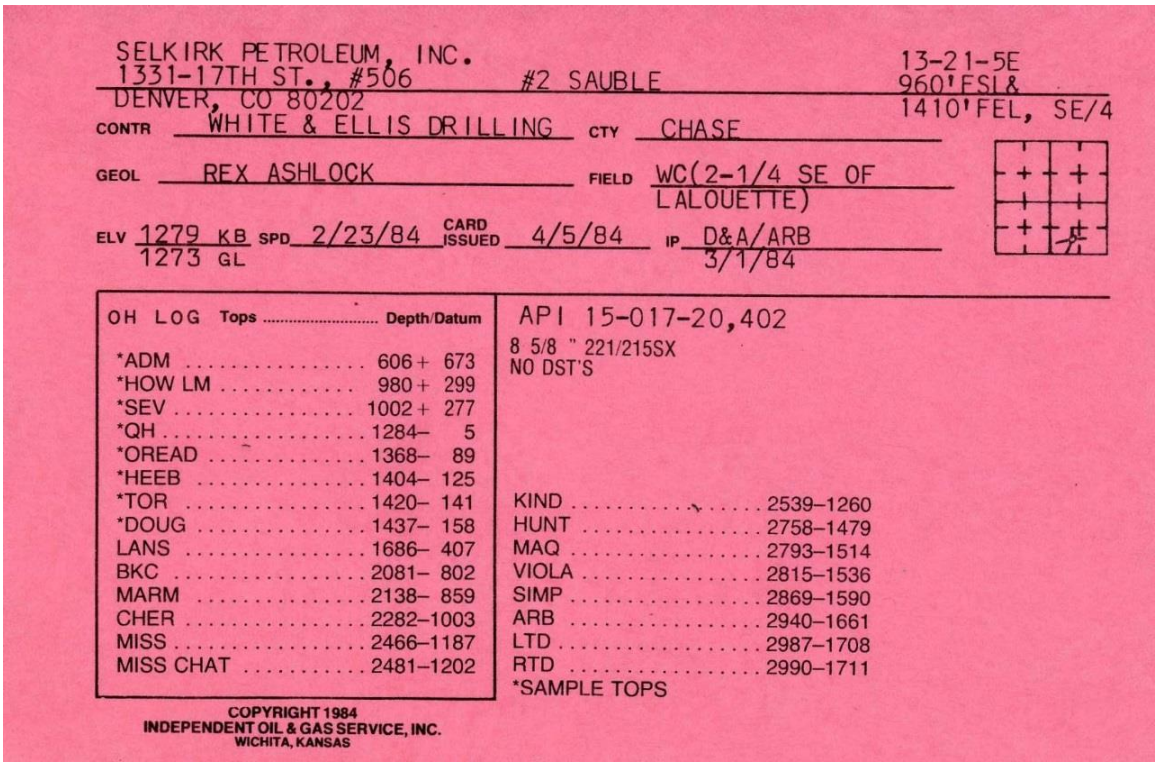

SELKIRK PETROLEUM, INC.
1331-17TH ST., #506
DENVER, CO 80202

#2 SAUBLE

13-21-5E
960'FSL &
1410'FEL, SE/4

CONTR WHITE & ELLIS DRILLING CTY CHASE

GEOL REX ASHLOCK FIELD WC(2-1/4 SE OF LALOUETTE)

ELV 1279 KB SPD 2/23/84 CARD ISSUED 4/5/84 IP D&A/ARB 3/1/84
1273 GL

OH LOG Tops ..... Depth/Datum

*ADM	606+	673
*HOW LM	980+	299
*SEV	1002+	277
*QH	1284–	5
*OREAD	1368–	89
*HEEB	1404–	125
*TOR	1420–	141
*DOUG	1437–	158
LANS	1686–	407
BKC	2081–	802
MARM	2138–	859
CHER	2282–	1003
MISS	2466–	1187
MISS CHAT	2481–	1202

API 15-017-20,402
8 5/8 " 221/215SX
NO DST'S

KIND	2539–1260
HUNT	2758–1479
MAQ	2793–1514
VIOLA	2815–1536
SIMP	2869–1590
ARB	2940–1661
LTD	2987–1708
RTD	2990–1711

*SAMPLE TOPS

Figure 8. A scout card from the collection at ESU. The location that the card corresponds to is printed in the top right corner. Section 13, Township 21, Row 5 East, Southeast quarter of the section 1410 feet from the East line, 960 feet from the South line. The location of the well in this section is marked in the small diagram.

The point was placed in a geospatial dataset by navigating to these coordinates and manually placing a point feature. The reason for doing this task was to see that the values made sense with what had previously been mapped, and to locate geologic features (Figure 9).

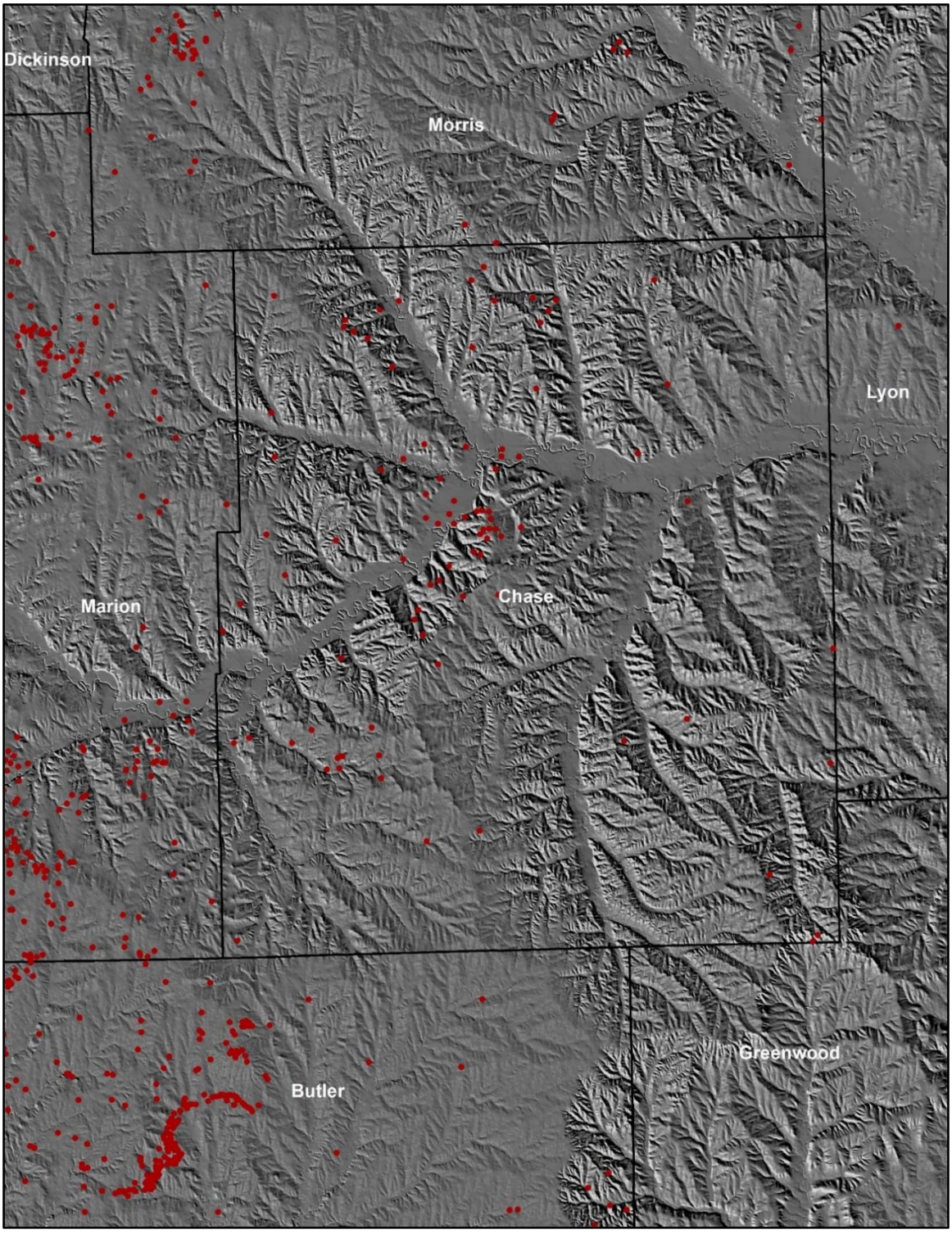

Figure 9. Wells used to confirm accuracy of Berendsen and Blairs (1986) structural contours.

Mapping Faults

As mentioned earlier, the geology of the Flint Hills, with the exception of the alluvial valleys, consists of layer cake geology, mainly nearly horizontal alternating layers of limestone and shale. Resistant beds of limestone form benches that are vertically interspaced with less competent layers of shale and mudstone in repeating sequences. These repeating sequences represent cyclothems that document successive transgressive and regressive stages of sea level during the Permian (West et al., 2010). When viewed from above, the limestone layers are clearly visible in 'so called' *stone lines*. If undisturbed by folding or faulting these stone lines are traceable for considerable distances in aerial photographs (Figure 10). Places where the observed stone lines are broken and offset horizontally represent locations where faulting has occurred. In these circumstances, faults are easily spotted from above as an offset in linear stone lines (Figure 11). These features may also be confirmed by field observation (Figure 12).

The full spectrum of available imagery was used in mapping these faults. Next Generation 911 (NG911) imagery was collected during the Fall of 2013 and Winter of 2014 at 0.3 meter resolution. This is useful because there are no leaves on the trees and because, in some cases, pastures have been burned leaving no vegetative cover and a black background that facilitates the tracing of white stone lines. The basemap imagery in ArcMAP is generally a seamless, leaf on high-resolution imagery at 0.3 meter resolution. In addition to the imagery described above that could be displayed in ArcMAP it was extremely helpful to scroll between different historical high-resolution imagery in Google EARTH. One section of a fault scarp may be visible in summer drought imagery, and another may be visible in early spring imagery.

Figure 10. Stone lines of the Council Grove Group as seen from leaf off high-resolution (DASC, 2014).

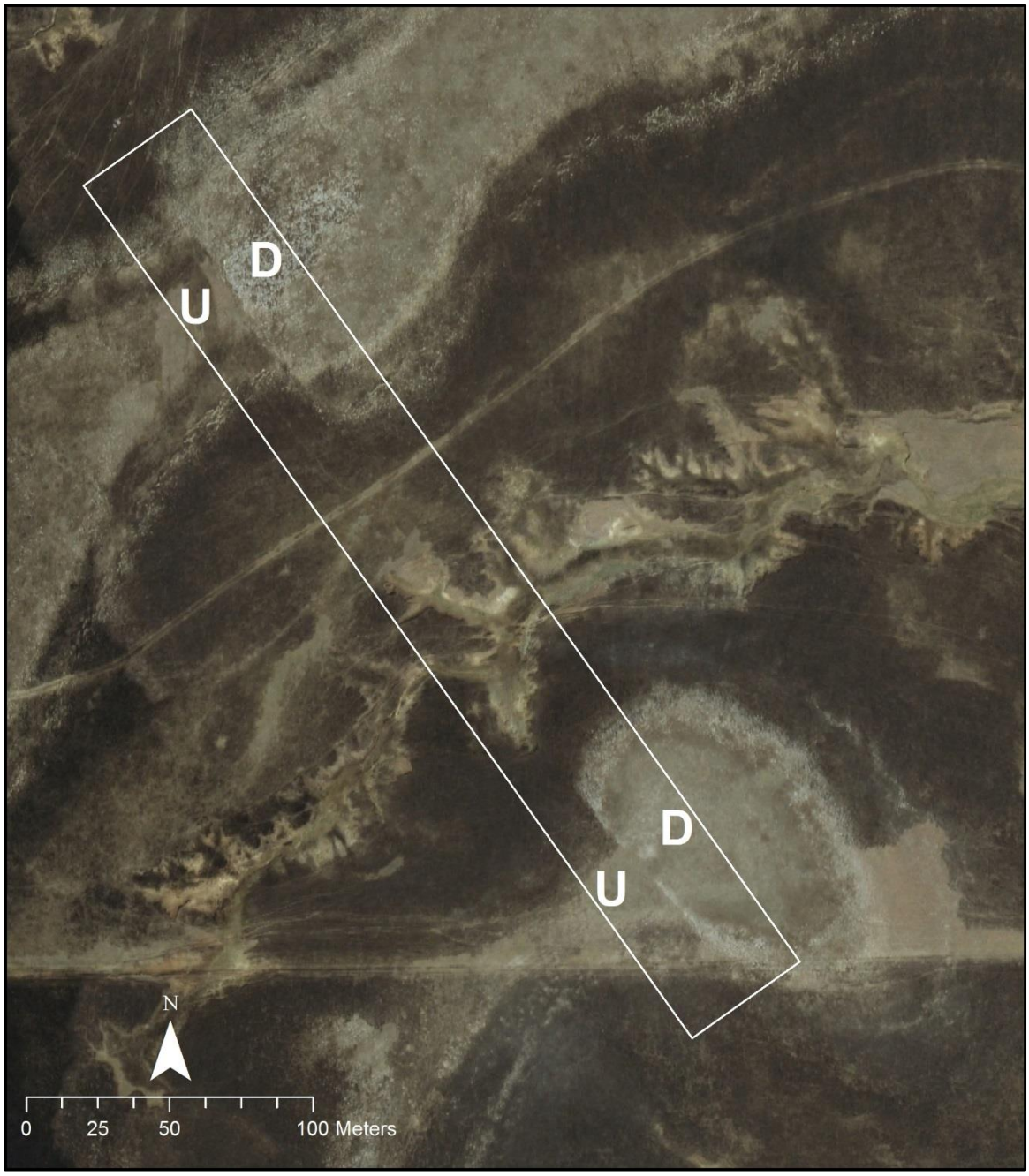

Figure 11. Offset in stone lines caused by vertical displacement along a fault scarp (DASC, 2014).

Figure 12. Looking ~SE down a fault scarp in the Neva Limestone Member. Photo location UTM zone 14N – E 707914, N 4249215.

Hillshade Analysis

Modern GIS software allows for the rapid generation of hillshades with the sun at any azimuth and orientation. Hillshades provide another analytical view of topography that might be used to look for anomalies caused by structural movements. Given the horizontal resolution of LiDAR available from Kansas Data Access and Support Center (1 meter), this is a vast improvement in what was previously available from ASTER backscan imagery (15 meters) and the National Elevation Dataset (~28 meters at this

latitude) in terms of surface elevation modeling for topographic analyses. The vertical resolution of the LiDAR used in this analysis has a root mean square error (RMSE) of 12.5 cm (DASC, 2011). This improvement in resolution permits a more detailed geomorphic analysis at a higher resolution than was previously possible (Figure 13) in search of structural anomalies expressed as topographic anomalies in hillshades. LiDAR hillshades are used throughout the text to show examples of geomorphic features and as basemaps. These data were acquired from the Kansas Data Access and Support Center (DASC) in 5000 x 5000 meter tiles and mosaicked together for the area of interest. This mosaic was then hillshaded. The hillshades in the text are shaded with an azimuth orientation of 315 degrees. In other words, the simulated sun is shining on the surface from the top left of the image (DASC, 2010-2105).

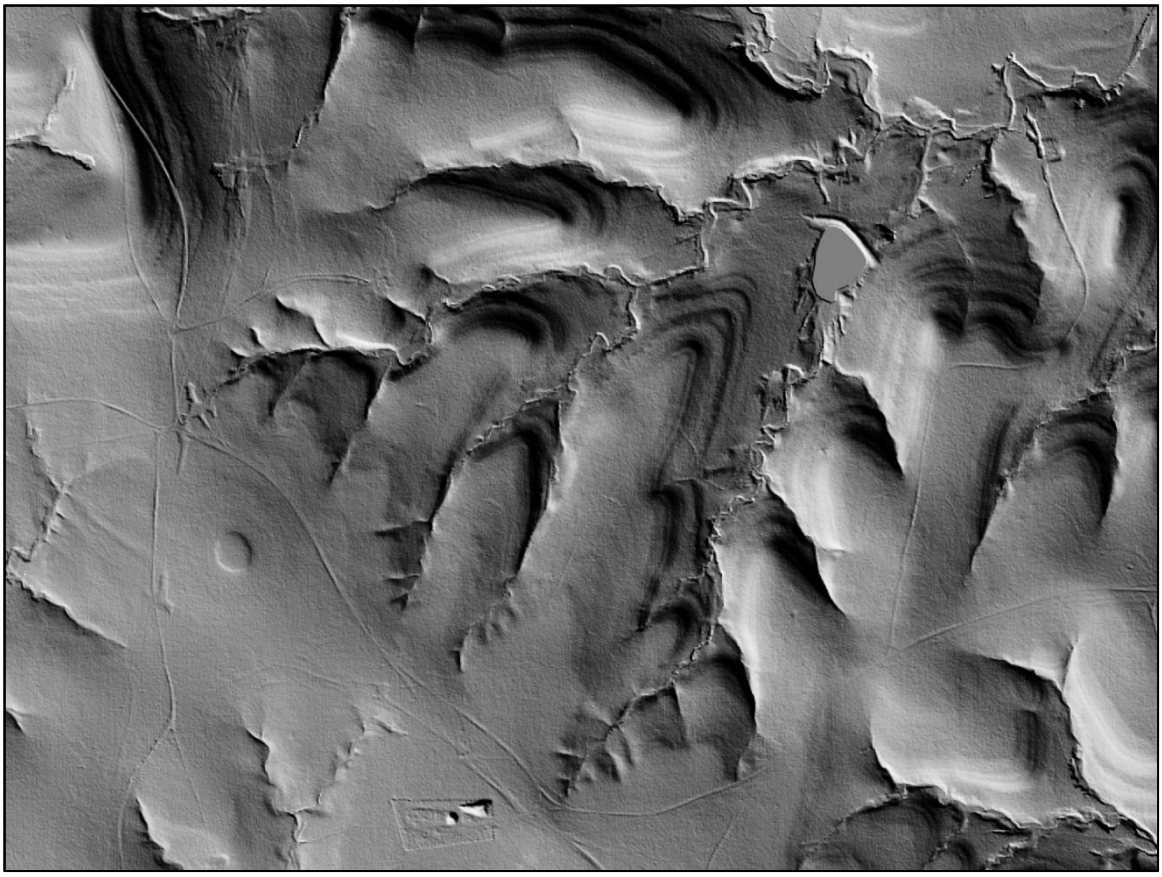

Figure 13. A one meter resolution hillshade of cliff and bench topography in the Flint Hills of Chase County. Individual stone lines are clearly visible.

Strike-and-Dip

One of the most basic field measurements performed by geologists to characterize geologic structure is the measurement of the dip magnitude and dip direction of inclined strata. Strike-and-dip measurements are the time-tested method for characterizing the orientation of planar strata in different three-dimensional orientations associated with folding and faulting. Most commonly strike-and-dip measurements are accomplished using a special compass called a pocket transit (e.g. Brunton Com Pro). The dip direction

and magnitude may also be measured using a simple surveyor's transit. To calculate the dip direction and magnitude of what is assumed to be a planar geologic feature with a transit, one must establish the relative elevation of three-points on that planar feature (Aber, 1988). These three-points should be placed in a configuration as close to an equilateral triangle as possible. This minimizes errors in the resulting dip direction and magnitude by placing each individual point as far away from the next as possible. If this could be accomplished accurately with existing high-resolution imagery and elevation datasets (e.g. DASC, 2010-2015, 2014) and GIS software (ArcGIS), then strike-and-dip of geologic strata could be measured in an automated way without the need of field work or permission from a land owner. One component of this research is to compare strike-and-dip acquired using a manual survey to a remote survey while using the same locations for both methods. In Figure 14, three points (yellow dots) located on visible stone lines have been placed in a triangular orientation as close to equilateral as possible.

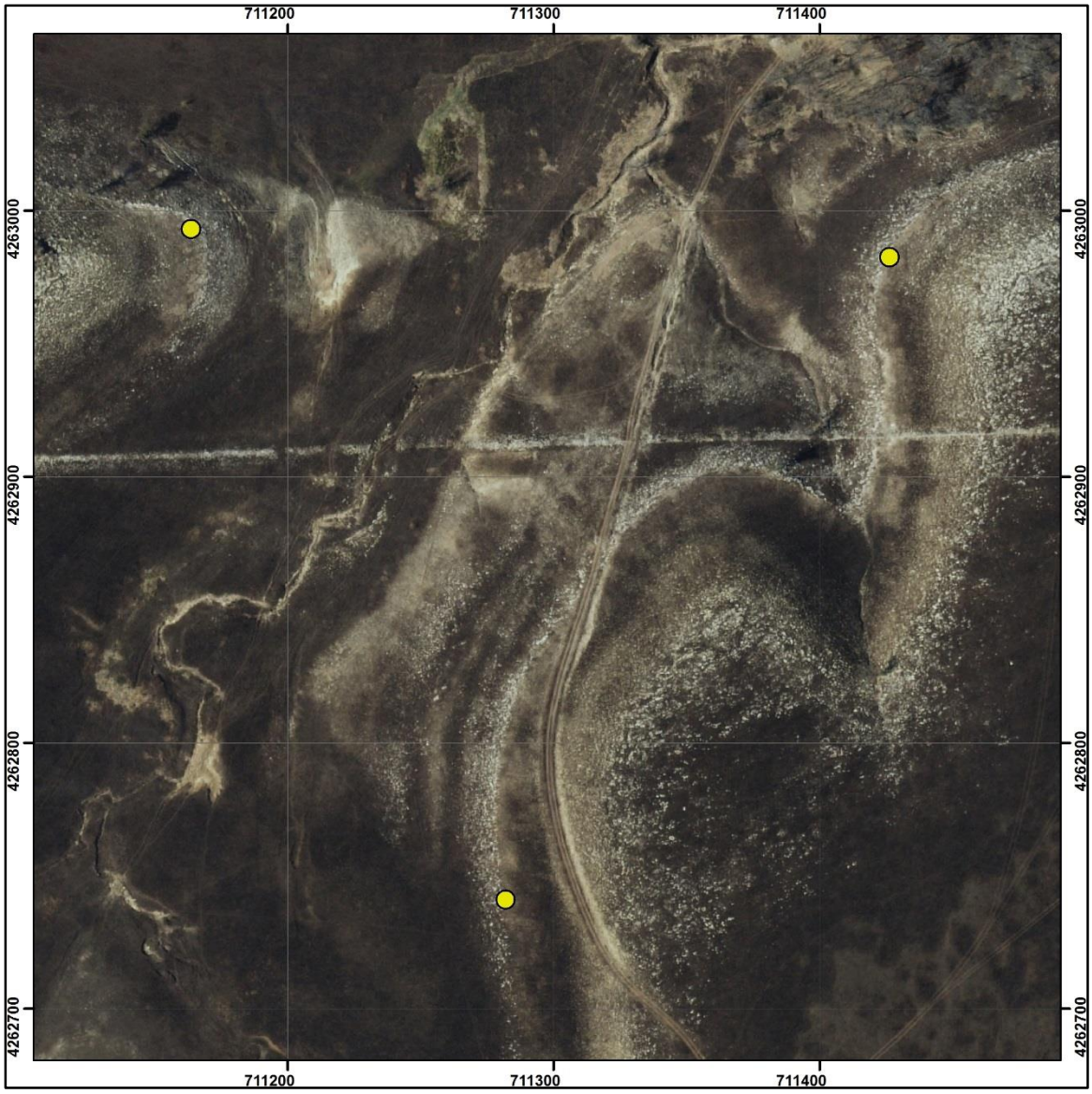

Figure 14. Three points placed on top of the Funston Limestone Member (DASC, 2014).

If it is possible to obtain accurate elevations from LiDAR, then it should be possible to derive the dip angle from the orientation of the strike. A horizontal line on the plane, strike, must be established first to derive dip. The strike line passes from the point of intermediate value through a line connecting the high point and the low point. This

point of intersection on the line connecting high and low points is calculated using this formula.

$$\frac{\boldsymbol{Elevation}\left(\boldsymbol{Intermediate\ Point}\right)-\boldsymbol{Elevation}\left(\boldsymbol{High\ Point}\right)}{\boldsymbol{Elevation}\left(\boldsymbol{Low\ Point}\right)-\boldsymbol{Elevation}\left(\boldsymbol{High\ Point}\right)}$$

$$=\frac{\boldsymbol{Distance}\left(\boldsymbol{High\ Point\ to\ Strike\ Intercept}\right)}{\boldsymbol{Distance}\left(\boldsymbol{High\ Point\ to\ Low\ Point}\right)}$$

Formula 1. The formula used to locate the strike-intercept point on the line connecting the highest and lowest points (Aber, 1988).

Dip is always perpendicular to the strike line, and in this example passes through the high point. The difference in elevation along that dip line, in combination with the length of the line segment, is used to calculate dip magnitude using this formula.

$$\frac{\boldsymbol{Elevation}\left(\boldsymbol{Strike\ Line}\right)-\boldsymbol{Elevation}\left(\boldsymbol{High\ Point}\right)}{\boldsymbol{Map\ Distance}\left(\boldsymbol{Strike\ Line\ to\ High\ Point}\right)}=\boldsymbol{tan}\left(\boldsymbol{Dip\ Angle}\right)$$

Formula 2. The formula used to derive dip magnitude given the difference in elevation of two points and the map distance between those two points (Aber, 1988).

A vector is not a vector without direction. The magnitude of dip must have a directional component. Here it is expressed as azimuth orientation in degrees from north.

To test the viability of measuring strike-and-dip remotely, the same three points used in the GIS analysis must be used to measure strike-and-dip with a transit. The results of these two methods of measurement were be compared statistically. To test the accuracy of the proposed GIS method, 30 separate three-point diagrams were completed remotely using GIS software, and at each site the elevation differences for the points were measured in the field with a surveyor's transit. Locations for the GIS and field measurements are shown in Figure 15. Figure 16 focuses on one location where the measurements were made utilizing an exposed stone line of the Funston Limestone Member.

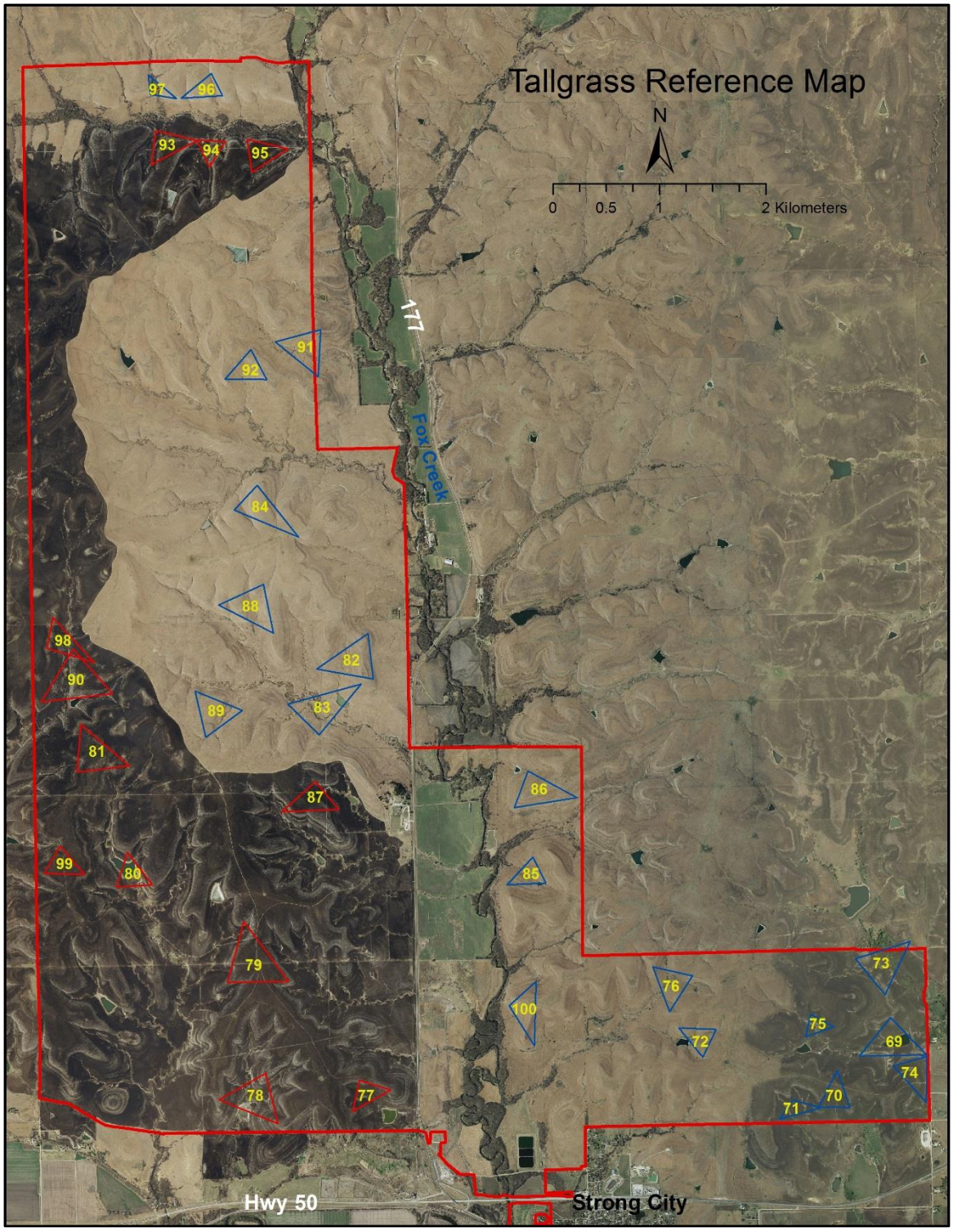

Figure 15. The field reference map that contains the location of all 30 three-point diagrams on the Tallgrass Prairie National Preserve (DASC, 2014).

The UTM coordinates of the points were marked on a reference map as well as the name of the limestone member. This was used for navigation in the field to each individual point (Figure 16).

Figure 16. A field reference map listing the UTM coordinates of each point as well as the limestone member that the points were placed on (DASC, 2014).

Remote Method

An automated method for calculating strike-and-dip using remote data was developed using ArcGIS software, its ModelBuilder module and several short Python programs. For each three-point diagram, three points were chosen on a prominent stone line. Point placement was selected based on several criteria:

1) The points need to be placed in a configuration as close to an equilateral triangle as possible. This minimizes any possible error coming from a faulty reading. The LiDAR supplied by Data Access and Support Center (DASC) at the Kansas Geological Survey has a reported 12.5 cm root mean square error (RMSE) for elevation which should be sufficiently accurate for this purpose.
2) The points were placed at least 200 m apart so as to minimize any resulting error in the dip direction or magnitude because of the acceptable RMSE. The purpose of this method is to identify relatively subtle features, hence the points were spaced at an appropriate distance to capture measurements at the appropriate scale.
3) Prominent stone lines were chosen to minimize any spatial error when visually placing a point on aerial imagery.
4) The points were placed on top of the limestone member where it was still obviously in place, not on float, talus, or scree derived from the limestone weathering out of the slope. Suitable locations are easily discerned in high-resolution imagery.

The three points now chosen and placed into a shapefile, were used as the input in a ModelBuilder model that includes Python scripts. This model, created using

ModelBuilder in ArcMAP, calculated the strike-and-dip of each three-point diagram in a number of steps. The first model nested within the whole extracts the LiDAR raster elevation value at each point, then it adds the X and Y Universal Transverse Mercator coordinates of each point. Next, it sorts them low to high based on elevation (Figure 17).

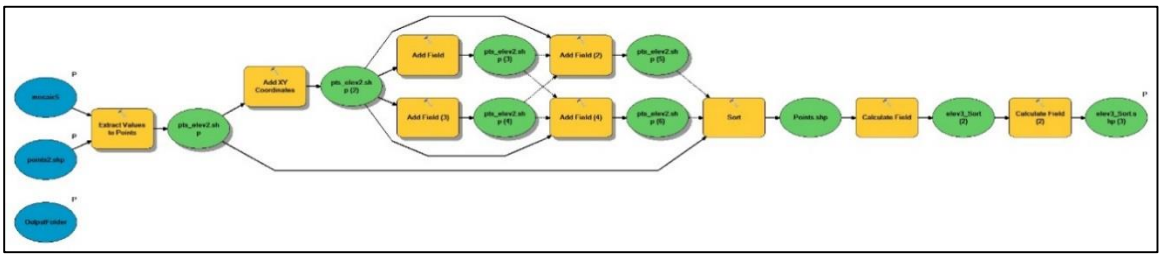

Figure 17. The first model in the series. Produced using ModelBuilder in ArcGIS.

The next model in the series splits each individual point into its own shapefile based on elevation with point one always being the lowest of the three and point three always being the highest (Figure 18).

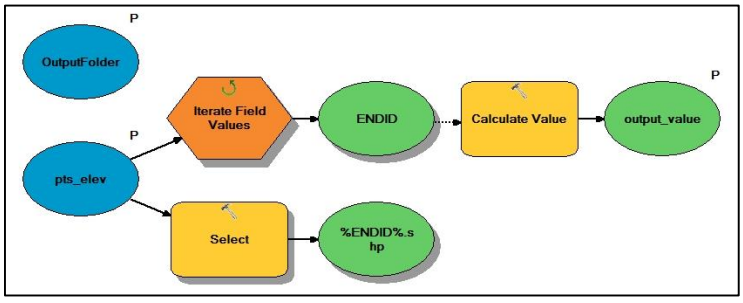

Figure 18. The second model in the series. Produced using ModelBuilder in ArcGIS.

The third model in the series adds the coordinates of the next point in rotation to the data table of each point based on elevation order. Point 1, being the lowest, adds the coordinates of point 3, point 3 adds the coordinates of point 2, and point 2 adds the coordinates of point 1 (Figure 19).

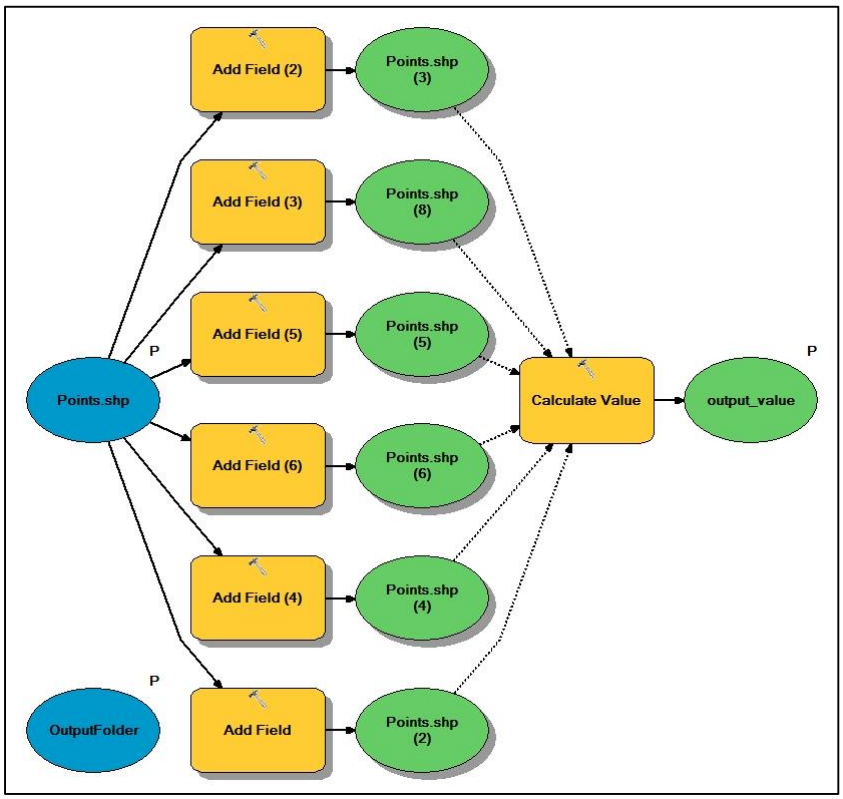

Figure 19. The third model in the series. Produced using ModelBuilder in ArcGIS.

The purpose of the previous step is to have the beginning and end coordinates for drawing a line between each point. The fourth model creates a line defined by the beginning and coordinates calculated in the third model (Figure 20). This creates a triangle.

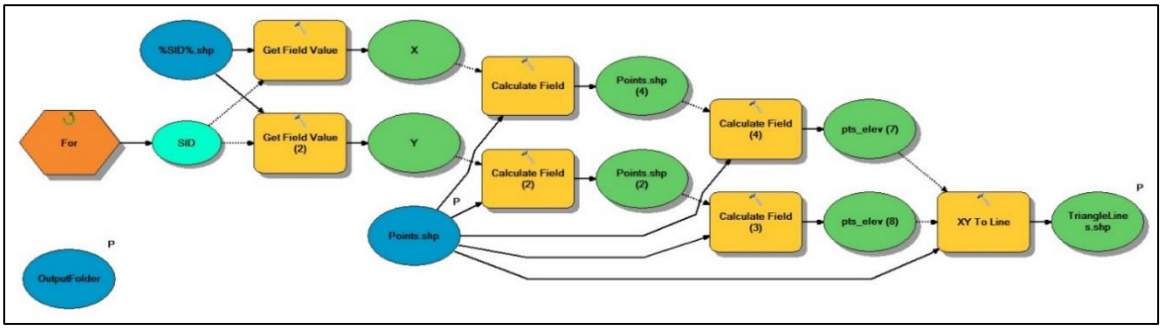

Figure 20. The fourth model in the series. Produced using ModelBuilder in ArcGIS.

The fifth model calculates the length of each line segment, adds it to the lines data table, then performs the strike-intercept formula. The distance from the high point to the strike-intercept point is used as an input on a Buffer Operation. This draws a circle at that specified radius from the high point. Where this circle intercepts the line connecting the high and low point is the strike-intercept point. An Intersect Operation is performed on the buffer and the high-low line. The coordinates of this intersection are used to draw a line from the strike-intercept point to the point of intermediate elevation. The new line is the strike line (Figure 21).

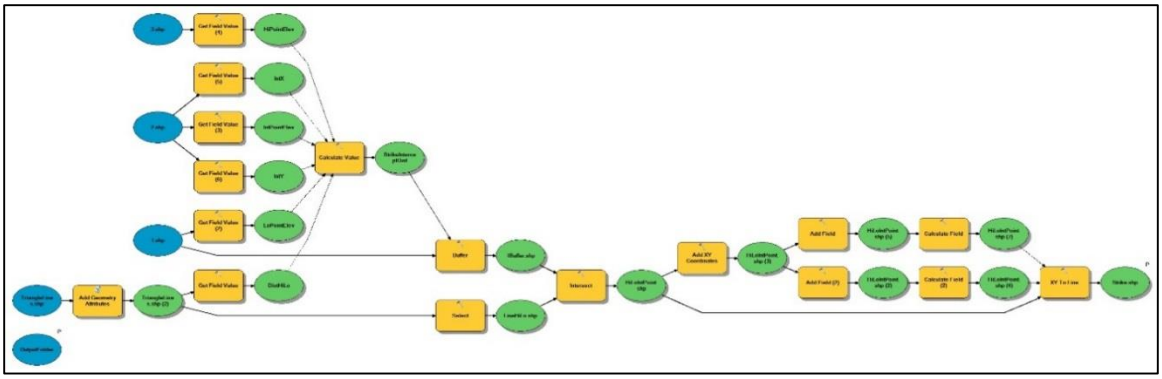

Figure 21. The fifth model in the series. Produced using ModelBuilder in ArcGIS.

The sixth model in the series of nested models performs a Near Operation from the low point to the strike line and from the high point to the strike line. The nearest place on the strike line to either the high point or the low point is a point that creates a line that is perpendicular to the strike line. The coordinates of the high point are used to draw a line from the high point to the coordinates determined by the Near analysis. This step is repeated with the low point. The length of the dip line is used in combination with the difference in elevation between the strike line and the high or low point using the formula from Formula 2 to calculate dip magnitude. The beginning and end coordinates of the new dip line are used to calculate azimuth orientation. Strike is derived by subtracting 90 from the azimuth value unless the azimuth value is less than 90. In this case, 270 is added to the azimuth value. This final step is accomplished using a Python script (Figure 22). The result follows the so-called 'right hand rule.' The right hand rule specifies that if the four fingers on your right hand are pointing down-dip, then the thumb points in the direction of strike.

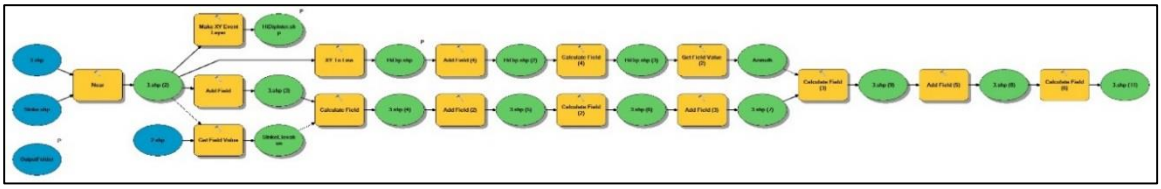

Figure 22. The sixth model in the series. Produced using ModelBuilder in ArcGIS.

Each submodel included in the string of models (Figure 23) was nested inside a larger model (Figure 24). When all six were run in sequence together, the iterators in ArcGIS that were used to make final calculations seemed to develop errors that caused the model to fail. Additionally, the clutter made it difficult to troubleshoot errors when assembling the model. The run time of the nested model is about 8 seconds. The steps accomplished in the model are shown graphically in Figure 25. The output of the nested model places dip magnitude, azimuth orientation, and strike at the end of the data table for the high and low points. Typical model output is shown in Figure 26.

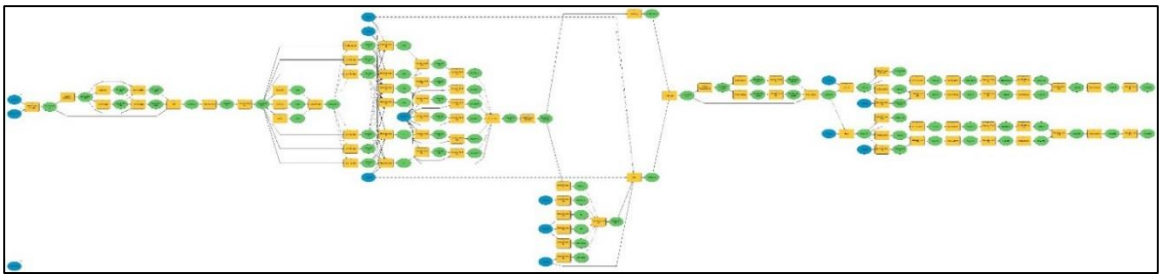

Figure 23. The ‘string model’ that includes all six model steps. Produced using ModelBuilder in ArcGIS.

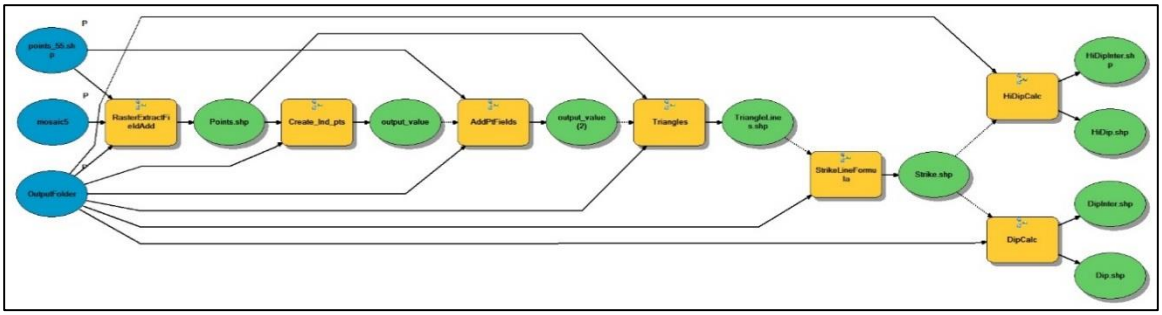

Figure 24. The 'nested model'. Produced using ModelBuilder in ArcGIS.

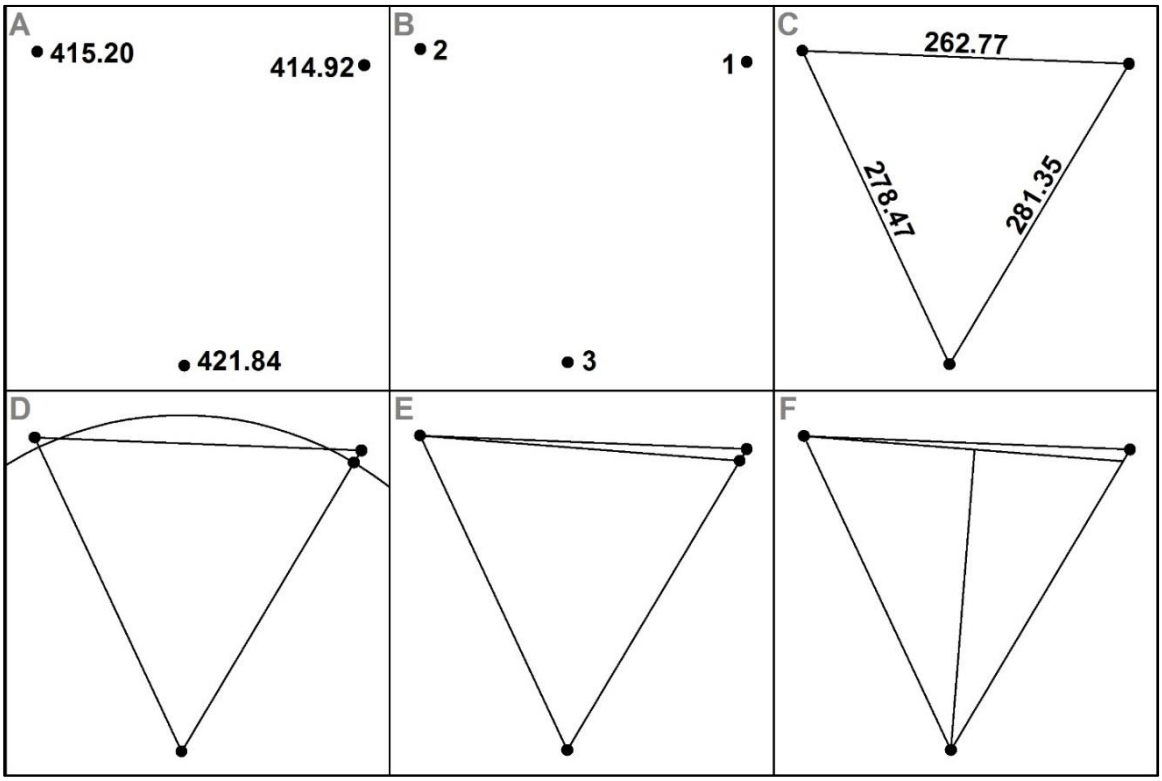

Figure 25. A graphical representation of the workflow required to calculate strike-and-dip.

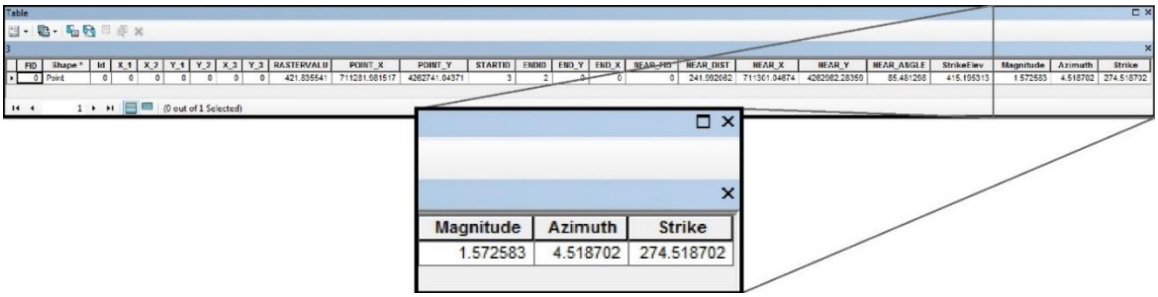

Figure 26. A typical data table for the high and low points, in this case the low point.

Field Methods

Field measurements of relative differences in elevation among each set of three points on exposed stone lines were performed using a 32 power CST/Berger optical transit (Figure 27) in combination with a metric stadia rod. Heat shimmer and distance between the transit and stadia rod made the numbers difficult to read sometimes. In this case, a piece of red duct tape was placed on the stadia rod. This allowed the person sighting through the transit to read constant elevation at a longer distance. Whether to move the tape up or down was communicated through two-way radio transceivers. When the tape was at a constant elevation with the transit, the person holding the stadia rod lowered it to read the number.

A field reference map was used to locate each of the three-point diagrams in the field (Figure 16). A handheld GPS unit was used to navigate to each point. When at the UTM coordinates listed on the reference map, the stadia rod was placed on top of the limestone where it was in place. The reading from the stadia rod was recorded for each point. This is a measure of how far below the transit the rock surface is located. If the elevation to the eyepiece is 1.86 meters and the reading on the stadia rod is 2.86 meters,

then the surface that the reading was taken from is 1 meter below the surface upon which the transit was set up.

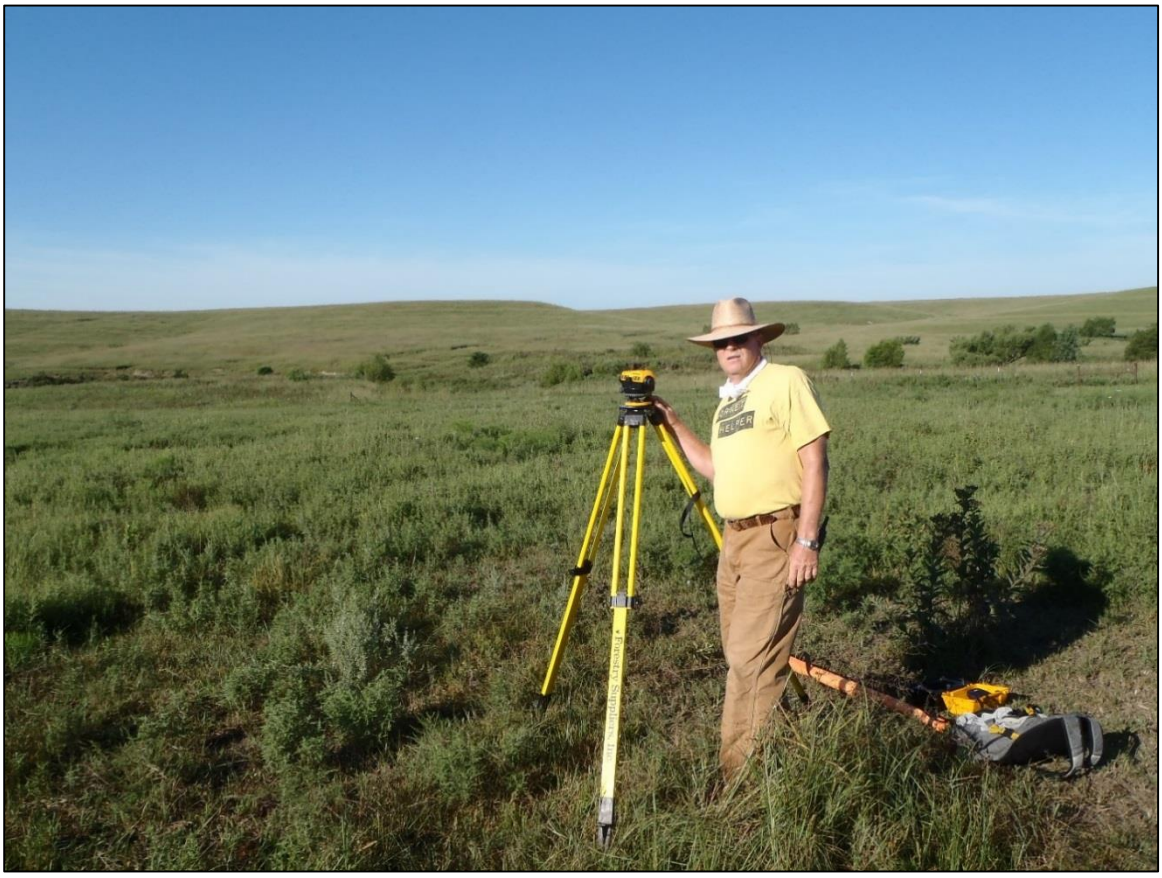

Figure 27. The optical transit used during the manual survey.

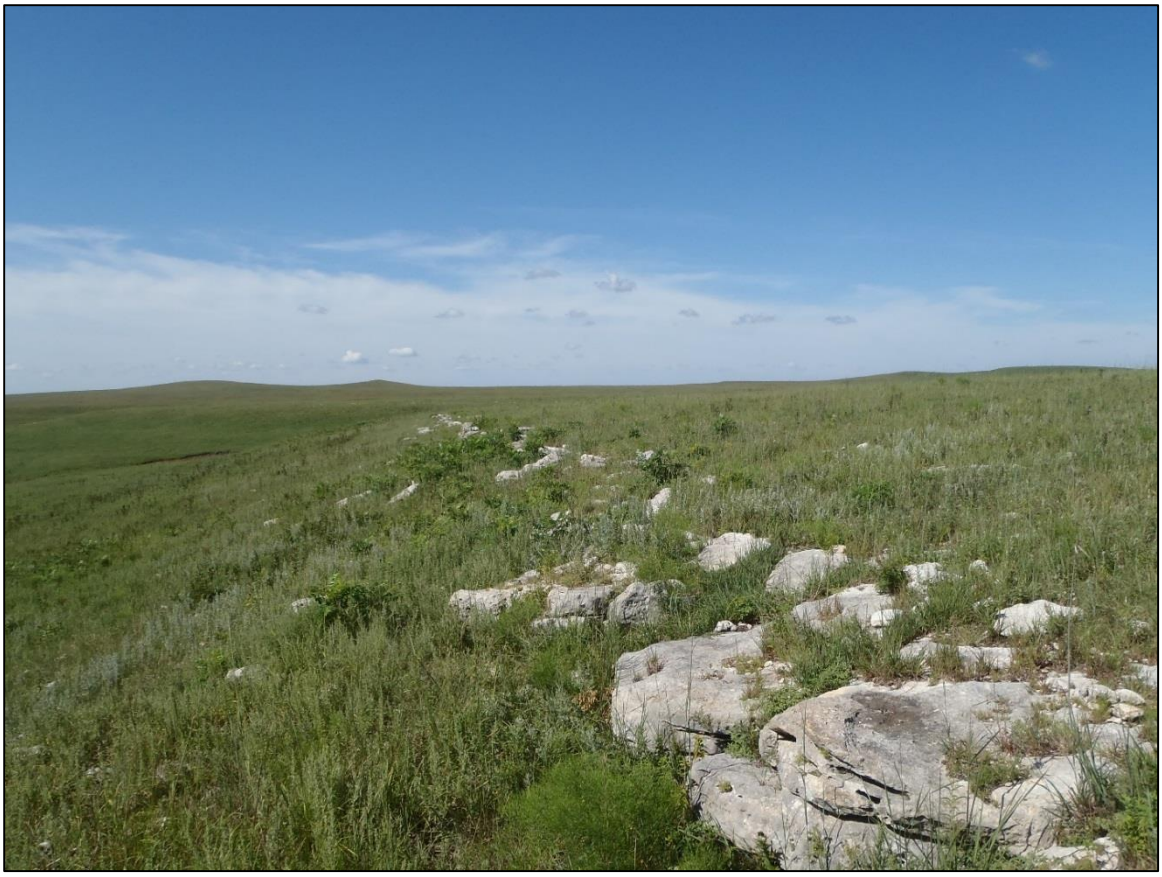

Figure 28. The ‘stone line’ or outcrop of the Threemile Limestone Member.

When calculating the strike-and-dip using the manual method, the map distance was taken from what was calculated using the GIS method because sighting distances were too great to precisely calculate distance optically. Figure 29 is a scanned paper diagram that was used to manually calculate strike-and-dip using field measurements. Note the UTM grid in the background used as a reference grid for measuring and marking angles.

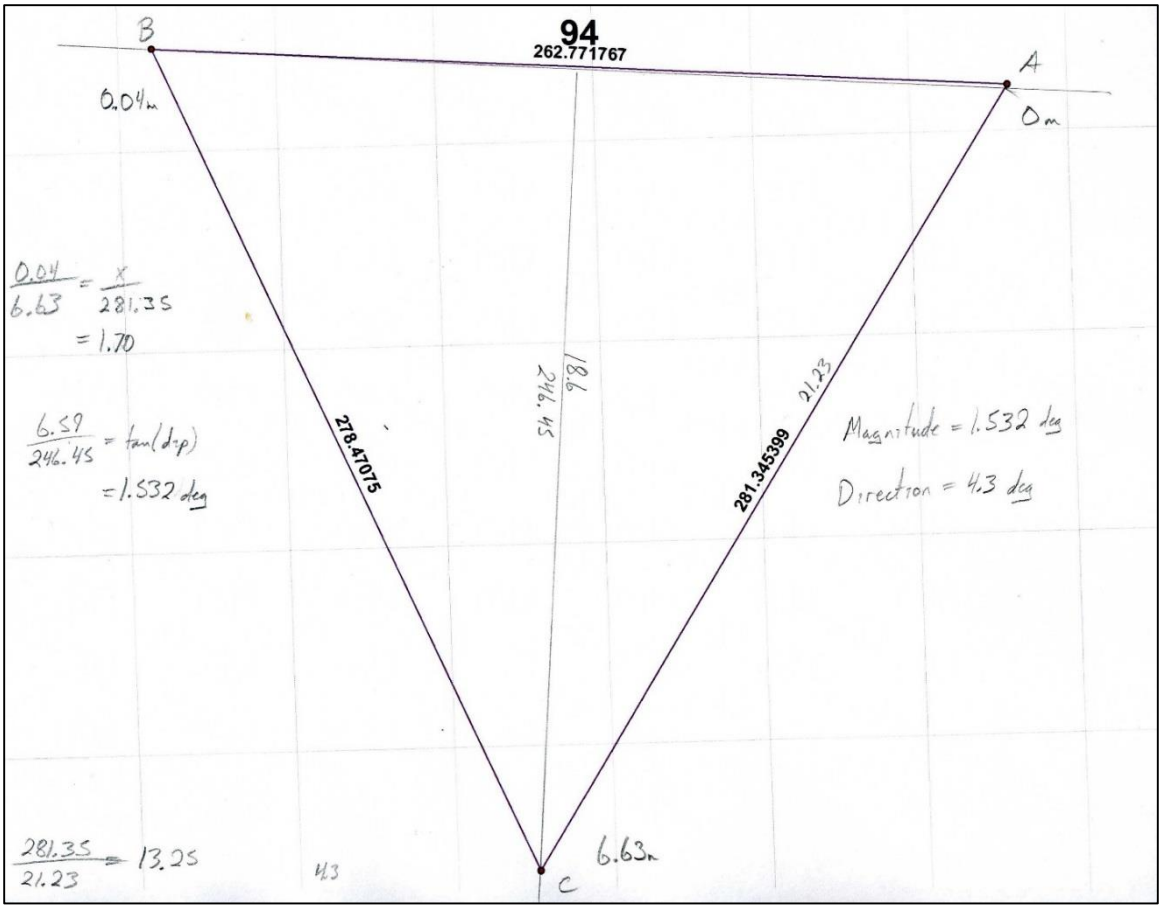

Figure 29. A diagram used in calculating strike-and-dip manually from field measurements. A UTM grid is seen in the background. The calculated magnitude and direction are seen on the right.

Chapter 3. Results

Calculating Strike-and-Dip Remotely

The magnitude of dip resulting from the manual survey was used as a baseline theoretical value in the percent error formula [%error = (#experimental - #theoretical) / #theoretical]. There were 30 individual three-point diagrams, thus there are 30 magnitude readings. The correlation between values from both methods is provided in Figure 30. One three-point, number 89, has been removed from this analysis. This three-point diagram was situated within the Bison enclosure at a location that the Bison frequented. Several attempts were made at taking readings here. The one semi-successful attempt allowed me to get the first two points without interruption. The third was hurried because of the approaching herd. This is seen in the values of the relative elevations at each point. The first two points are comparable to the values extracted from LiDAR. The third is less precise. Having been warned by the staff at the Tallgrass Prairie National Preserve concerning the sometimes aggressive nature of Bison, I did not feel comfortable allowing the herd to approach any closer.

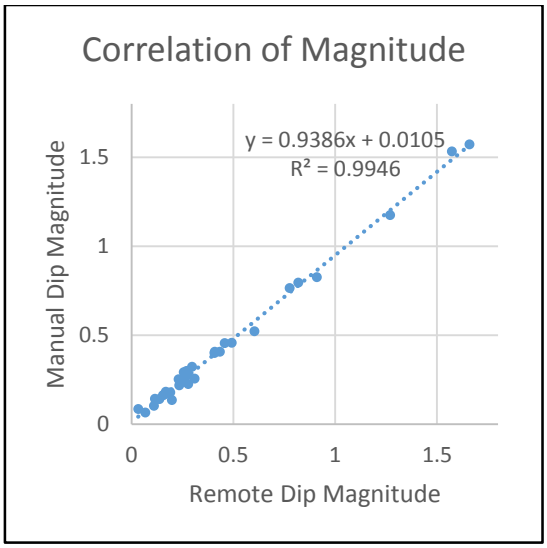

Figure 30. Correlation of remote magnitude readings and manual magnitude readings. n=29.

The same analysis was applied to all 99 individual points used in both methods (Figure 31). In this case, one point value was removed from the data (number 89) for the reason explained above. Two points were removed from diagram number 95, and one point was removed from diagram number 84. In each of these cases, the error was attributable to a difficulty in the field (operator error).

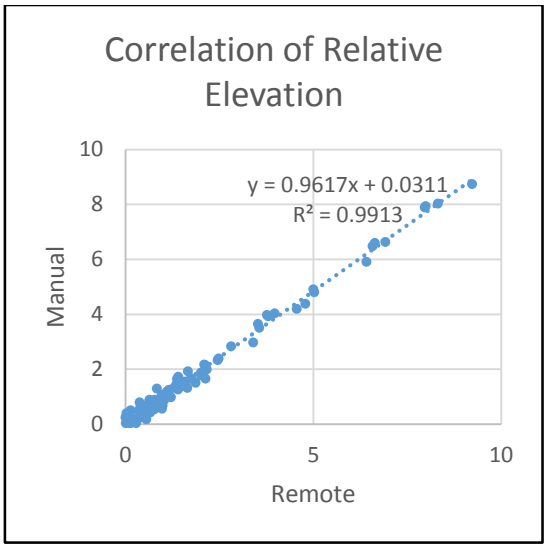

Figure 31. Correlation of relative elevation values from each method. n=95.

The R-squared value for both of these analyses indicate that the remote survey method produces similar results to those acquired using the manual method. One issue to consider is that the time required to perform all processes requisite to completing these 30, three-point diagrams used in this analysis took a couple of hours in one day. The time required to evaluate the precision of these measurements in the field at the same, difficult to access, locations was multiple weeks.

There are many variables that affect field work, some that cannot be controlled: landowner permission, animal interference, weather, operator error, accessing remote areas, vegetative conditions, and expense are some. All of these were encountered at one time or another during this survey. When conducting the same survey using the remote method, several different sources of imagery were used. Access to drought-era imagery, post-burn imagery (DASC, 2014), and leaf-on imagery (ArcGIS, 2016) helped

immensely when used in combination for the best placement configuration of each point in every three-point diagram. The same thing done in the field without an eagle eye view makes point placement less consistent in my estimation. This area is conducive to both survey methods. The reasons for this are self-evident: originally horizontal strata, distinct marker beds, minimal agricultural activity, and minimal tree cover. An outcrop, or stone line, may not be visible in aerial imagery from mid-June because of vegetative cover. The grass of the Flint Hills is burned periodically to control weeds and encroachment by trees. This is done to maximize potential grazing. The stone line is most likely to be visible in post-burn spring imagery. This analysis would not have been possible 10 years ago given the availability of LiDAR and the resolution and variety of available imagery.

The results of both the manual and remote survey methods are shown in map view below in Figure 32. Upon visual inspection, the two methods would seem to produce similar results. Diagram 89, described at the beginning of the section as one that was difficult to acquire, is marked in blue on both diagrams. Notice that this diagram exhibits the greatest difference graphically between the two survey methods.

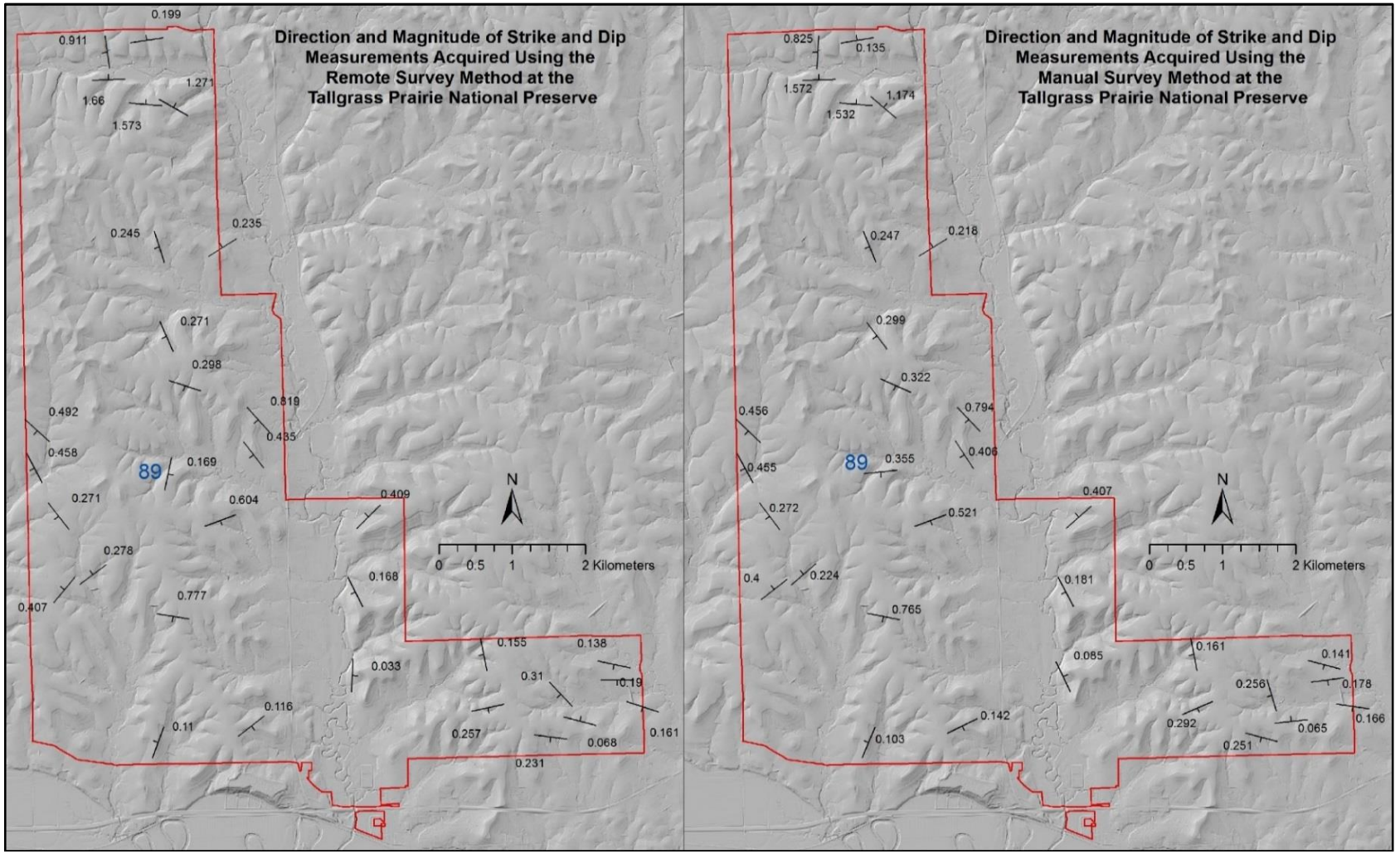

Figure 32. The results of the remote (left) and manual survey (right) methods within the confines of the Tallgrass Prairie National Preserve. Diagram 89 is marked in blue.

Mapping Faults

High-resolution aerial imagery may be used to detect small faults and study their spatial patterns. The same may be said of mapping surface rupturing faults using imagery and LiDAR as was said earlier concerning strike-and-dip. This application was not possible 10 years ago. The area is uniquely suited to this pursuit given the surficial geology, vegetative cover, and land use. The relatively recent release of a variety of high-resolution imagery and LiDAR has facilitated this pursuit. Some of the faults were obvious in the field such as ones that present a profile in a hillside (Figure 33 below). After the eye is trained to locate these features in imagery, it is relatively easy to do so. By comparison, many of these features are difficult to spot in the field unless the exact location and alignment is known (Figures 12, 34, 35).

Figure 33. Looking north, there is a visible offset in the Cottonwood Limestone Member (roughly 2 meters). The west side (left) is up in this instance. This configuration is variable in mapped faults for the fault trend that extends from Elmdale westward. It is likely that many more faults in this trend are concealed by terrace and alluvial deposits. Photo location: UTM zone 14N – E 704902, N 4253975.

The majority of the surface rupturing faults that were mapped had less than 1 meter of offset. Some were nearly invisible to the naked eye unless their existence was known beforehand from imagery. Figure 34 shows a small fault on Elmdale Hill. In all cases where the joint pattern is visible in the space between the hanging wall and foot wall, it displays a dominant orientation parallel with the individual fault. Figure 35

shows a small fault as it passes through road Yy in Chase County, one mile west of the Lyon County border.

Figure 34. Looking approximately northwest down a fault scarp in the Cottonwood Limestone Member on Elmdale Hill (UTM zone 14N – E 707878, N 4249343). Notice the alignment of limestone blocks between the hanging wall and foot wall. This linear configuration of joint patterns parallel to the overall fault trend between the hanging wall and foot wall is ubiquitous in the faults surveyed in the study area.

These faults do not seem to occur as isolated structures. Where they are visible they seem to cluster together in swarms indicating that the rocks were stressed and fractured over larger areas than each individual fault would indicate. In the digitizing process it became obvious that when one fault was found, a comprehensive search of the surrounding area would generally yield additional faults. One of the research questions to be addressed in this project involved an analysis of the spatial pattern of occurrence for swarms of faults visible in high-resolution aerial photography and analyzed via geographic information systems software.

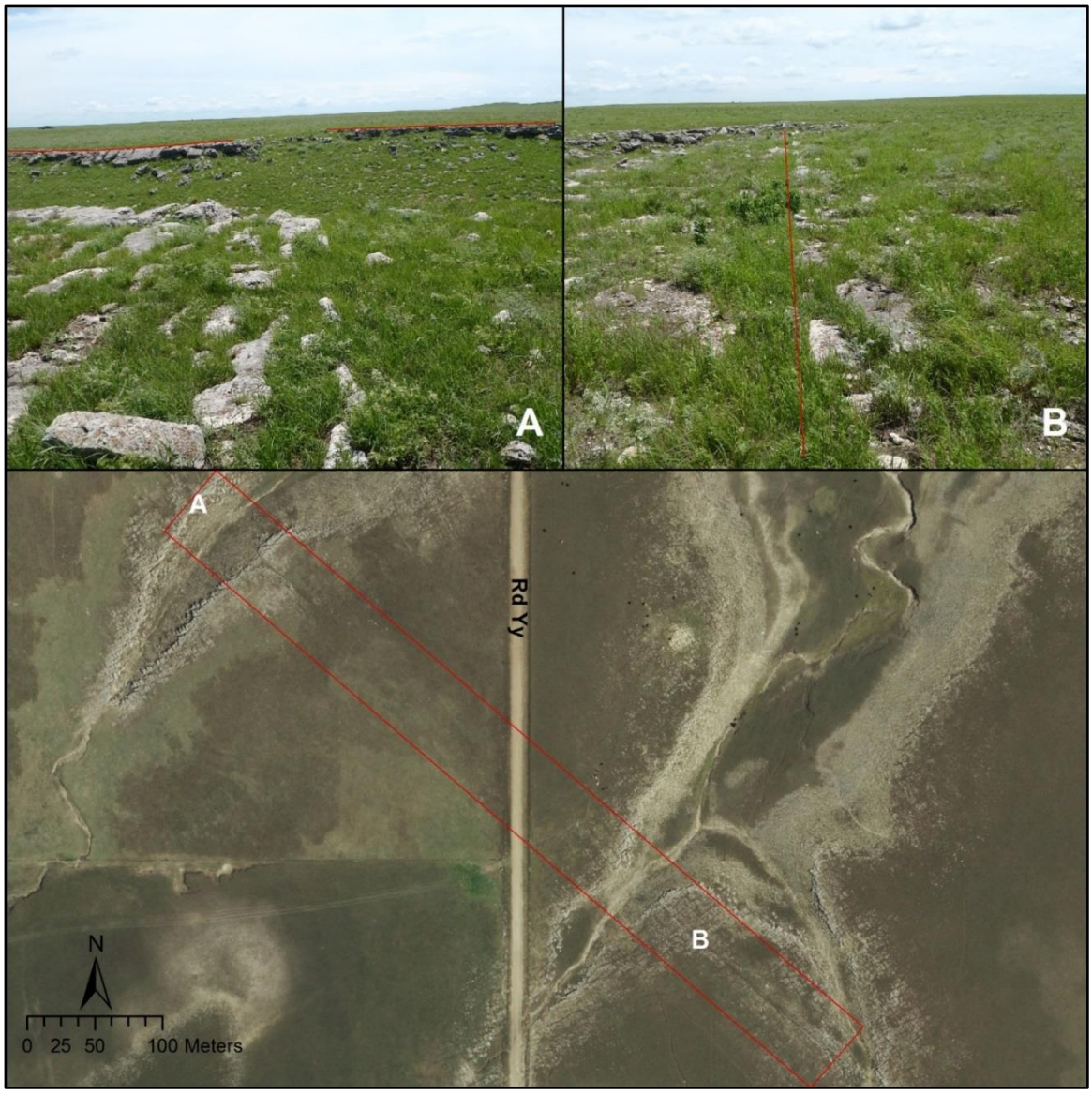

Figure 35. A fault with ~0.3 meters of offset in the Neva Limestone Member. Photo A and B were taken looking SE down the fault scarp. The purpose of this figure is to show that relatively minor offset is clearly visible in modern imagery (DASC, 2014).

The fault shown in Figure 35 is part of a trend of Riedel shears that extends to the west 6 kilometers. A schematic diagram of the formation of Riedel shears is shown in

Figure 36. Strata on the northern side of the trend follow the regional dip. Strata on the southern side of the trend dip to the south-southwest in a narrow band that marks a hinge point before they return to the regional dip further south. The surface trend of Riedel shears, also known as shear gashes, En-echelon faults, and tension gashes, is inferred to demarcate the northern side of a basement boundary. This area is shown in detail in Figure 37.

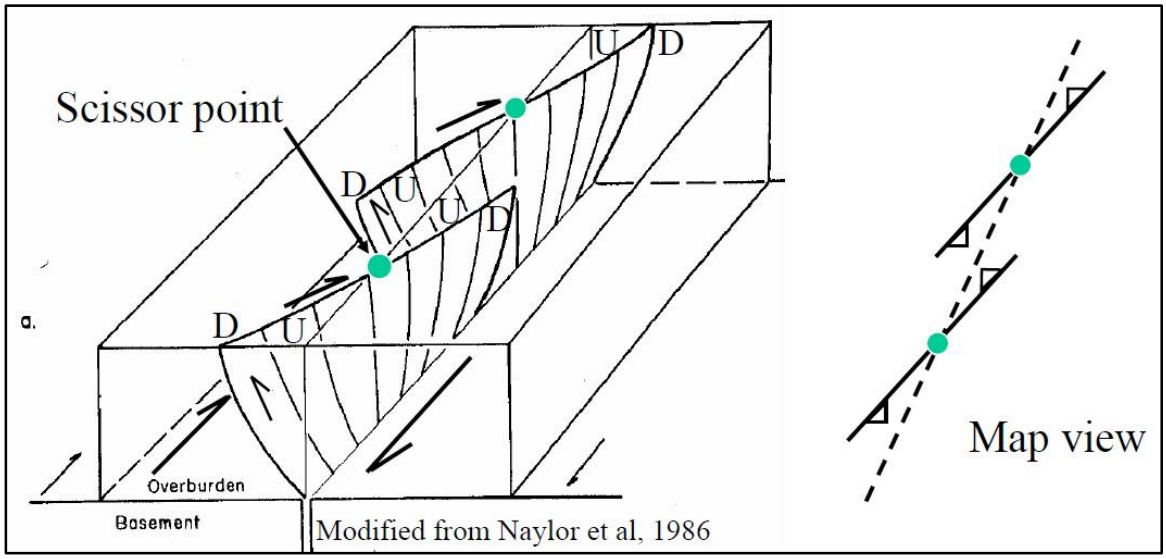

Figure 36. Schematic diagram of Riedel shears (Smith, 2005).

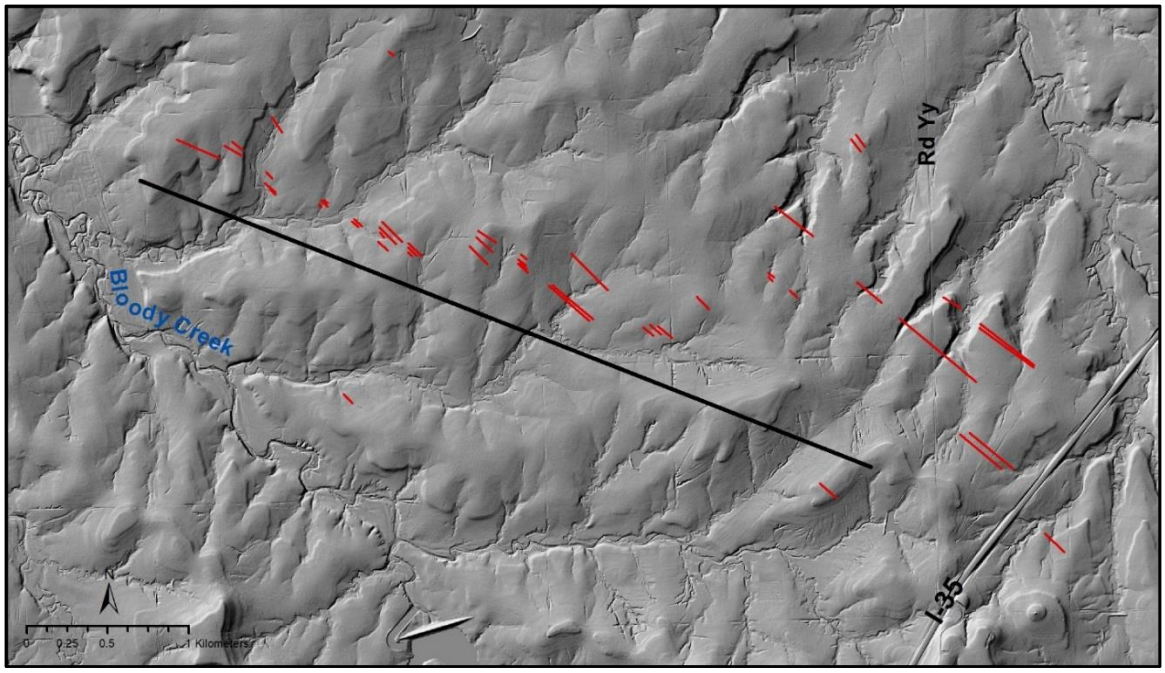

Figure 37. A trend of Riedel shears in eastern Chase County with minimal offset. The black line marks the approximate trend of the strata dipping toward the SSW.

Movement along this basement boundary was likely oblique given the trend of Riedel shears accompanied by a parallel trend of dipping strata. This pattern comprising a trend of Riedel shears paralleled by a trend of dipping strata is found in several other locations along the Nemaha Anticline in this area. In each case it exerts some structural control on the drainage. In each case, minor tributaries parallel the Riedel shears while the larger stream or creek that these minor tributaries feed parallels the overall trend of the Riedel shears. Middle Creek is paralleled by a much larger trend of Riedel shears that extend for more than 25 kilometers (Figure 38 below). An oblique view of this area is seen from a perspective over Neva in Figure 39. Strata are clearly visible dipping from

the left of the image to the right into the alluvial valley. This, also, must be the surface expression of movement along a previously unmapped basement fault.

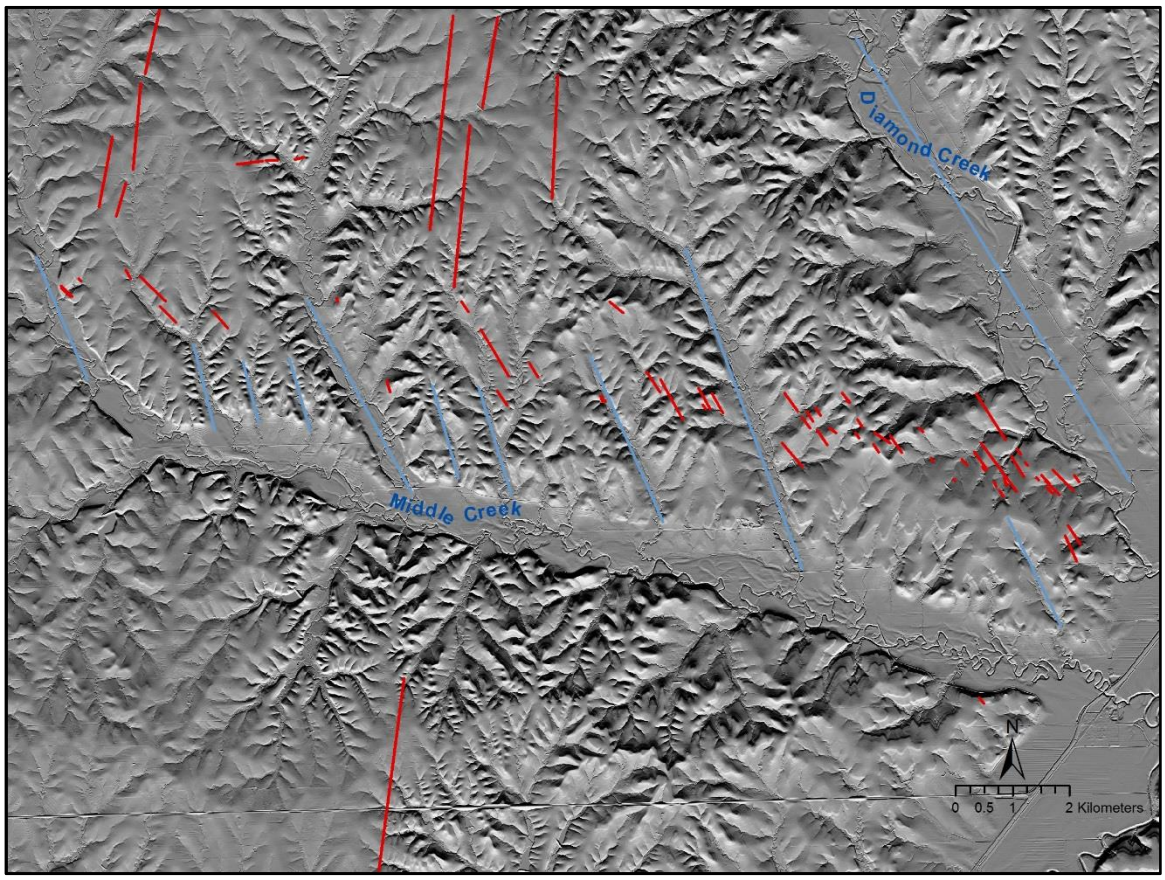

Figure 38. Mapped surface rupturing faults in (red), and drainage alignment (blue) north of Middle Creek and west of Elmdale. Linear features aligned N-S are seen cutting across this trend of Riedel shears.

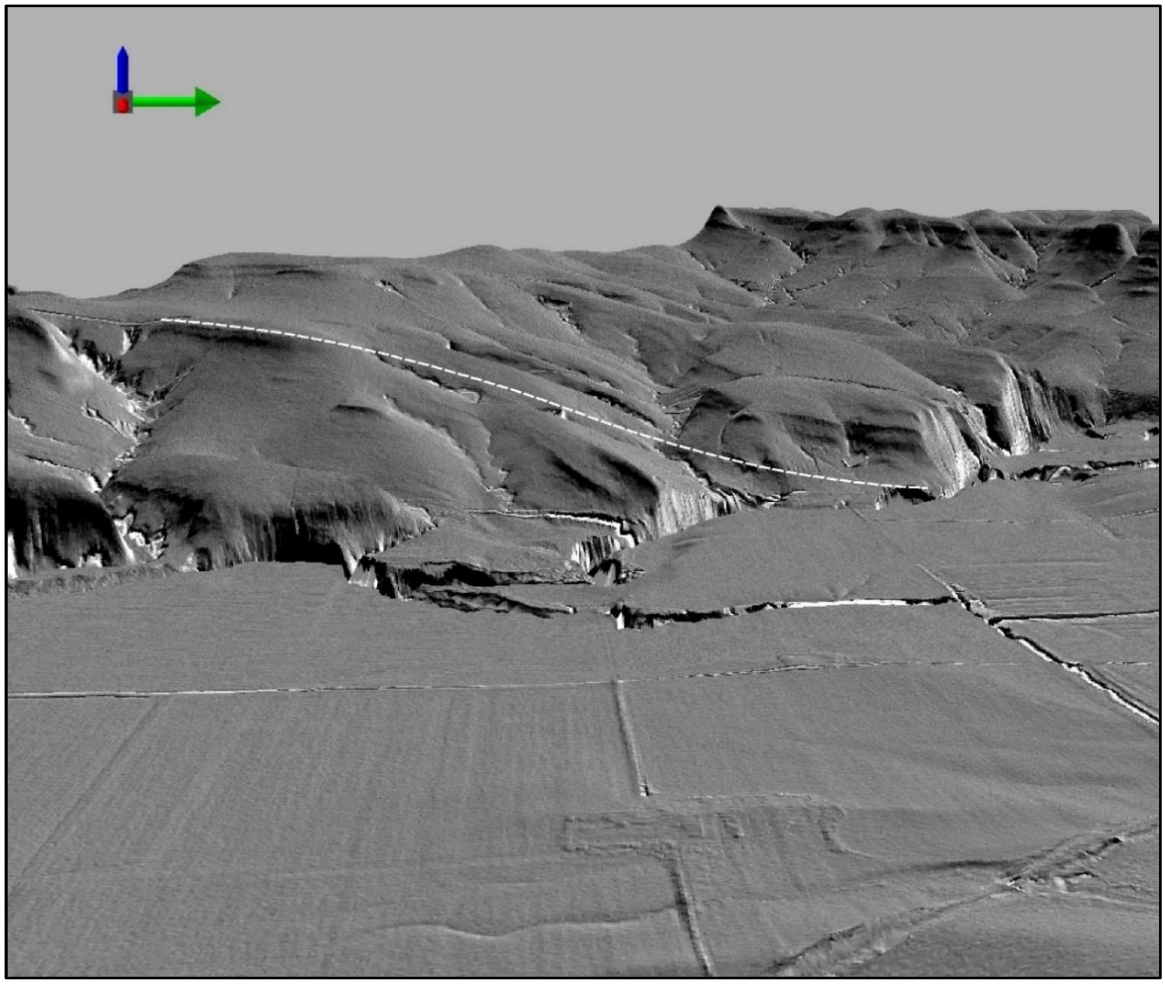

Figure 39. An oblique view of the southern side of Diamond Creek valley. The Neva and Burr Limestone Members dip into the Diamond Creek alluvial valley at center. The viewpoint is roughly 1.5 km north of Neva looking west. Vertical exaggeration = 10x. This trend of dipping strata is sub-parallel to Diamond Creek valley to the northwest for at least 8 kilometers. The trend of dipping strata would appear to be the surface expression of the Lost Springs trend. The green arrow points north.

The same configuration is found along Palmer Creek in northern Chase County. This trend of Riedels extends for at least 12 kilometers from the eastern limits of Palmer

Creek to the west. It passes over the drainage divide to the west and is paralleled by two unnamed tributaries of Schaffer Creek (Figure 40 below).

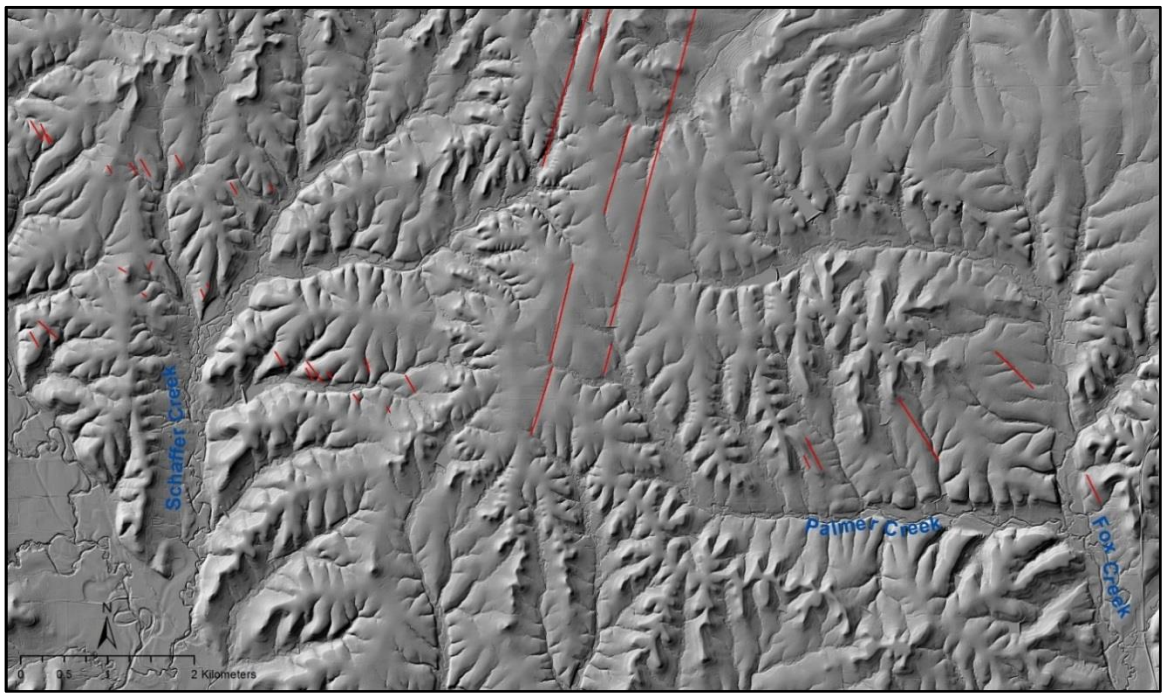

Figure 40. The drainage pattern of Palmer Creek is similar to that of Middle Creek, although at a smaller scale. Faults marked in red parallel the drainage pattern. Again, strata dip relatively steeply to the north on the southern side of the Palmer Creek alluvial valley. Once again, linear features in the style shown in Figure 18 are seen trending NNE to the west of the Humboldt Fault.

Another cluster of faults were detected in the study area on the southern portion of the Elmdale Dome along Holmes Creek. A photo of a fault scarp is shown in Figure 41. The main cluster is ~5 kilometers northeast of the basement fault separating the Elmdale

Dome from the Cedar Creek syncline. This is labeled on Berendsen and Blairs' (1986) Basement Structure map as the Elmdale Fault. The visible faults terminate in the Cottonwood River valley to the northwest and at the trend of moderately dipping strata associated with the Humboldt fault to the southeast. This assemblage of faults is substantially spatially denser than trends found elsewhere in the study area. In the field, these faults appear to be normal faults (Figure 42, 43). It is particularly noteworthy that where this assemblage of faults intersects the dipping strata associated with the Humboldt Fault, the dipping strata that, in this area, trending NNE-SSW, have an offset to the east of approximately 1 kilometer (Figure 44). The faults are roughly parallel to each other and to the overall trend. This is not the case in the Riedel trends discussed above, whereupon the orientation of individual faults deviate from the overall trend of the cluster of faults (Figure 36). There also appears to be an arcuate component to their overall configuration. At the surface, strata begin to dip into the Cedar Creek syncline ~4 kilometers to the southwest of the main cluster of faults at this location. There are many flowing springs in the area that have been modified by the rancher to water cattle.

Figure 41. Looking approximately southeast down a fault scarp near the southern limit of the Elmdale Dome (UTM zone 14N – E 703225, N 4242555).

Figure 42. A fault scarp exposed in a small creek on the southern side of the Elmdale Dome (UTM zone 14N – E 704034, N 4241583). The scarp is roughly 30 degrees from vertical. Notice the slickensides and iron scale. Recemented fault breccia is visible near the right side of the image below the rock hammer. This is the best example of an exposed fault scarp encountered in the field during the course of this study.

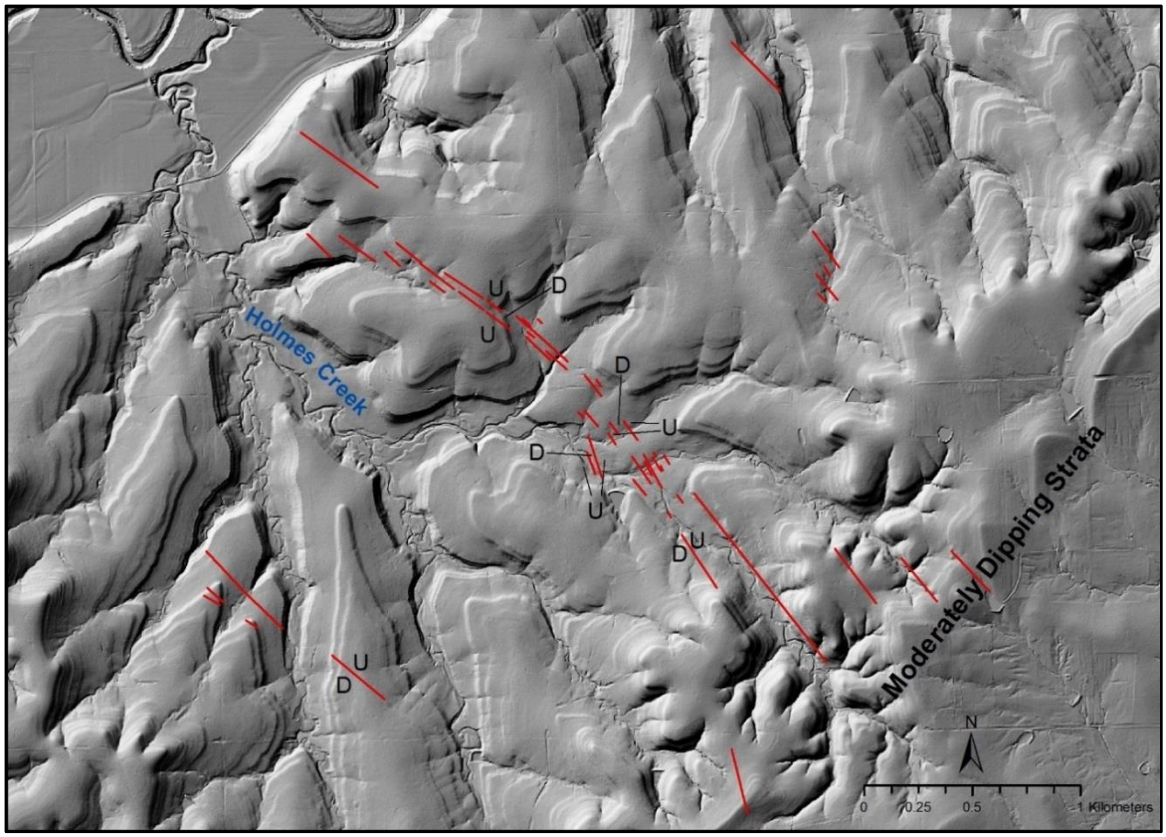

Figure 43. Faults mapped near the southern edge of the Elmdale Dome (red). The moderately dipping strata associated with the eastern edge of the Nemaha are visible as flat irons in the SE corner of the image.

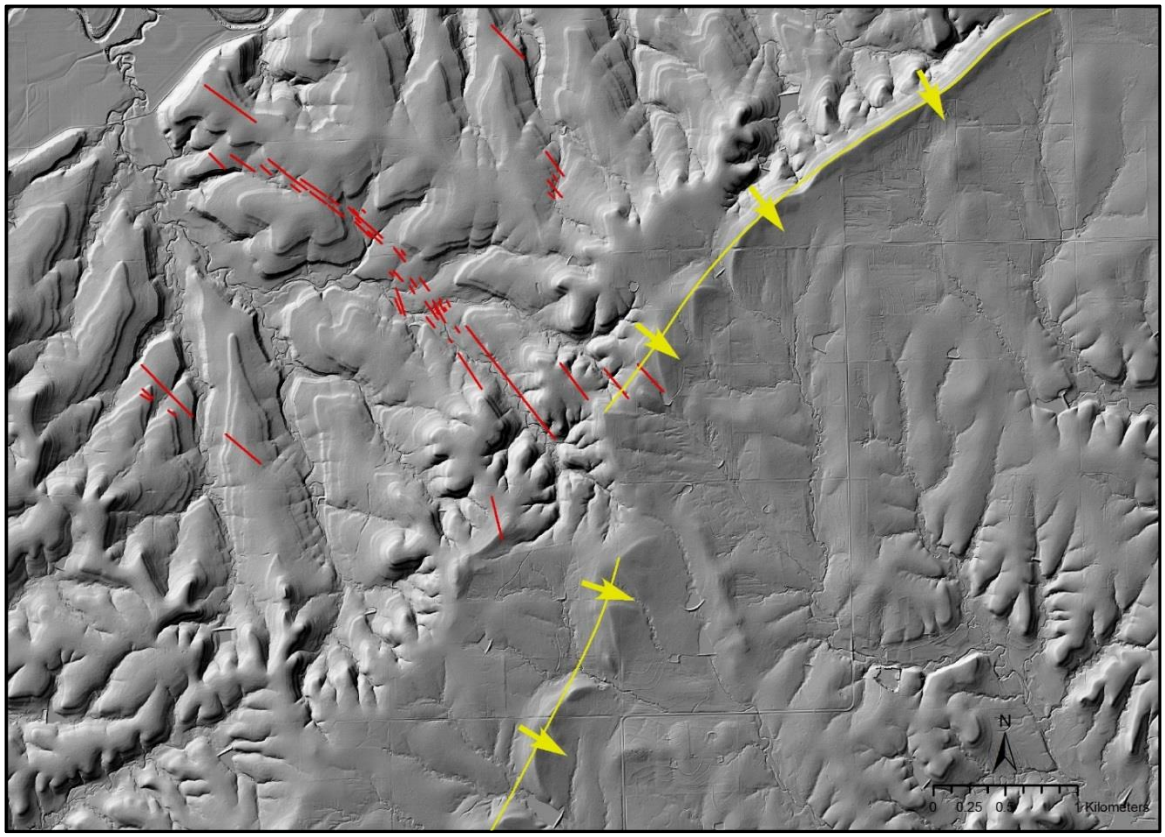

Figure 44. Offset in the dipping strata associated with the Humboldt Fault (yellow) where it intersects what is informally referred to in this thesis as the "Holmes Creek Fault Trend" (red). The flat-irons in the image are composed of the Barneston Formation.

Another example of a fault system with a similar configuration is found on the eastern edge of Butler County, approximately 9 kilometers northeast of Rosalia. This assemblage of faults is located just east of the escarpment of the Flint Hills. To the west, the land surface is not dissected to the same degree that it is to the west of the escarpment. It is likely that the faults continue to the northwest given that the measured offset of the fault marked as A in Figure 45 below is approximately 3 meters, but they are not visible. The fault marked as A is most visible in the Funston Limestone Member.

Again, there is an arcuate component to the mapped faults. Less literature is available on the basement structure in this location and access in the field to the majority of the faults was out of the question because of the typical landowner-operator arrangements seen in this portion of the Flint Hills. In this case, the lake and surrounding land was a vacation home for a landowner that resided elsewhere.

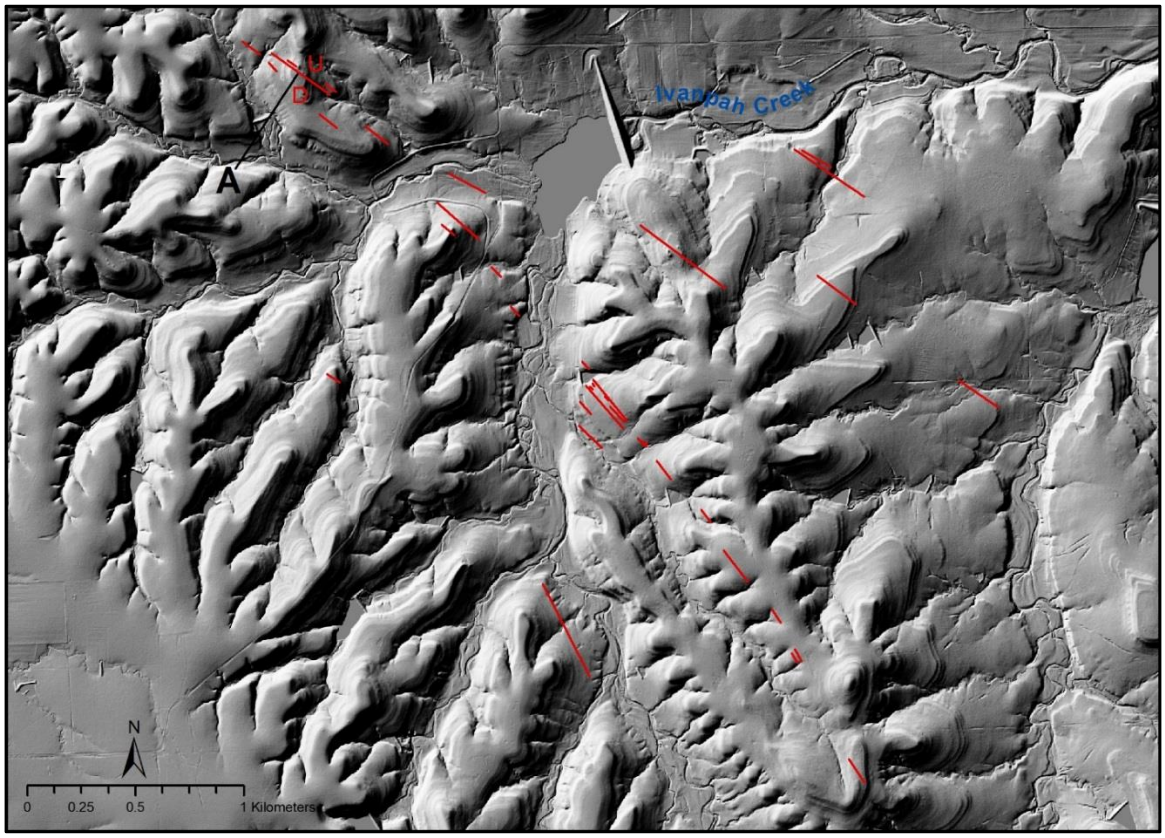

Figure 45. An assemblage of faults ~9 km NE of Rosalia. The coordinates of the fault marked as A are: UTM zone 14N – E 714261, N 4195585.

Interpreting Hillshaded LiDAR

Hillshading bare earth LiDAR allows the viewer to interpret geomorphic features at an ultrafine scale with vegetative cover mathematically removed by selecting for the lowest return in the area detected in the original .las dataset. Modern software allows for the production of multiple hillshades with a simulated sun shining from multiple directions at a fine scale, and over a relatively large area. It is possible to accomplish this task in a relatively short amount of time. This is a direct result of the increased processing power of modern computing systems and the resolution of modern datasets.

Geomorphic interpretation using LiDAR is much improved compared with the National Elevation Dataset. In properly hillshaded LiDAR with the correct contrast and appropriately stretched color ramp, features become visible that would not otherwise be visible. Some features are visible in a LiDAR hillshade that are not easy to discern in the field. Cattle trails, individual stone lines, terraces, fence lines, and even rows of crops are visible in some cases using 1 meter LiDAR. This is an incredible new tool for geomorphic analysis. In the well-established geological setting of Kansas this makes spotting geomorphic anomalies relatively easy. Dipping strata along the Nemaha Fault become obvious (Figure 46 below).

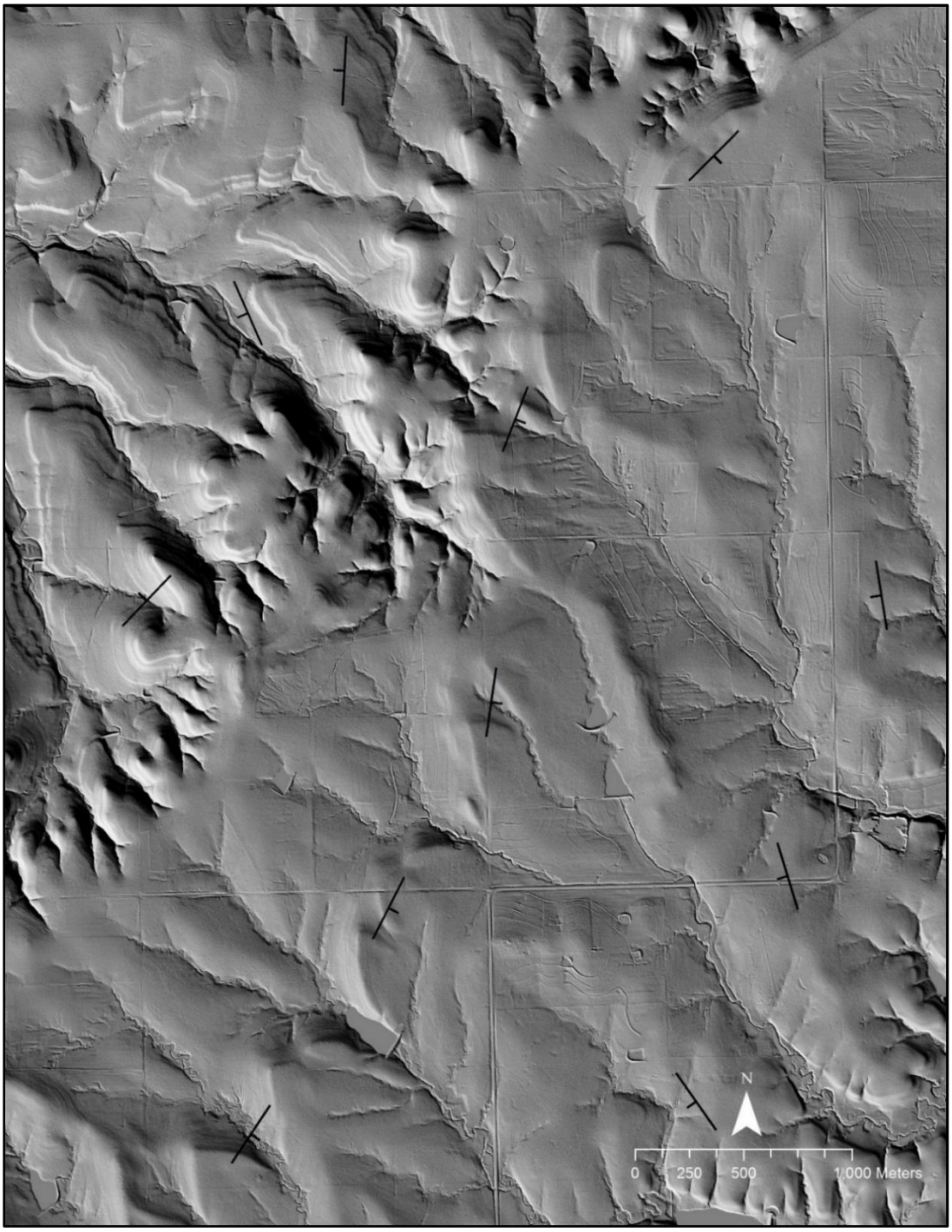

Figure 46. Flat Irons marking the easternmost extent of the Elmdale Dome. These extend from the bottom left portion of the image to the top right. Note that the dipping strata are highly localized in this lineament. Strata to the west and east of the pictured trend generally dip ~0.3° to the west.

Modern software also allows the user to create orthographic views of areas of interest. It is possible to exaggerate the vertical axis to make the muted topographic features of Kansas easily visible. Examples of this are seen in Figure 39, and Figure 47 below.

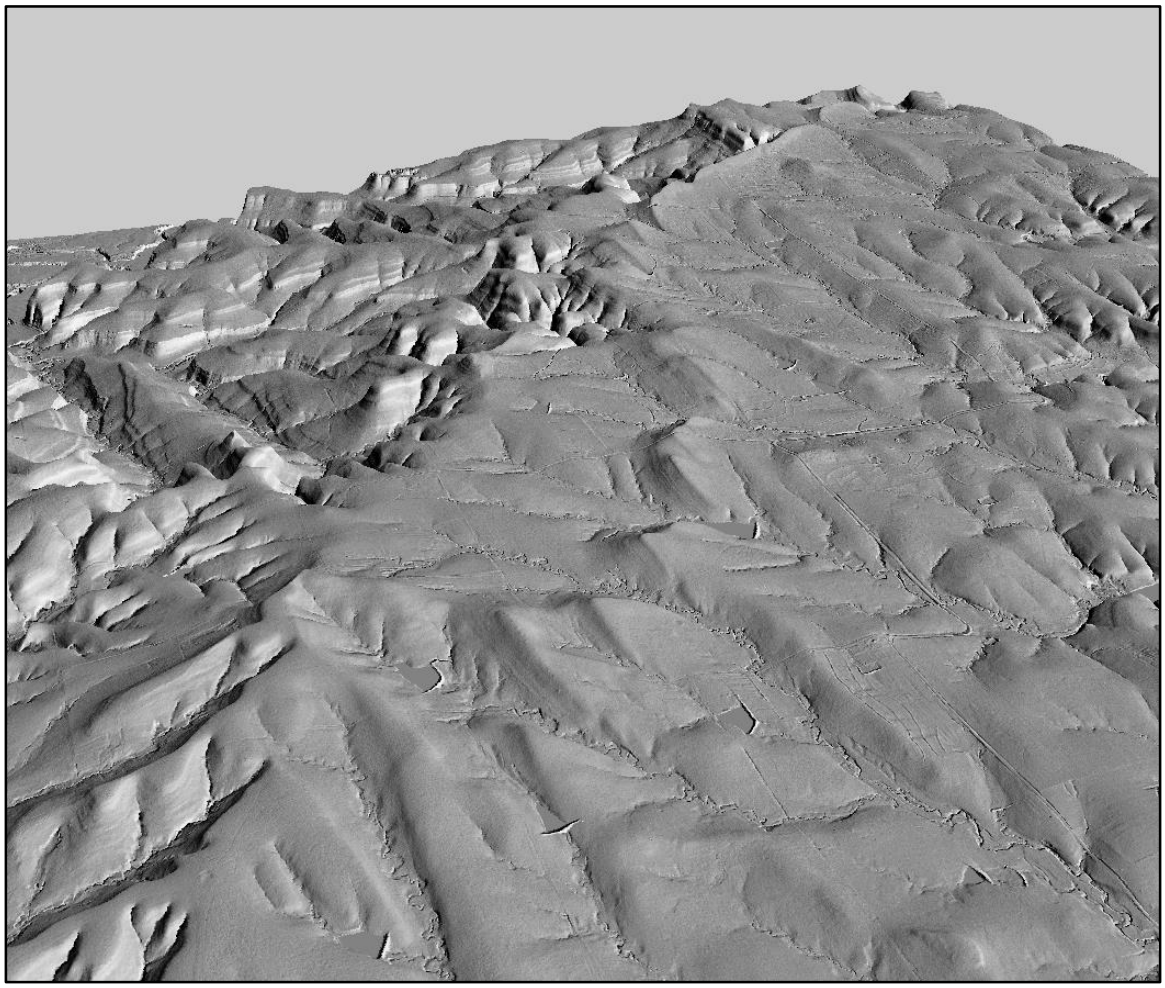

Figure 47. A three-dimensional view of the same area shown in Figure 46 looking NNE along the dipping strata. Vertical exaggeration = 10x.

Linear features become visible using hillshaded LiDAR as well (Figure 48 below). This linear feature shown crossing Highway 50 northwest of Clements, KS is a feature commonly found roughly parallel to and west of the Nemaha front.

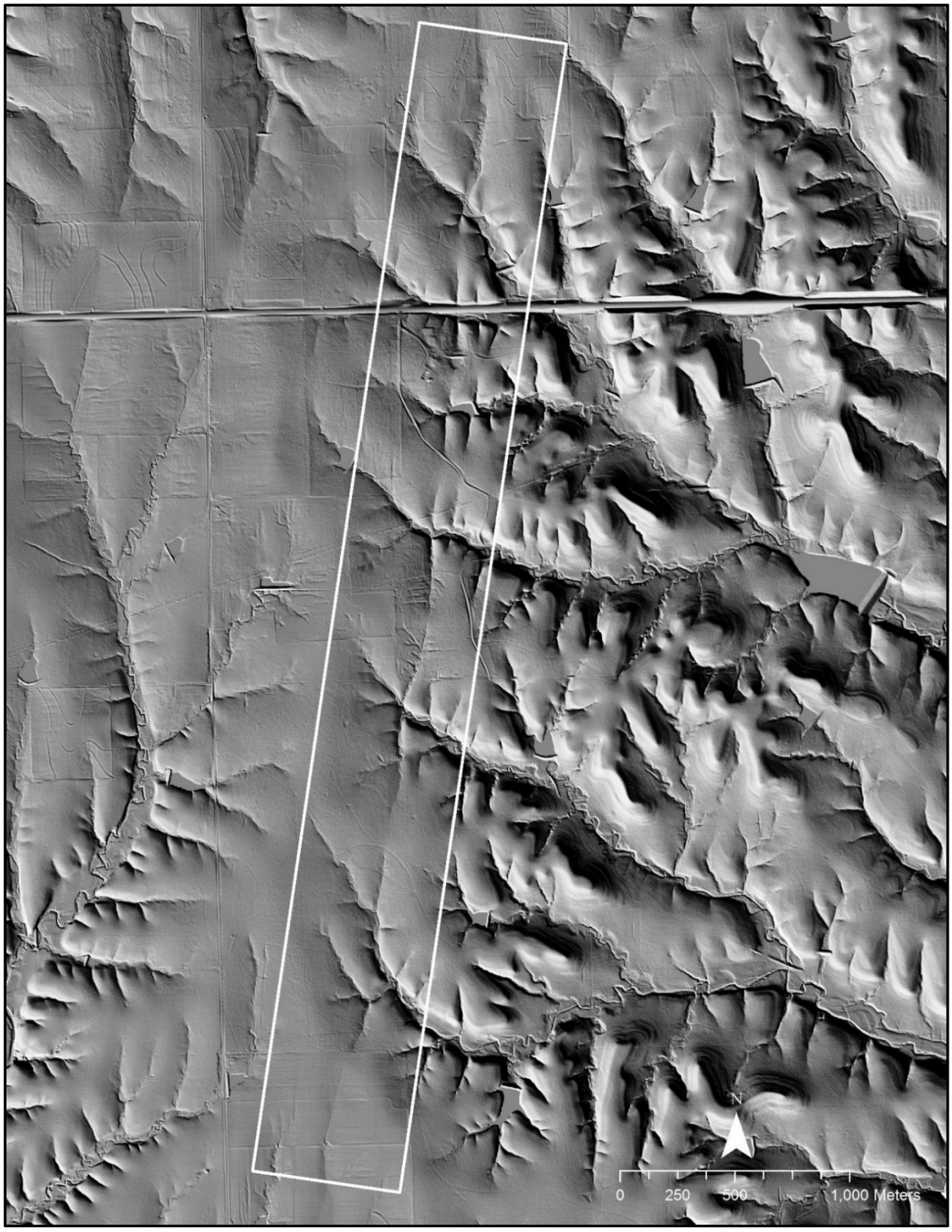

Figure 48. A linear feature assumed to be a fault zone ~12.5 km west of the Elmdale. K-150 crosses the image near the top.

Previously Unknown Ridge Features

A previously unknown geomorphic feature was found during the course of this study as well. These features are seen as muted linear ridges shown in Figure 49 and an oblique view of the same area in Figure 50. When digitizing these features, care was taken to not include features that may have been confused with them, i.e., dunes. For self-evident reasons, these features were not typically found in alluvial valleys. In many cases they paralleled drainages. In the examples presented, accelerated erosion from agriculture has not yet completely erased these features. Additionally, these features are old enough to have influenced the course of drainage in the area. The cluster of features shown in Figure 49 lie parallel to, but ~2.5 km west of a basement fault associated with the Lost Springs Oil Field (Berendsen and Blair, 1986). Elsewhere, in many cases the orientation and clustering of these features tends to be associated with other mapped basement faults and other structural features seen in Berendsen and Blair (1986). A graph of elevation along a transect that crosses the ridges shown in Figure 49 is shown in Figure 51. Elevation was derived from LiDAR.

Figure 49. Pressure ridges overlying multiple faults ~8 kilometers west of the town of Lost Springs. Incidentally the Santa Fe Trail crosses the image at center.

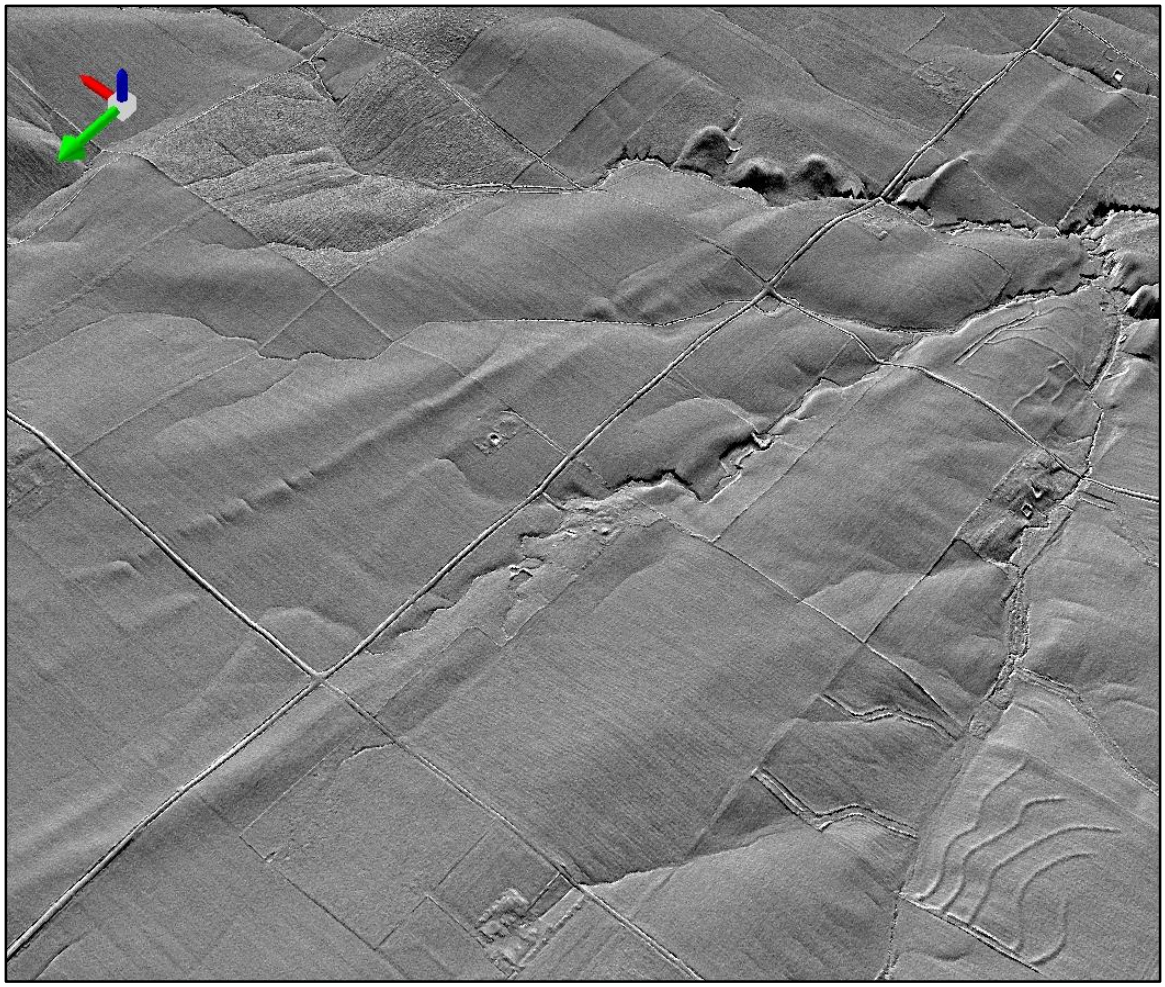

Figure 50. A three-dimensional view of the pressure ridges west of Lost Springs. The green arrow points north. These features are extremely muted when seen in person. Vertical exaggeration = 10x.

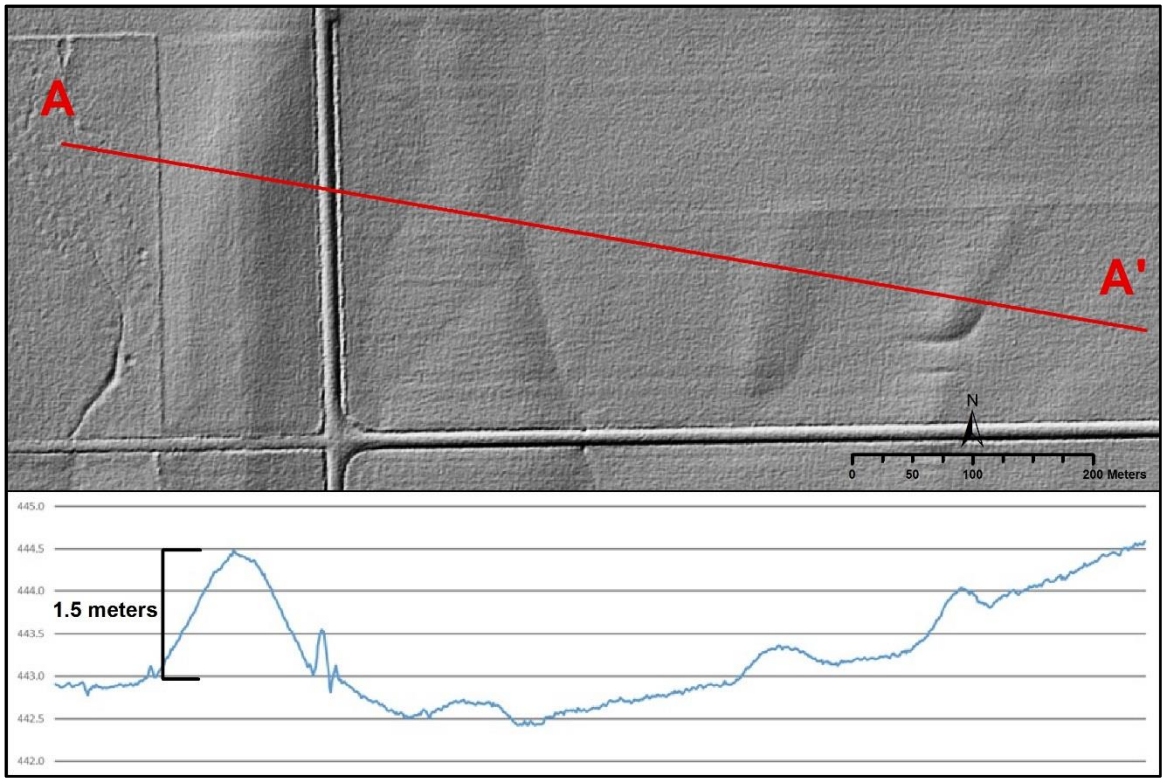

Figure 51. A transect across the Lost Springs pressure ridges showing elevation in meters from LiDAR. The transect A-A' is 913 meters in length.

Figure 52. A pressure ridge west of Lost Springs. The ridge runs from the left of the image (north) near the grain silos to the right. It is seen as a slight hump in the road marked by the arrow. Photo taken facing east at: UTM zone 14N – E 669203, N 4268762.

These features are almost exclusively found to the west of the Nemaha fault. One exception is found east of the Humboldt Fault in Butler County. The examples shown in Figure 53 roughly parallel I-35 approximately 12 kilometers SW of Cassoday, KS.

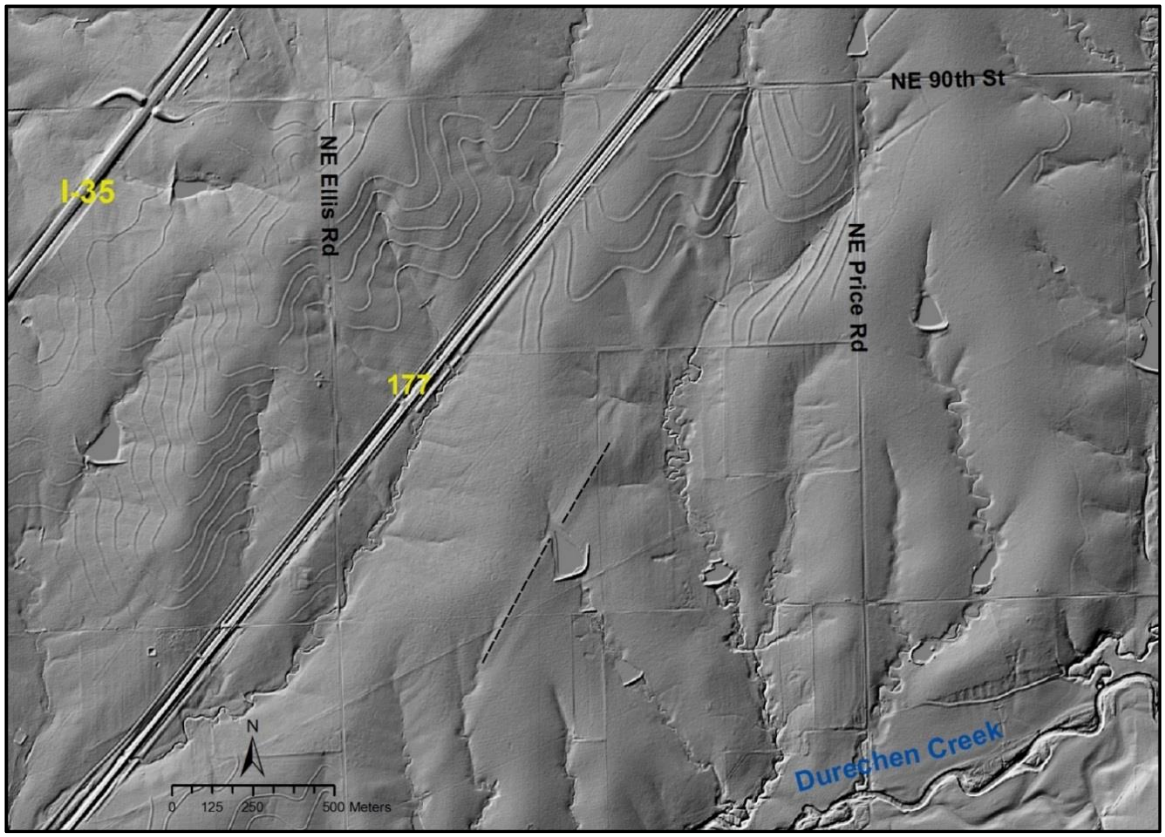

Figure 53. Some of the pressure ridges found east of the Humboldt Fault. This assemblage is found ~12 km SW of Cassoday, KS. Two are marked with a dashed line to aid the reader in locating these features.

Chapter 4. Discussion and Interpretation

The aforementioned methods, when combined, are an effective tool for interpreting the structural history of this portion of the Flint Hills, one caveat being that the author is, so to say, standing on the shoulders of giants. The wealth of data and research done in the study area and adjacent areas provided much in the way of context for the interpretation of the structures discussed in the text. Previous looks at the area through a geospatial lens lacked the spatial resolution available in modern high-resolution imagery and LiDAR (Figure 54).

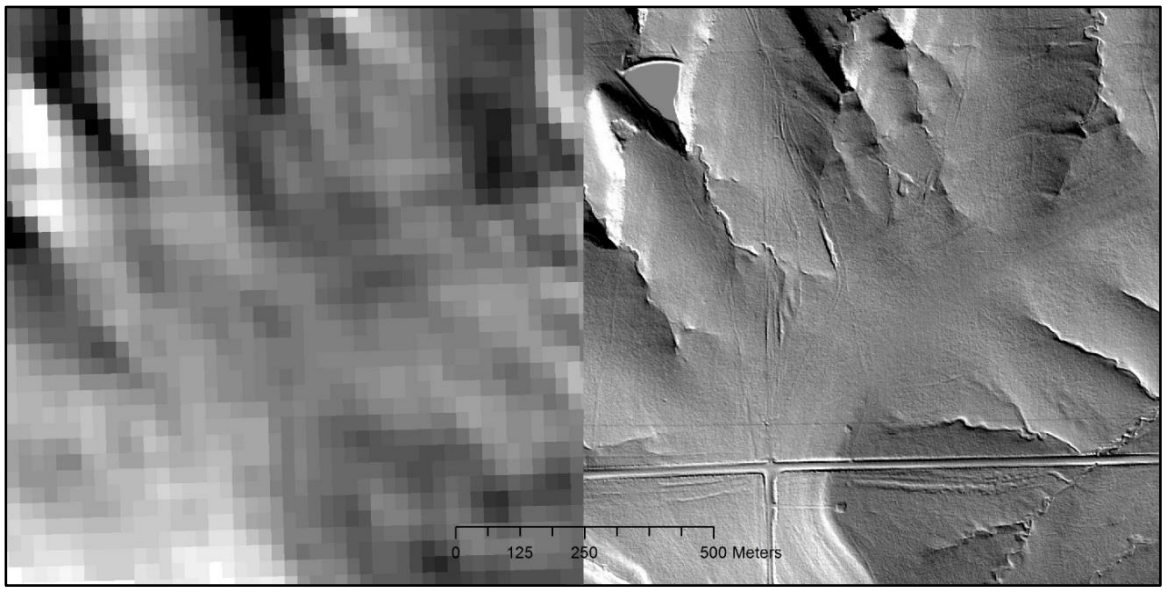

Figure 54. The difference in resolution between National Elevation Dataset (NED) digital elevation model data (left) and 1 meter LiDAR (right) (DASC, 2010-2015). The NED has a resolution of 1/3 arc second, ~28 meters at this latitude (USGS, 2016). The same area, Elmdale Hill, is shown in both images.

The gross structure postulated by Berendsen and Blair (1986) largely matches what is visible in newer datasets. Many previously unmapped minor structures not included by Berendsen and Blair are now visible using this combination of new datasets.

Faults west of the Humboldt Fault

Given the location and orientation of the linear features, shown in Figure 48 and discussed in Figures 38, and 340, relative to the Nemaha front, it is likely that these are associated with slight adjustments along basement structures parallel to and west of the Nemaha front. Taking the currently accepted model for the gross structure of the Nemaha fault (Figure 55) into consideration, I would tend to suggest that these are the surface expression of reverse/backthrust faults directly related to the primary thrust of the Nemaha Fault.

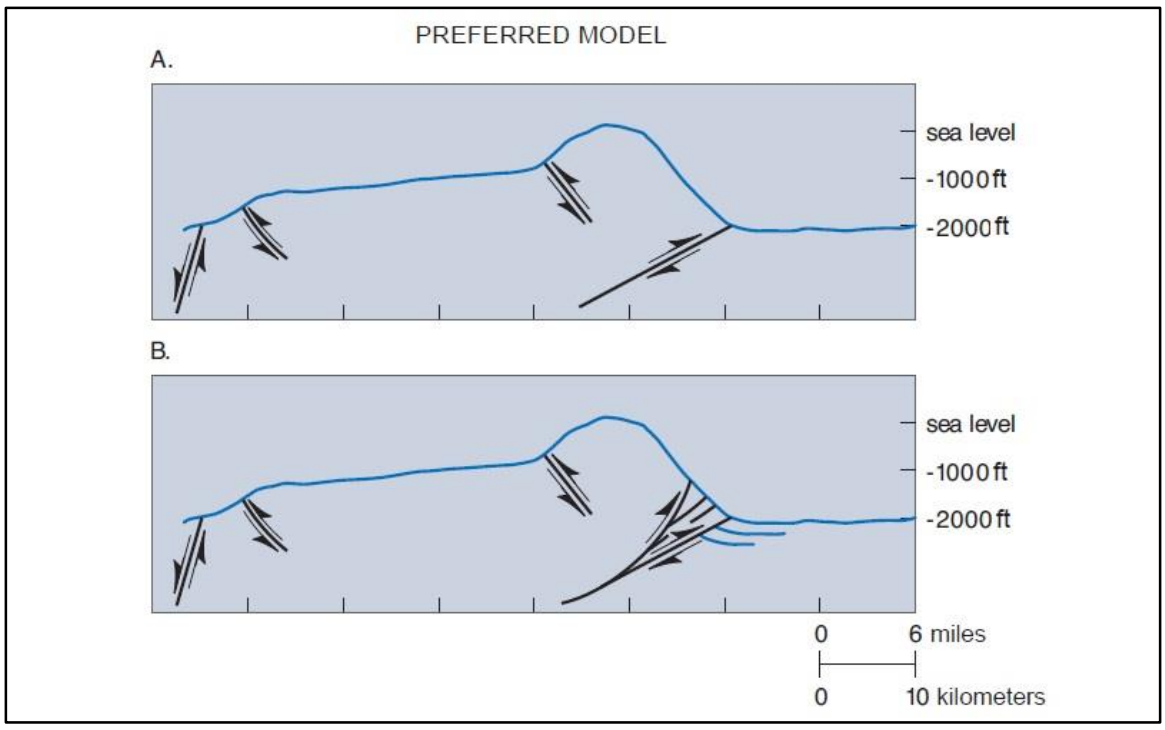

Figure 55. The model for the basement structure of the Nemaha fault proposed by Gerhard (2004).

Pressure Ridges

A map of faults, linear features, pressure ridges, and lineaments of dipping strata is shown below in Figure 56. There are multiple configurations that these ridges are found in. One, in particular, has a similar configuration to those identified as Riedel shears. An example of this pattern is evident in eastern Harvey County. This assembly of faults trends north and is parallel to but far removed to the west of the Whitewater Fault.

A second configuration seen in the image is more linear. Several, long-running, assemblies of ridges parallel to the Halstead Fault are found in the south-west corner of

the image and elsewhere. These assemblies consist of a continuous, sometimes broken ridge where interrupted by erosional crosscutting and agricultural activity.

In many cases, these features overlie or are parallel to known basement faults. In many other cases they parallel recognized structural features such as those associated with mapped oil fields. An example of this is seen in the eastern lobe of the Ritz-Canton oil field, and by extension, the Halstead and Graber oil fields (Figure 56). They are expressed as a ridge where visible. They exert some structural control of drainage where they cross a drainage. These appear to be the surface expression of faults in some capacity. Where these features do not overlie a recognized structural feature, I would suggest that they are the surface expression of a yet unmapped fault trend.

Concerning their expression as ridges at the surface, I would like to propose two possible modes of genesis.

1. These ridges are so-called pressure ridges composed of fault breccia expelled at the surface. In this case, the ridges exist because of movement along a fault that is recent enough that the expelled fault breccia lies in a linear mound overlying the near surface trace of the fault. In this proposed mode of formation, the ridges exist because relatively recent movement along a fault plane.
2. These ridges are the result of groundwater escaping along a plane of weakness (a fault). Minerals held in solution at depth were precipitated as conditions changed on approach to the surface. This is to say that the strata along the fault are better cemented than those adjacent. In this proposed mode of formation, the ridges exist because of erosional processes.

In this geological context, I would favor the second mode of formation. It is possible that in some cases it is the first, or a combination of the two. A small percentage of the ridge features mapped exhibited vertical offset along the fault scarp. In this case, the feature is visible because of vertical offset between hanging wall and foot wall that has not yet been erased by erosion. These do not appear as ridges in hillshaded LiDAR. These appear as a linear bench.

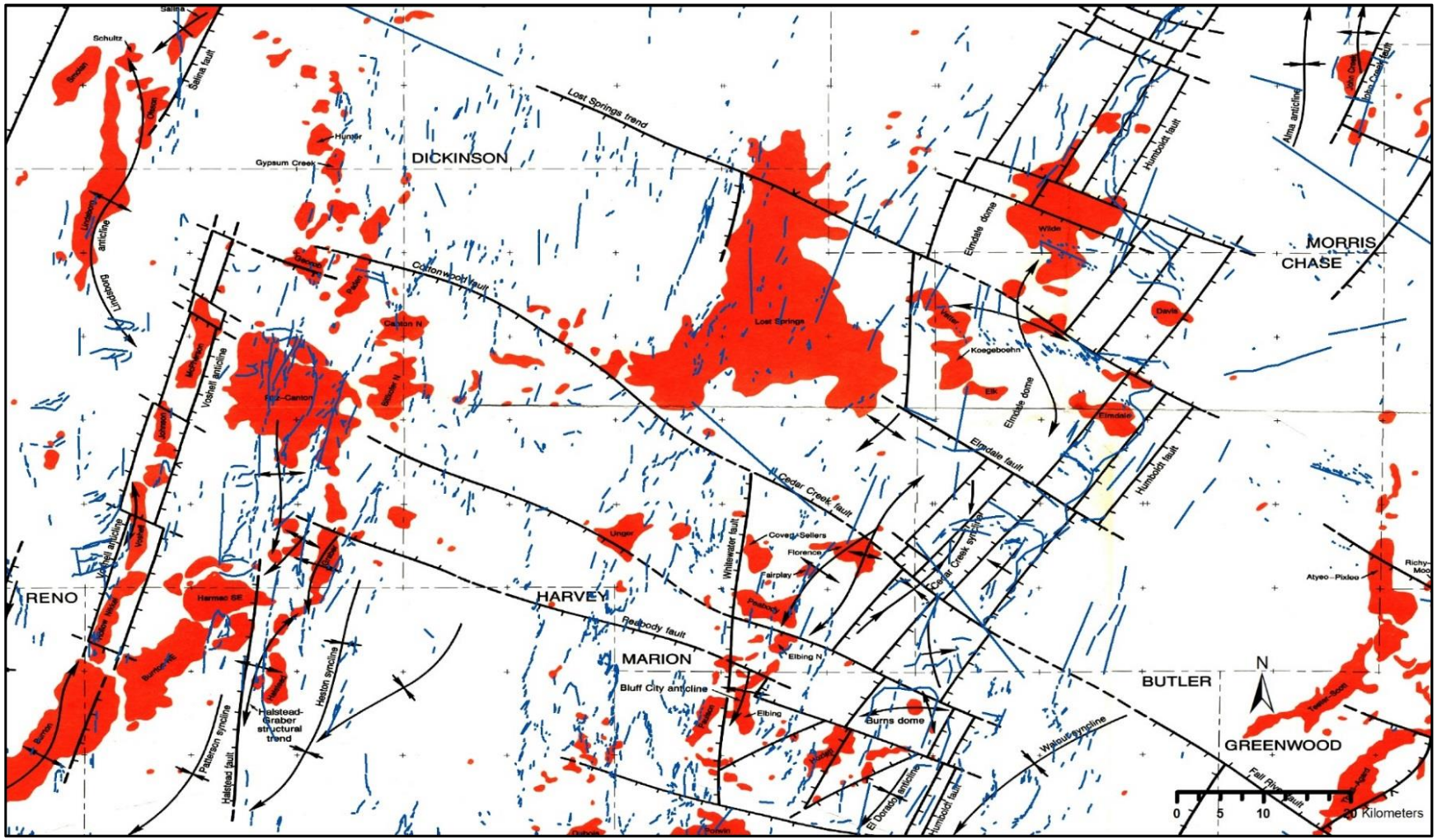

Figure 56. Mapped faults, linear features, pressure ridges, and lineaments of dipping strata overlain on the generalized tectonic map from Berendsen and Blair (1986). The mapped fault trends appear to parallel previously recognized structures in the area.

Interpretation of the Collected Data

The directional forces required to produce a Riedel configuration is well understood (Naylor, et al., 1986; Petit, 1987; Ahlgren, 1999; Davis, et al., 1999; Atmaoui, 2005). The assembly of faults and ridges with this configuration are shown in Figure 57. The collective orientation of mapped surface rupturing Riedel shears represents one axis of release. The trend of ridges with a Riedel configuration in eastern Harvey County have another. Given the bimodal arrangement of these trends it likely represents a structural release along two different axes. Each one of these trends of Riedel shears is likely the surface expression of movement along a basement fault.

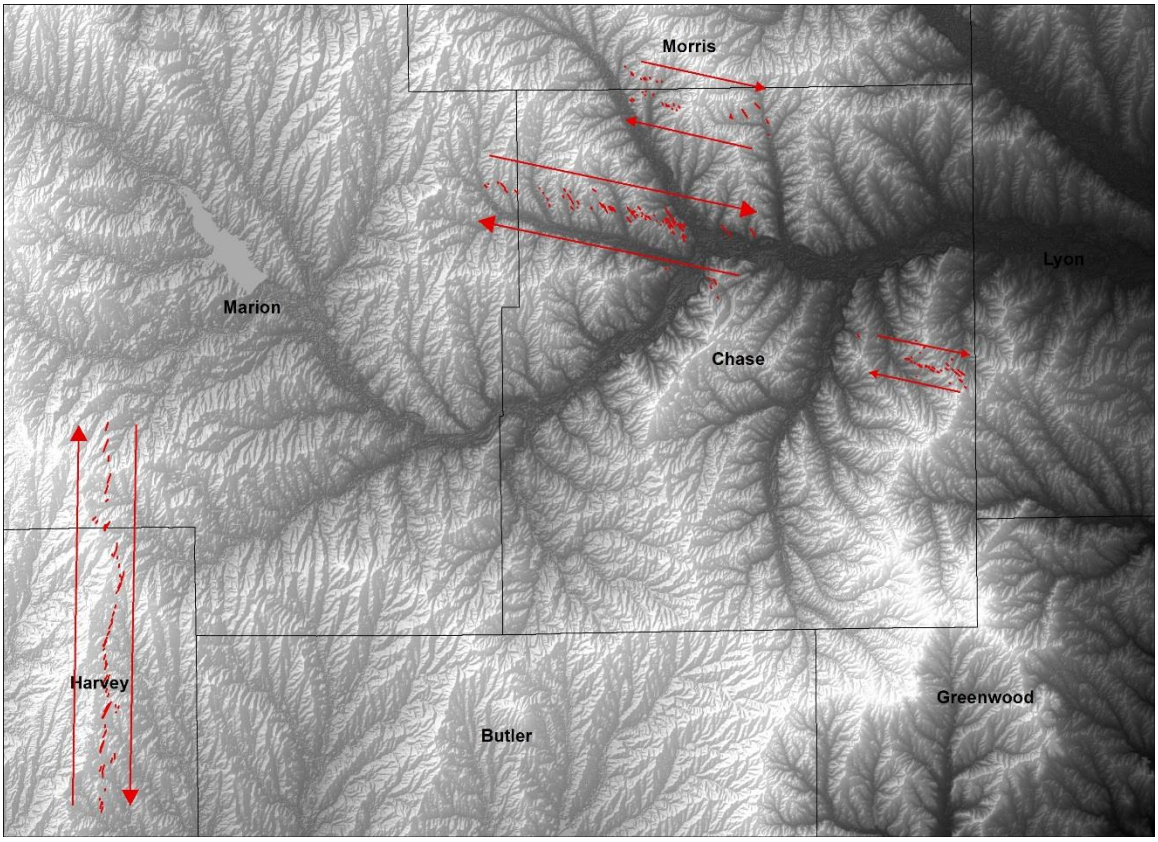

Figure 57. The configuration of the Riedel trends (red) showing the directional shear forces required to create these trends. 1/3 arc-second NED is used as a basemap.

Strata dips gently to the southwest near the transition from the Elmdale Dome to the Cedar Creek syncline. The strata begins to deviate from the regional dip directly southwest of the informally named "Holmes Creek Fault Trend" (Figure 43). This localized change in direction of dip is also accompanied by a left-lateral offset in the moderately dipping strata of the Humboldt Fault (Figure 44). I would like to suggest that this is another unmapped basement fault that lies northeast of, but parallel to the Elmdale fault as shown on Berendsen and Blairs (1986). An image of this area is shown in Figure 58 below.

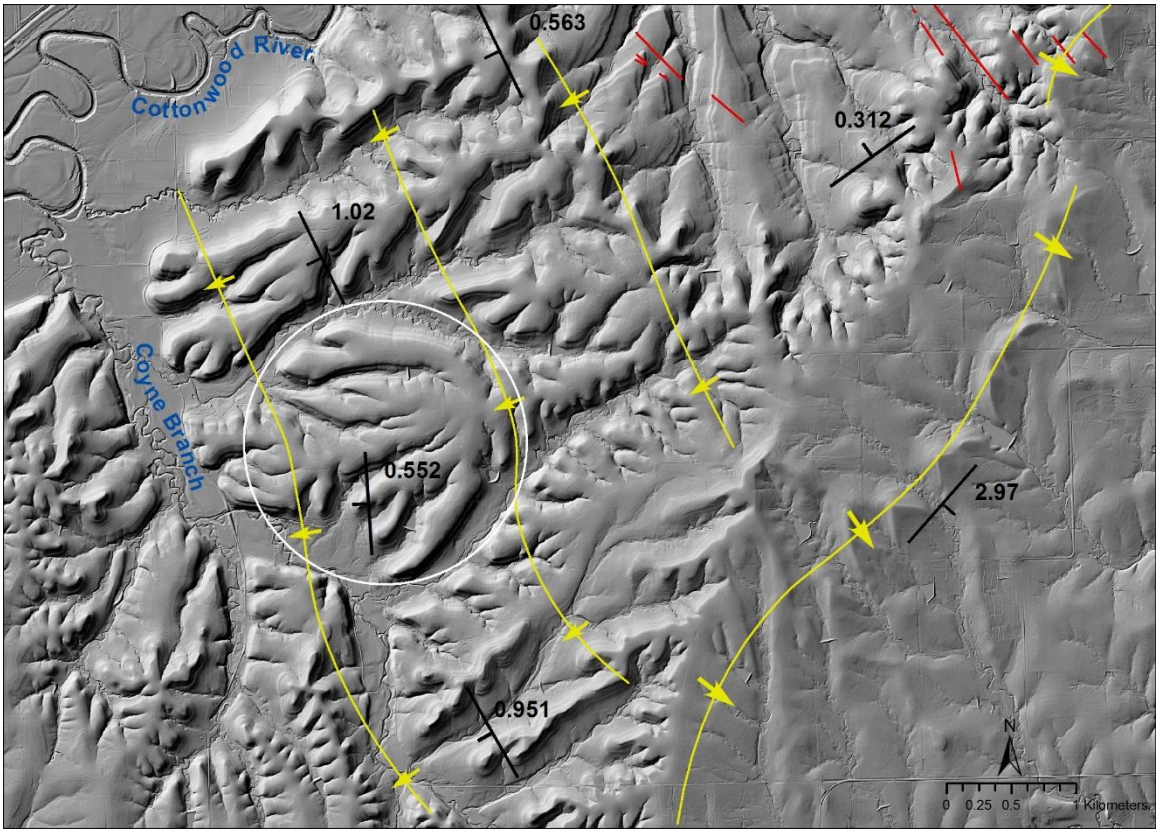

Figure 58. Dipping Strata (yellow), and strike-and-dip measurements (black). A broad plane of dipping strata west of the Humboldt Fault dips to the SW near the transition from the Elmdale Dome (NE) to the Cedar Creek syncline (SW). Notice the dissected flat-iron structure at left-center (circled in white). The dipping strata associated with the Humboldt Fault is seen dipping to the SE in the right side of the image. Note the offset in the dipping strata in the top right corner of the image where the "Holmes Creek Fault Trend" (red) terminates against the flat-irons at its southeastern limit.

The general surface structure of the Elmdale/Neva area is shown in Figure 59. Middle Creek is paralleled by a trend of Riedel shears for approximately 25 kilometers to the west of Neva. Dipping strata occupies the same space as the cluster of Riedel shears

west of Neva. As this trend passes through the Diamond Creek Valley northwest of Neva, it produces a linear ridge. This is possible evidence for structural movement during the Holocene given that this structure lies within the alluvial valley. It continues eastward to its terminus at the dipping strata associated with the Humboldt Fault. This trend of Riedel shears is likely the surface expression of a basement fault that has not been previously mapped. The anticline mentioned by Prosser and Beede (1904) north of Neva is in actuality the result of strata dipping northward exposed in a hillside.

South-east of Elmdale, the dipping strata defining the Humboldt Fault trend northeast-southwest. As this trend travels northward it bends westward then bends generally back to the east as it passes into the Cottonwood River Valley in an 'S' curve. The valley upstream of Chase State Fishing Lake lies near the trough of a plunging syncline. The continuation of this trend of dipping strata to the north into the river valley is likely a plunging anticline. This supposition is reinforced by the dip readings on the northern side of the valley opposite Elmdale Hill (Figure 59).

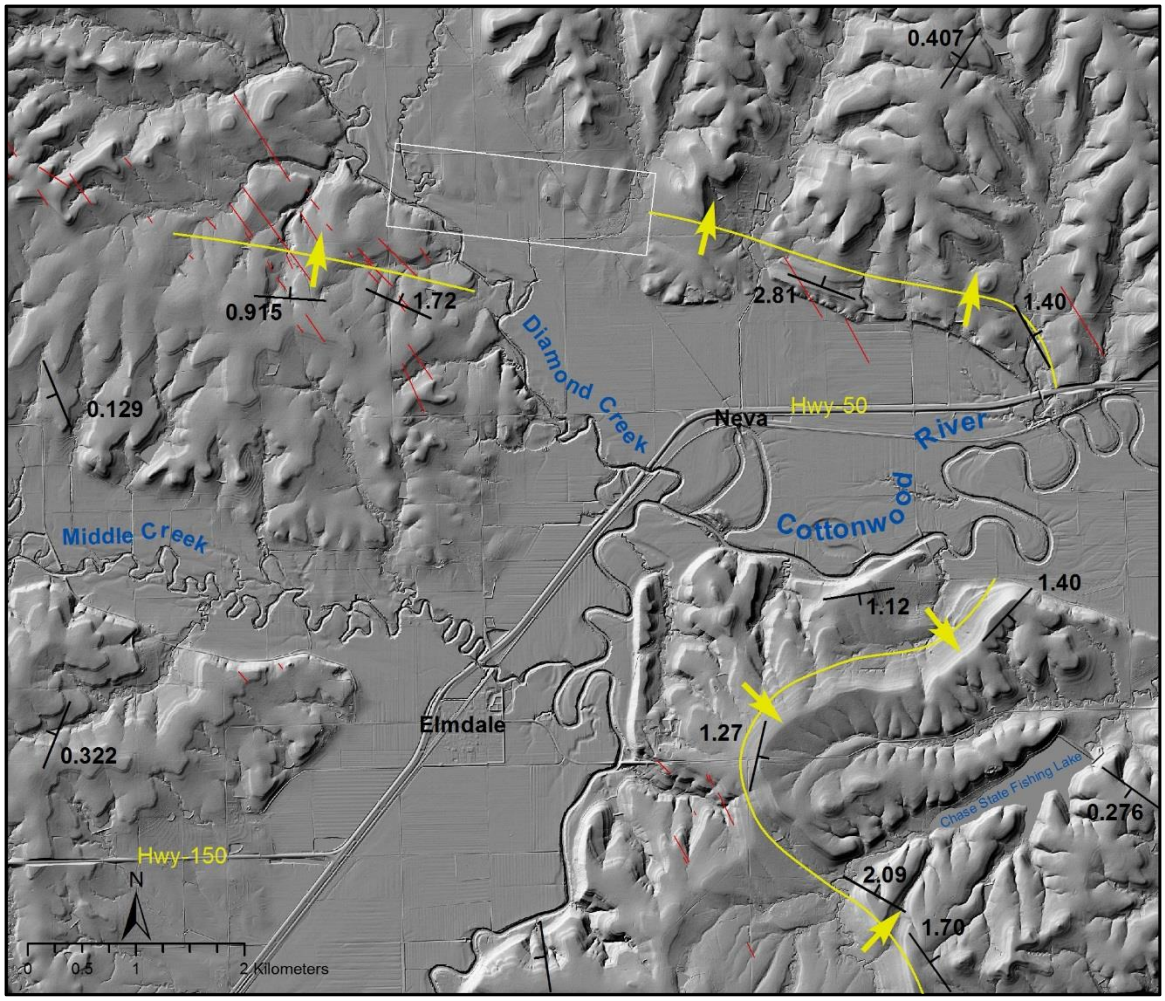

Figure 59. Bands of dipping strata (yellow), and faults (red) in the vicinity of the town of Elmdale, KS. Notice the bench highlighted by the white box that marks the continuation of dipping strata across the Diamond Creek Valley. The top of Elmdale Hill is a plunging syncline. The Cottonwood River valley north of Elmdale Hill is likely a plunging anticline.

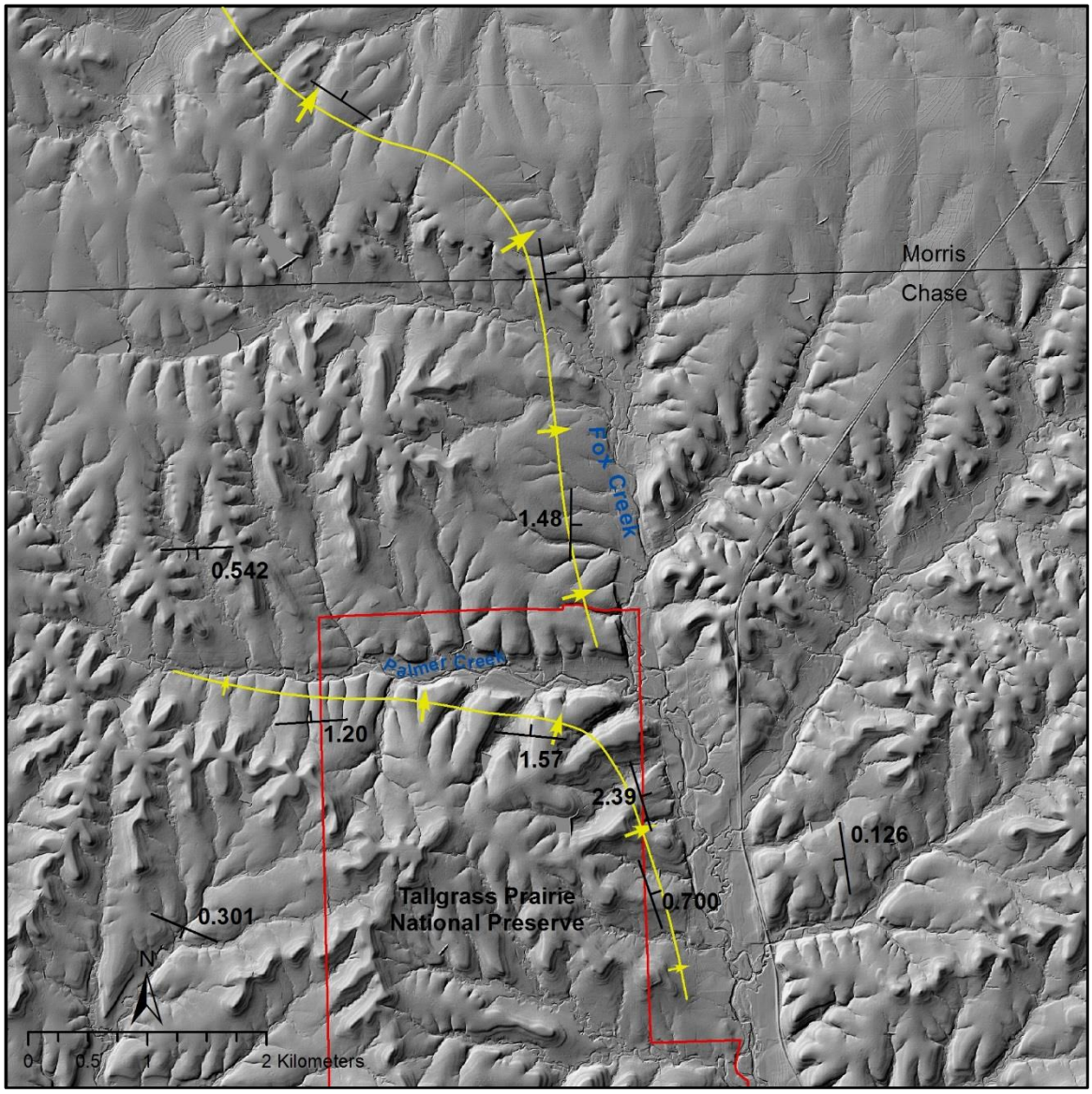

Figure 60. Linear trends of dipping strata in the northern portion of Fox Creek drainage. The vertical offset between one side of northern Fox Creek Valley and the other mentioned by Prosser and Beede (1904) virtually disappears on its way south to the north of Tallgrass Prairie National Preserve headquarters. The fault proposed in 1904 as a mechanism for the offset between east and west valley walls is accounted for entirely by the moderately dipping strata overlying the Humboldt Fault.

Moderately dipping strata associated with the eastern boundary of the Nemaha Fault found when mapping strike-and-dip, or analyzing hillshaded LiDAR, overlie subsurface faults previously mapped by Berendsen and Blair (1986).

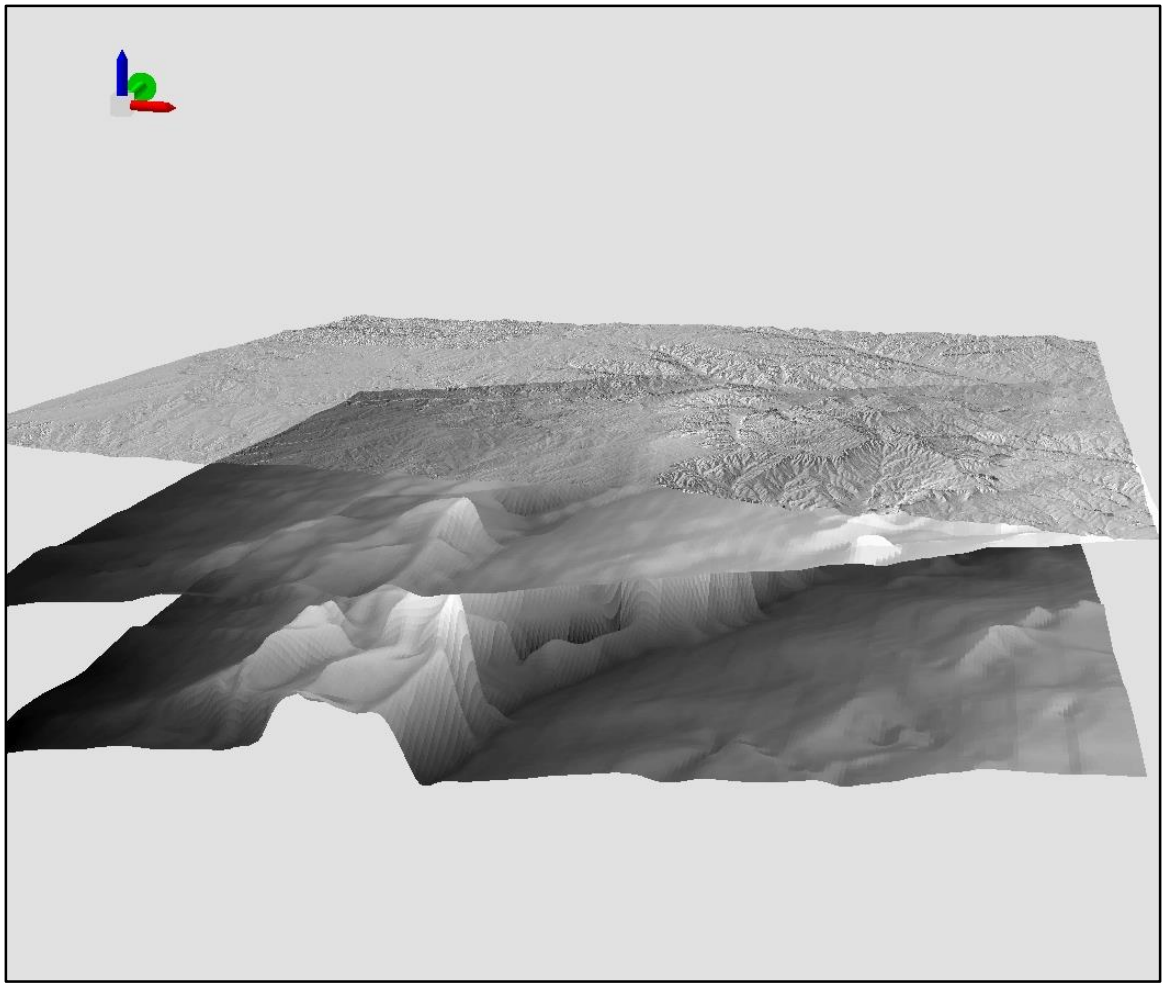

Figure 61. A three-dimensional display of the land surface (top) (USGS, 2016), the top of the Lansing Group (middle), and the Arbuckle Group (bottom). The Cedar Creek syncline is seen as a depression in both the Lansing and the Arbuckle. It is sandwiched between the Burns Dome to the south and the Elmdale Dome to the north. These surfaces are derived from contours in the map series from Berendsen and Blair (1986). Vertical exaggeration = 20x. The green arrow points north.

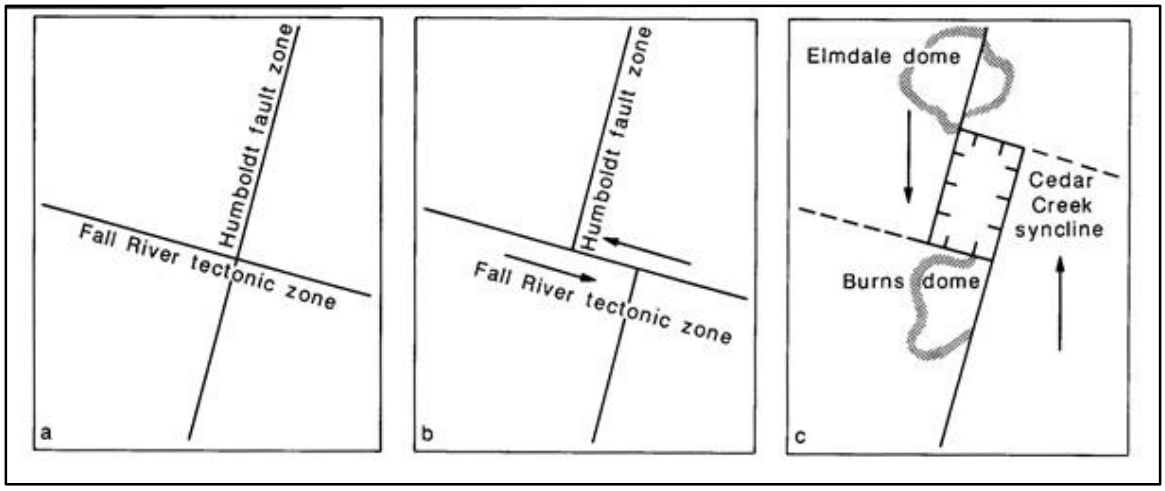

Figure 62. Tectonic model for the Cedar Creek syncline and adjacent structures. a) Structural configuration post MCR. b) Left lateral motion along the Fall River tectonic zone as a result of the Taconic and Acadian Orogenies that exploited the extension of transform fracture zones associated with mid-ocean rifting (Figure 64). c) The creation of the horst, graben, horst structure that is the Elmdale Dome, Cedar Creek syncline, and Burns Dome. This is suggested to be the result of oblique compression during the uplift of the Ouachita and Ancestral Rocky Mountains (Berendsen and Blair, 1986, Figure 6).

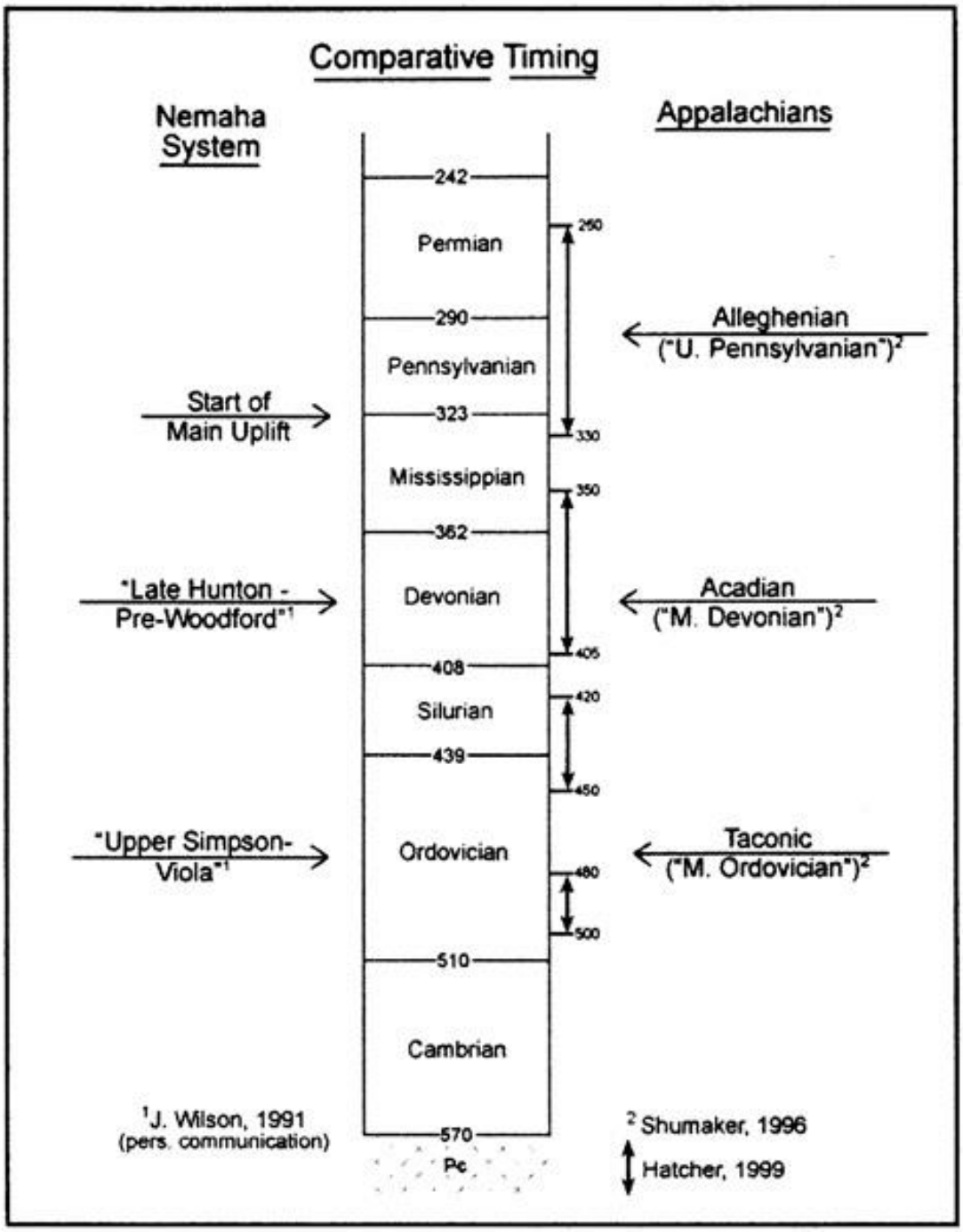

Figure 63. Comparative timing of the three major Paleozoic orogenies on the eastern margin of Laurentia shown in combination with episodes of uplift on the Nemaha System. Ages are in millions of years (Gay, 2003; Figure 37).

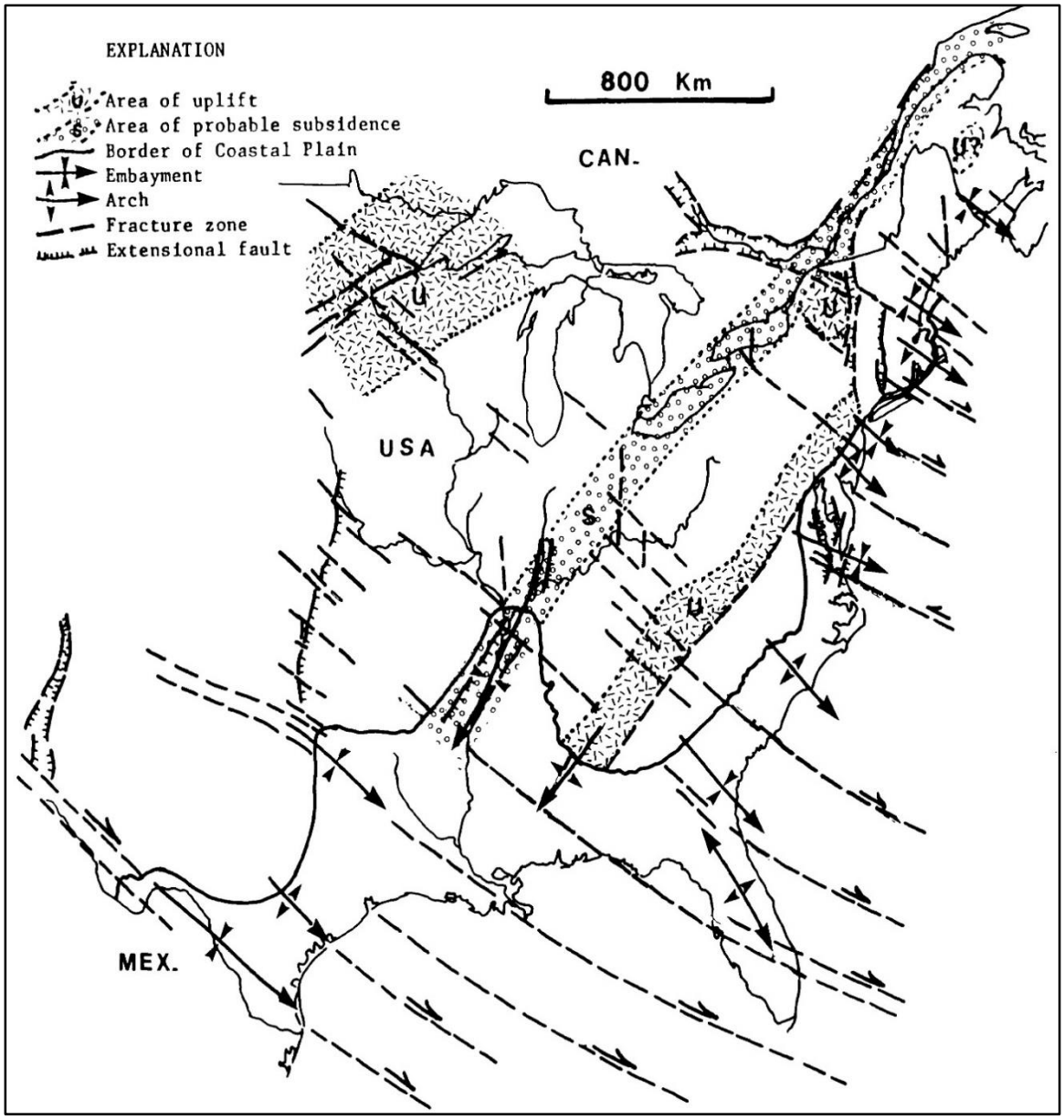

Figure 64. The extension of transverse fracture zones and their associated displacement with spreading at the Mid-Atlantic Ridge into the cratonic interior (Barosh, 1990, Figure 21).

Chapter 5. Conclusions

The wealth of previous geological work done in central and eastern Kansas is of immense help in interpreting newly available data such as high-resolution imagery and LiDAR. The surficial geology (easily defined marker beds of white limestone), land cover (grasses), typical land use (typically untilled), and difficulty in gaining physical access in this region make it particularly well suited to investigation through remote means.

1. The ability to input older, analog data into a geospatial dataset allows for the simultaneous viewing of older data alongside new datasets. Data visualization capabilities of GIS software aid in interpretation of a complex collection of data.
2. LiDAR DEM hillshades are a much improved method for interpreting structurally controlled geomorphic features. The density of ground control points is superior to what was typically available.
3. In this region, acquiring strike-and-dip remotely is preferable to the manual survey method. This assessment takes into consideration the difficulties in getting permission and the time and cost of manually surveying a large area.
4. It is possible to detect and map surface rupturing faults using a variety of high-resolution imagery. The overall configuration of faults within a fault trend may be used to interpret the structural forces that created them.

The area covered in this study overlies a complex collection of basement faults. These basement faults have been activated and reactivated in the past due to a variety of tectonic events. The Nemaha Fault Zone is thought to be the result of spreading at the

Midcontinent Rift farther to the west. This collection of rhombic basement blocks was reactivated later as terranes collided with the now eastern and southeastern margin of the craton during the Paleozoic. Episodes of Paleozoic mountain building introduced a rotational aspect to structural deformation at the Nemaha System through time. Forces transmitted across the North American craton by these and other collisions exploited preexisting basement faults. Some of these are extensions of transverse fractures zones extending all the way to the Atlantic Mid-Ocean Ridge. These structures are inferred to account for the Fall River, Chesapeake, Bolivar-Mansfield, and Central Missouri Tectonic Zones among others. These structures likely are the result of earlier intracratonic rifting created by the MCR or Reelfoot Rift.

The structural anomaly that is Elmdale Dome and its adjacent structures were recognized early in the 20th century. It has been the focus of further study in the time since then. The application of new technology and data to the study of this region in this thesis has uncovered yet again more information concerning the structure of the region.

The dipping strata and associated landforms overlying the Humboldt Fault may be easily traced from north-central Oklahoma to the glaciated region of northeastern Kansas. Moderately dipping strata associated with the eastern boundary of the Nemaha Fault found when mapping strike-and-dip, or analyzing hillshaded LiDAR, generally match subsurface faults previously mapped by Berendsen and Blair (1986). Areas with localized anomalous dips generally overlie recognized structural features. Newly mapped fault trends sometimes match recognized basement faults and structures, while some do not. These likely overlie unrecognized basement structures.

Oblique movement is recorded in various Riedel trends and associated dipping strata in Chase and surrounding counties. The fault trend and associated dipping strata that cross the Diamond Creek valley are possible evidence of Holocene adjustment along this particular fault trend. This feature is visible as an escarpment that crosses the Diamond Creek valley.

The fault zone that parallels Holmes Creek and the fault zone found in the headwaters of Ivanpah Creek share a similar arcuate configuration. The fault zone paralleling Holmes Creek lies parallel to but roughly five kilometer northeast of the Elmdale Fault. Approximately one kilometer of horizontal offset in the dipping strata overlying the Humboldt Fault is visible where this trend intersects said dipping strata. These fault trends appear to be normal in nature.

Linear fault zones west of the Humboldt front parallel the orientation of the Humboldt Fault (south-southwest to north-northeast). These are possibly the result of adjustments along backthrusts or reverse faults created by the main thrust of the Nemaha Fault Zone during the active period of the Midcontinent Rift ending ~1.1 Ga. These and other basement structures were reactivated later during Paleozoic and more recent Laurentian orogenies. It is also likely that displacement along transverse faults associated with sea floor spreading in the Atlantic was transmitted into the cratonic interior during the Mesozoic and Cenozoic exploiting transverse faults created by earlier intracratonic rifts (MCR, Reelfoot Rift) and orogenies (Grenville). Adjustments along basement structures was transmitted upwards through the sedimentary column.

New technology allows for new methods of data collection and visualization in this realm. The introduction of LiDAR and a wide variety of high-resolution imagery

allow for the analysis of structural features in this context at a much improved scale relative to what was available a decade ago. This trend of improving geospatial data and the accompanying improved possibility for analysis is likely to continue to advance.

References

Aber, J. S., 1988. Structural Geology Exercises with Glaciotectonic Examples. Hunter Textbooks, Winston-Salem, North Carolina, p. 140. Earth Science Department, Emporia State University. Emporia, Kansas 66801.

Ahlgren, S. G., 1999. The Nucleation and Evolution of Riedel Shear Zones as Deformation Bands in Porous Sandstone. A prepublication manuscript submitted to the faculty of the Department of Geosciences in partial fulfillment of the requirements for the Degree of Master of Science in the Graduate College, The University of Arizona.

ArcGIS® software by ESRI, 2016. World Imagery Basemaps. ArcGIS® and ArcMap™ are the intellectual property of Esri and are used herein under license. Copyright © Esri. All rights reserved. For more information about Esri® software, please visit www.esri.com.

Atmaoui, N., 2005. Development of Pull-Apart Basins and Associated Structures by the Reidel Shear Mechanism: Insight from Scaled Clay Analogue Models. Der Fakultät für Geowissenschaften der Ruhr-Universität Bochum zur Erlangung des Doktorgrades der Naturwissenschaften.

Barosh, P. J., 1990. Neotectonic movement and earthquake assessment in the eastern United States. Geological Society of America. Reviews in Engineering Geology, v. 8, ch. 5, p. 77-109.

Baars, D. L., 1995. Basement Tectonic Configuration in Kansas. Kansas Geological Survey, Bulletin 237. The University of Kansas, Lawrence, KS 66047.

Berendsen, P., Blair, K. P., 1995. Structural Development of the Nemaha Tectonic Zone in Kansas. Oklahoma Geological Survey Circular 97, p. 208-214.

Berendsen, P., Blair, K. P., 1986. Subsurface structural maps over the Central North American rift system (CNARS), central Kansas, with discussion. Kansas Geological Survey, Subsurface Geology Series 8.

Berendsen, P., Borcherding, R. M., Doveton, J., Gerhard, L., Newell, K. D., Steeples, D., Watney, W. L., 1988. Texaco Poersch #1, Washington County, Kansas—Preliminary geologic report of the pre-Phanerozoic rocks. Kansas Geological Survey, Texaco USA. Open-file Report 88-22.

Data Access and Support Center (DASC), 1997. Public Land Survey System (PLSS). Township and Range. Kansas Geological Survey, August 27, 1997. http://kansasgis.org/catalog/index.cfm?data_id=1762&show_cat=1

Data Access and Support Center (DASC), 2011. Kansas LiDAR Data Acquisition. Kansas Geological Survey. The University of Kansas. Lawrence, Kansas 66047. http://www.kansasgis.org.

Data Access and Support Center (DASC), 2012. TIGER 2010, Census Counties. http://kansasgis.org/catalog/index.cfm?data_id=1561&show_cat=1.

Data Access and Support Center (DASC), (2010-2015). Kansas LIDAR. Kansas GIS Policy Board, Topeka, KS. LIDAR 2010-LIDAR2015. http://kansasgis.org.

Data Access and Support Center (DASC), 2014. NG911 Imagery. 1-foot pixel resolution. Collected fall 2013 and winter 2014.

Davis, G. H., Bump, A. P., Garcia, P. E., Ahlgren, S. G., 1999. Conjugate Riedel deformation band shear zones. The Department of Geosciences, The University of Arizona, Tucson, Arizona 85721, USA. Journal of Structural Geology, v. 22, p. 169-190.

Gay, S. P. Jr., 1989. "Graniteville-type" Proterozoic igneous intrusions mapped in southeast Kansas. Kansas Geological Survey, Bulletin 226. Geophysics in Kansas, p. 229-243. Applied Geophysics, Inc. Salt Lake City, Utah 84111.

Gay, S. P. Jr., 2003. The Nemaha Trend-A System of Compressional Thrust-Fold, Strike-Slip Structural Features in Kansas and Oklahoma, Part1. The Shale Shaker, v. 54, issue 1, p. 9-17.

Gerhard, L. C., 2004. A New look at an old Petroleum Province. Kansas Geological Survey, Bulletin 250, part 1. The University of Kansas, Lawrence, KS 66047, USA

Hauser, E. C., 1996. Midcontinent rifting in a Grenville embrace. Geological Society of America Special Paper 308. Institute for the Study of the Continents, Cornell University, Ithaca, New York 14853.

Horrall, K. B., Hagni, R. D., Kisvarsanyi, G., 1982. Mineralogical, textural, and paragenetic studies of selected deposits of the southeast Missouri lead-zinc-copper district and their genetic implications. International conference on Mississippi Valley type lead-zinc deposits. Proceedings Volume, p. 289-316. University of Missouri, Rolla.

Haworth, E., 1915. The Crystalline Rocks of Kansas. Kansas Geological Survey, Bulletin 2, p. 27-29.

Jewett, J. M., Moore, R. C., O'Connor, H. G., Smith, R. K.., 1951. Geology, Mineral Resources, and Ground-water Resources of Chase County, Kansas. State Geological Survey of Kansas, v. 11. University of Kansas Publications.

Kansas Geological Survey Interactive Oil and Gas Wells and Fields Map, 2016. http://chasm.kgs.ku.edu/ords/qualified.well_page.DisplayWell?f_kid=1006513368. Well Report. Accessed October 2016.

Keller, G. R., Lidiak, E. G., Hinze, W. J., Braile, L. W., 1983. The Role of Rifting in the Tectonic Development of the Midcontinent, U.S.A. Tectonophysics, v. 94, p. 391-412.

McBee, W., Jr., 2003. Nemaha Strike-Slip Fault Zone. Adapted from oral presentation at AAPG Mid-Continent Section Meeting, October 13 2003. Search and Discovery Article #10055.

Merriam, D. F., 2010. Evolution of thought on the Buried Precambrian Rocks of Kansas. Transactions of the Kansas Academy of Science, v. 113(1/2), p. 71-90.

Naylor, M. A., Mandl, G., Sijpesteijn, C. H. K., 1986. Fault geometries in basement-induced wrench faulting under different initial stress states. Journal of Structural Geology, v. 8, Issue 7, p. 737-752.

Petit, J. P., 1987. Criteria for the sense of movement on fault surfaces in brittle rocks. Journal of Structural Geology, v. 9, Issue 5-6, p. 597-608.

Prosser, C. S., Beede, J. W., 1904. Cottonwood Falls Folio. Folios of the Geologic Atlas 109. United States Geological Survey. Washington D.C.

Sims, P. K., 1990. Precambrian Basement Map of the Northern Mid-Continent U.S.A. United States Geological Survey, IMAP series 1853. Denver, Colorado

Smith, T., Nyahay, R., 2005. Wrench Fault Architecture of Trenton Black River Hydrothermal Dolomite Reservoirs. New York State Museum. Presented at ES-AAPG 2005 Meeting. http://www.wvgs.wvnet.edu/www/tbr/docs/050920_ESAAPG05_Smith.pdf

Somanas, C., Knapp, R. W., Yarger, H. L., Steeples, D. W., 1989. Geophysical model of the Midontinent Geophysical Anomaly in northeastern Kansas. Kansas Geological Survey, Lawrence, Kansas 66046. Bulletin 226 p. 215-228.

U. S. Geological Survey (USGS), 2016. USGS NED 1/3 arc-second ArcGrid 2016. Multiple 1 x 1 degree tiles. https://viewer.nationalmap.gov/basic/?basemap=b1&category=ned,nedsrc&title=3DEP%20View.

West, R. R., Miller, K. B., Watney, W. L., 2010. The Permian System in Kansas. Kansas Geological Survey Bulletin 257. Lawrence, Kansas 66047.

I, Alan Edward Peterson , hereby submit this thesis/report to Emporia State University as partial fulfillment of the requirements for an advanced degree. I agree that the Library of the University may make it available to use in accordance with its regulations governing materials of this type. I further agree that quoting, photocopying, digitizing or other reproduction of this document is allowed for private study, scholarship (including teaching) and research purposes of a nonprofit nature. No copying which involves potential financial gain will be allowed without written permission of the author. I also agree to permit the Graduate School at Emporia State University to digitize and place this thesis in the ESU institutional repository.

_____

Signature of Author

_____

Date

NEW GEOSPATIAL TECHNIQUES AND METHODS APPLIED TO STRUCTURAL GEOLOGY IN EAST-CENTRAL KANSAS

Title of Thesis

_____

Signature of Graduate School Staff

_____

Date Received